Magma Mixing
Interaction Between Rhyolitic and Basaltic Melt

Daniele Morgavi

München 2013

Magma Mixing
Interaction Between Rhyolitic and Basaltic Melts

Daniele Morgavi

Dissertation
an der Fakultat fur Geowissenschaften
der Ludwig-Maximilians-Universität
München

vorgelegt von
Daniele Morgavi
aus Roma, Italia

München, den May, 2013

Erstgutachter:	DONALD B. DINGWELL
Zweitgutachter:	DIEGO PERUGINI
Tag der mündlichen Prüfung:	14. 01. 2014

To all the Friend and lovers
that have shared a peace of their
life with me

In my life
(Lennon and McCartney)

There are places I remember
All my life, though some have changed
Some forever not for better
Some have gone and some remain
All these places have their moments
With lovers and friends I still can recall
Some are dead and some are living
In my life I've loved them all

But of all these friends and lovers
There is no one compares with you
And these memories lose their meaning
When I think of love as something new
Though I know I'll never lose affection
For people and things that went before
I know I'll often stop and think about them
In my life I love you more

Though I know I'll never lose affection
For people and things that went before
I know I'll often stop and think about them
In my life I love you more
In my life I love you more

Table of content

List of Figures

List of table

Prologue

All of the data presented in this doctoral dissertation have been published in scientific journals or are in the review process:

1. **Daniele Morgavi**, Diego Perugini, Cristina P. De Campos, Werner Ertel-Ingrisch, Yan Lavallée, Lisa Morgan, Donald B. Dingwell, 2012. Interactions between rhyolitic and basaltic melts unraveled by chaotic mixing experiments. *Chemical Geology, Volume 346, 2013, Page 199-212*

2. **Daniele Morgavi**, Diego Perugini, Cristina P. De Campos, Werner Ertel-Ingrisch, Donald B. Dingwell,. Time Evolution of Chemical Exchanges During Mixing of Rhyolitic and Basaltic Melts. *Contribution to Mineralogy and Petrology, 2013, Volume 166 issue 2 pp 615-638*

3. **Daniele Morgavi**, Diego Perugini, Cristina P. De Campos, Werner Ertel-Ingrisch, Donald B. Dingwell., 2013 Morphochemistry of patterns produced by mixing of rhyolitic and basaltic melts. *Journal of volcanology and Geothermal Reaserch 2013 volume 253, pages 87-93*

This Ph.D. thesis is subdivided in 5 chapters. The first 4 chapters have their own summary and conclusion. The 5th chapter there is an outlook that explains the important goals achived by this research and the potentials for future investigation.

Summary

In order to increase our understanding of magma mixing processes and their impact on the geochemical evolution of silicate melt we present in the following works, the first set of experiments performed using natural basaltic and rhyolitic melts. In particular, we investigate the interplay of physical dynamics and chemical exchanges between these two melts using time-series mixing experiments performed under controlled, chaotic, dynamical conditions. The variation of major and trace elements is studied in detail by electron microprobe (EMPA) and Laser Ablation ICP-MS (LA-ICP-MS) and the time-evolution of chemical exchanges during mixing is investigated. Using the concentration variance as a proxy to measure the rate of chemical element homogenization in time, a model to quantify chemical element mobility during chaotic mixing of natural silicate melts is proposed.

The morphology of mixing patterns at different times is quantified by measuring their fractal dimension and an empirical relationship between mixing time and morphological complexity is derived. The complexity of mixing patterns is also compared to the degree of homogenization of chemical elements during mixing and empirical relationships are established between the fractal dimension and the variation of concentration variance of chemical elements in time. Finally we discuss the petrological and volcanological implications of this work.

Enjoy

Zusammenfassung

Um unser Verständnis über die Prozesse bei der Vermischung von Magmen und dessen Auswirkungen auf die geochemische Entwicklung von Silikatschmelzen zu verbessern, werden in dieser Arbeit erstmalig eine Reihe von „Magma Mixing“ Experimenten vorgestellt, in der natürliche Basalte und Rhyolite verwendet werden.

In dynamischen Zeitreihen-Mischungsexperimenten, die unter kontrollierten, chaotischen, dynamischen, Bedingungen abliefen, wurde vor allem das Zusammenspiel der physikalischen Prozessen durch das mechanische Vermengen zweier Schmelzen und der resultierenden chemischen Austauschreaktionen durch Diffusion an den Grenzflächen zwischen diesen beiden Schmelzen untersucht.

Die Variation von Haupt- und Spurenelementen wurde mittels Elektronen-Mikrosonde (EMPA) und Laser Ablation ICP-MS (LA-ICP-MS) im Detail untersucht und zusätzlich konnte die zeitliche Entwicklung des chemischen Austauschs während des Mischungsvorgang dargestellt werden.

Die Varianz der Konzentration einzelner Elemente über die Grenzflächen zwischen Basalt und Rhyolit hinweg wurde als Proxy verwendet, um die Homogenisierungsrate der chemischen Elemente bezogen auf die Zeit zu bestimmen.

Dies wird als Modell vorgeschlagen, mit dem die Mobilität chemischer Elemente während chaotischem Mischens von natürlichen Silikatschmelzen quantifiziert werden kann.

Im Weiteren wurde mit Hilfe von Fraktalanalyse die Morphologie der Mischungsmustern zu unterschiedlichen Zeiten quantifiziert und eine empirische Beziehung zwischen Mischzeit und morphologischer Komplexität abgeleitet.

Die Komplexität der Mischungsmuster wurde zudem mit dem Grad der Homogenisierung der chemischen Elemente während des Mischens verglichen.

Dadurch konnten empirische Beziehungen zwischen der fraktalen Dimension von Mischungsmorphologien und der zeitlichen Variation der Konzentration von chemischen Elementen abgeleitet werden.

Im Laufe dieser Arbeit werden zudem die petrologischen und vulkanologischen Auswirkungen diskutiert.

Chapter 1

INTRODUCTION

1.1 Magma mixing: the idea of R.W. Bunsen

In the history of geosciences the idea of magma mixing went through a long period of strong opposition and delays in acceptance.

The first investigation on magma mixing dates back to 1851, when the chemist Robert W. Bunsen from the University of Heidelberg published a research on the chemical variation of some igneous rock samples collected in the western region of Iceland. In his study he determined the concentration of seven major oxides (SiO_2, Al_2O_3, FeO_{tot}, Cao, MgO, K_2O, Na_2O).

Figure 1 (Rober Willem Bunsen 30 March 1811– 16 August 1899)

What came out from his work was that elements seem to show linear trends in binary plots. This lead him to propose the idea that chemical variation in those rocks could be considered as a "simple" binary mixing between two distinct magmas with different initial compositions.

In order to determine the degree of magma mixing Bunsen had to face the most complex part of the magma mixing research: the determination of the end-members. Any error in this part of the work could completely compromise the final interpretation.

He chose, as end-members, the average of the chemical analysis of six rocks of the most felsic group and the average of six from the most mafic. Using those two extreme chemical

compositions he proposed a model to calculate the hypothetical hybrid given the starting proportion of the two initial end-members.

Bunsen published this data set in which, for the first time, magma mixing was taken into account for explaining the chemical variation of a suite of igneous rocks and presented his hypothesis to the geological community. His idea attracted critical response from the geological society which stressed the fact that he was proposing a major petrological theory in a discipline which was not his own. The strongest opposition against the mixing theory came from the most expert geologist at that time of the Icelandic and Etna volcano, Wolfgang Sartorius Freiherr von Waltershausen. He mostly argued against the method used by Bunsen of averaging the rock analysis in order to calculate the end-members.

Sartorius not only criticized the arbitrary choice of the end-members but also disliked the idea from Bunsen of an extensive felsic/mafic layer of magma underneath the Iceland. From 1857 to 1866 several authors (Durocher 1957 a-b; Roth 1861; Zirkel 1966) have deliberately ignored the theory of magma mixing of Bunsen and more in detail in Lehrbuch der Petrographie (Zirkel 1866), in a section on the origin of igneous rock series, assessed Bunsen's hypothesis of magma mixing concluding that Bunsen had probably pushed things too far in suggesting that all igneous rocks were to be explained as a mixture between two magmas.

In the end of the 19th century works from (Roth 1861) contributed to reject the hypothesis of magma mixing proposed by Bunsen. In particular the publication from Rosenbusch (1889) and Iddings (1892) on igneous differentiation finally posed a gravestone on the magma mixing theory.

Since the beginning of the 20th century the experimental and thermodynamic work of Bowen (e.g. Bowen, 1926) had a profound influence in petrology. Although Bowen did not explicitly deny the possibility of magma mixing, he reinterpreted field evidence of magma mixing rather as immiscibility of liquids (see Bowen, 1926).

Some 50 years passed by before geoscientists started, once more, to recognize magma mixing evidence in rocks at different length scales.

1.2 Magma mixing in the modern times

Since the first hypothesis for the origin of mixed igneous rocks (e.g. Bunsen 1851), a plenty of evidence of magma mixing processes, in all tectonic environments, throughout geological times, has been recorded (e.g. Eichelberger 1978, 1980; Blundy and Sparks 1992; Wiebe 1994 ; De Campos et al. 2004a ; Kratzmann et al. 2009 Perugini e Poli 2012).

Magma mixing in the modern petrological and volcanological community is understood as a physical process by which two batches of magma mingle, followed by a diffusion process by which the chemical elements are exchanged between magmas (e.g. Flinders and Clemens, 1996). Much effort has been spent, trying to constrain the complexities of magma mixing. Physically, magma mingling is controlled by the viscosity of each end-member melt, with the premise that mingling can primarily occur if the viscosity contrast is relatively low (e.g. Sparks and Marshall, 1986; Grasset and Albarede, 1994; Bateman, 1995; Poli et al., 1996; Perugini and Poli, 2005). Chemically, magma mixing is driven by the variable kinetics of chemical element diffusion exerted by chemical gradients of a multi-component system (e.g. Lesher, 1990; Baker, 1990) and it has been classically described through the geochemical observation of linear variations in inter-elemental plots (e.g. Fourcade and Allegre, 1981).

Magma mixing is nowadays regarded as a major process affecting compositional variability of igneous rocks in the Earth system (e.g. Anderson 1976; 1982; Hibbard, 1981). It is a fundamental phenomenon responsible for a wide range of compositions in both intrusive and extrusive igneous environments (e.g. Wiebe, 1994; De Rosa et al., 1996; Perugini and Poli, 2005; Kratzmann et al., 2009) and its occurrence has been commonly inferred as an eruption trigger (e.g. Sparks and Sigurdsson, 1977; Druitt et al., 2012; Leonard et al., 2002; Martin et al., 2008). The ubiquity of the process is observed at different scales in the rock

record, evident through variable structural and textural patterns and morphologies such as filament-like structures, enclaves, syn-magmatic dykes and mineral phases showing physico-chemical disequilibrium (e.g. Walker and Skelhorn, 1966; Didier and Barbarin, 1991; Hibbard, 1995; Flinders and Clemens, 1996; Perugini et al., 2002; Perugini et al., 2003). Some of the most striking evidence of magma mixing in igneous rocks is the occurrence of textural heterogeneity, and the processes responsible have been discussed extensively (e.g. Eichelberger, 1975; Anderson, 1976; Bacon, 1986; Snyder, 2000; Perugini and Poli, 2005; Perugini and Poli, 2012). This heterogeneity includes enclaves, banding, and "streaky" structures (e.g. Didier and Barbarin, 1991; Wada, 1995; De Rosa et al., 1996; Ventura, 1998; Smith; 2000; De Rosa et al., 2002; Perugini and Poli, 2002; Perugini et al., 2007). The development of these structures is modulated by the dynamics of physico-chemical processes arising during mixing (e.g. Flinders and Clemens, 1996; Perugini et al., 2003). An understanding of the details of magma mixing, therefore, is of primary importance for petrology and volcanology, with direct implications for the interpretation of the compositional variability of igneous rocks as well as in hazard assessment in active volcanic areas.

1.3 Numerical and experimental study: new ideas for understanding magma mixing

Studies focused on numerical and experimental investigation of mixing dynamics (e.g. Perugini et al. 2003; Perugini et al. 2008; De Campos et al., 2004; 2008, 2011; Petrelli et al. 2011) have highlighted a great complexity of this process, whose evolution is governed by a continuous interplay between physical dispersion of melts and chemical exchanges. One of the most striking results arising from these studies is that, during mixing, chemical elements experience a diffusive fractionation process due to the development in time of chaotic mixing dynamics (Perugini et al. 2006, 2008). This process is considered the source of the strong deviations of many chemical elements from the linear variations in inter-elemental plots that would otherwise be expected based on a conceptual model classically adopted in the geochemical modeling of magma mixing processes (e.g. Fourcade and Allegre 1981). The

false assumption of evidence for a linear trend poses problems in the study of rocks generated by magma mixing because it may lead to an erroneous interpretation and reconstruction of the mixing end-members with important consequences on the reconstruction of the geochemical features of source regions and associated geological and geodynamic interpretations. Current efforts rather attempt to constrain the intricacies of the physico-chemical nature of magma mixing through chaotic mixing dynamics for which mathematical solutions exist and describe the physical interaction of the mixing end-members (e.g. Perugini et al., 2006, 2008).

1.4 Chaotic Mixing Experiments

To shed new light on the complexity of magma mixing processes, a new experimental apparatus has been developed which is able to perform experiments using high viscosity silicate melts at high temperature (De Campos et al. 2011; Perugini et al. 2012 Morgavi et al. 2012a, 2012b). This device has been used to study the mixing process between "low-complexity" synthetic silicate melts composed of a few chemical elements enabling the study of the modulation of chaotic dynamics on the geochemical evolution of the mixing system.

Recent studies on the mineralogical and geochemical features of mixed rocks (e.g. Hibbard et al., 1981; 1995; Wallace and Bergantz, 2002; Costa and Chakraborty, 2004; Perugini et al., 2005; Slaby et al., 2010; 2011), as well as those focused on quantitative analyses of morphologies related to textural heterogeneity (e.g. Wada, 1995; De Rosa et al., 2002; Perugini and Poli, 2002; Perugini et al., 2002; 2004) have highlighted the dominant role played by chaotic mixing dynamics in producing the substantial complexity of geochemical variations and textural patterns found in the resultant rocks (e.g. Flinders and Clemens, 1996; De Campos et al., 2011; Morgavi et al., 2012; Perugini et al., 2012). Despite significant attention in the past, however, few works have focused on the understanding of the relationship between the morphology of the mixing patterns and the geochemical variability of the system (e.g. De Rosa et al., 2002; Perugini et al., 2004). There is a paucity of data concerning the link between the complexity of mixing patterns and the compositional

heterogeneity triggered by the mutual dispersion of melts with different initial compositions. Yet this aspect appears particularly relevant in the light of recent results obtained from natural samples, numerical simulations and experiments that indicate a key role being played by chaotic mixing processes in generating scale-invariant mixing patterns (i.e. fractals) propagating from the meter to the micrometer length scale in the magmatic mass (e.g. Perugini et al., 2003; Perugini et al., 2008; De Campos et al., 2008, 2011; Petrelli et al., 2011; Morgavi et al., 2012). The generation of such structures implies the development of large contact interfaces between interacting melts through which chemical exchanges are strongly amplified leading to highly variable degrees of homogenization depending on the different mobility of chemical elements (e.g. Perugini et al., 2006; 2008; De Campos et al., 2004; 2008; 2011; Perugini et al., 2012; Perugini and Poli, 2012; Morgavi et al., 2012). In addition, preliminary results indicate that the study of the time evolution of compositional exchanges between magmas can be effectively modeled, leading to the prospect that the record of magma mixing processes may serve as chronometers to estimate the time interval between mixing and eruption (Perugini et al., 2010).

Chapter 2

INTERACTION BETWEEN RHYOLITIC AND BASALTIC MELTS UNRAVELED BY CHAOTIC MIXING EXPERIMENTS

Summary

Magma mixing may operate at any stage in the evolution of a magmatic system. The development of mixing is strongly controlled by fluid dynamics and its understanding requires a comprehensive physico-chemical approach in order to identify and interpret its occurrence in nature. Here, we experimentally study the physical and chemical interplays during the mixing of basaltic and rhyolitic natural melts from the Snake River Plains, USA. In particular, we present the results of the first high-temperature mixing experiments performed under controlled chaotic dynamic conditions, providing a new methodological approach to constrain the complexities of the mixing process between natural, silicate melts.

The mixing process is initially governed by the dynamics of stretching and folding of the melts, producing alternating flow bands. These bands increase the contact area between the end-members, which subsequently enhance chemical exchanges and thus contribute to the generation of regions with variable degrees of hybridization. We quantified the mobility of major and trace elements across contact areas, and analyzed the concentration variance decay induced by chemical diffusion. The analysis shows that elements diffuse with different efficiencies as the chemical gradient evolves and therefore, the achievement of hybrid compositions contrasts between elements. The approach introduced in this study can, in principle, be applied to mixing trends observed in nature in order to estimate the time-scales and degree of magma mixing evidenced across volcanic rocks/deposits.

2.1. Introduction

Magma mixing is regarded as a major process affecting compositional variability of igneous rocks in the Earth system (e.g. Anderson 1976; 1982; Hibbard, 1981). It is a fundamental phenomenon responsible for a wide range of compositions in both intrusive and extrusive igneous environments (e.g. Wiebe, 1994; De Rosa et al., 1996; Perugini and Poli, 2005; Kratzmann et al., 2009) and its occurrence has been commonly inferred as an eruption trigger (e.g. Sparks and Sigurdsson, 1977; Druitt et al., 2012; Leonard et al., 2002; Martin et al., 2008). The ubiquity of the process is observed at different scales in the rock record, evident through variable structural and textural patterns and morphologies such as filament-like structures, enclaves, syn-magmatic dykes and mineral phases showing physico-chemical disequilibrium (e.g. Walker and Skelhorn, 1966; Didier and Barbarin, 1991; Hibbard, 1995; Flinders and Clemens, 1996; Perugini et al., 2002; Perugini et al., 2003). The development of these structures is modulated by the dynamics of physico-chemical processes arising during mixing (e.g. Flinders and Clemens, 1996; Perugini et al., 2003).

Magma mixing is generally understood as a physical process by which two batches of magma mingle, followed by a diffusion process by which the chemical elements are exchanged between magmas (e.g. Flinders and Clemens, 1996). Much effort has been spent, trying to constrain the complexities of magma mixing. Physically, magma mingling is controlled by the viscosity of each end-member melt with the premise that mingling can primarily occur if the viscosity contrast is relatively low (e.g. Sparks and Marshall, 1986; Grasset and Albarede, 1994; Bateman, 1995; Poli et al., 1996; Perugini and Poli, 2005). Chemically, magma mixing is driven by the variable kinetics of chemical element diffusion exerted by chemical gradients of a multi-component system (e.g. Lesher, 1990; Baker, 1990) and it has been classically described through the geochemical observation of linear variations in inter-elemental plots (e.g. Fourcade and Allegre, 1981). In recent years, numerical and experimental studies of mixing dynamics have offered a new level of complexity of the physico-chemical process that represent magma mixing (e.g. Poli and Perugini, 2002;

Perugini et al., 2003; Perugini et al., 2008; De Campos et al., 2008, 2011; Petrelli et al., 2011). In particular, it has been suggested that the combined action of physical mixing and chemical diffusion during chaotic mixing induces the diffusive fractionation of chemical elements (Perugini et al., 2006, 2008). Such characteristics of elements to fractionate as well as to homogenize may thus be responsible for the deviation of the expected linear chemical variation in inter-elemental plots (Perugini et al., 2006, 2008), therefore thwarting our ability to describe magma mixing through such a simple geochemical model (e.g. Fourcade and Allegre, 1981). Current efforts rather attempt to constrain the intricacies of the physico-chemical nature of magma mixing through chaotic mixing dynamics for which mathematical solutions exist and describe the physical interaction of the mixing end-members (e.g. Perugini et al., 2006, 2008).

Here, we present the very first findings of a study on the physical and chemical interplays between natural basaltic and rhyolitic melts in controlled chaotic dynamic conditions. Geochemical analysis of major and trace elements across mixing structures are used to provide a new scheme to interpret observed modulations of chemical elements during the mixing of magmas.

2.2 End-members and experimental setup

2.2.1 End-member selection and preparation

Experiments were performed using natural samples from the Bruneau Jarbidge eruptive center in the Snake River Plain (USA). In particular, the Mary's Creek basalt and the Cougar Point Tuff (CPT) rhyolite (unit V) were selected as end-members. Further details about petrographic features and geochemical composition of these rocks can be found in Bonnichsen (1982) and Cathey and Nash (2009).

Rock powder from each end-member was melted and homogenized using a concentric cylinder viscometer (Dingwell, 1986). The melts were held at 1600 °C inside a $Pt_{80}Rh_{20}$ crucible (5.0 cm long, 2.5 cm inner diameter, 0.1 cm wall thickness) and stirred with a

$Pt_{80}Rh_{20}$ spindle for 48 and 6 hours for the rhyolite and the basalt, respectively. This procedure yields chemically homogeneous, bubble- and crystal-free melts, which after quenching to glasses, were prepared and used in the chaotic mixing experiments (Table 1).

	Basalt	Rhyolite
SiO_2	48.44	78.64
Al_2O_3	16.30	9.75
TiO_2	1.77	0.23
FeO_{tot}	12.20	1.83
MgO	7.47	0.12
CaO	11.54	0.82
MnO	0.28	bdl
Na_2O	1.95	3.45
K_2O	0.31	4.50
P_2O_5	0.43	bdl
Rb	4	195
Sr	220	50
Y	18	47
Zr	112	360
Nb	10	45
Ba	190	790
La	13	88
Ce	27	175
Pr	3.6	16.0
Nd	14	58
Sm	3.3	12.0
Eu	2.0	0.5
Gd	1.3	10.0
Dy	1.7	8.5
Yb	1.5	6.0
Th	0.9	33.0
U	0.2	7.5
η (log Pas) @ 1350°C	0.86	4.75
η (log Pas) @ 1400°C	0.66	4.43
ρ (g/cm^3) @ 1350°C	2.98	2.33
ρ (g/cm^3) @ 1400°C	2.96	2.33

Table 1: Concentrations of major and trace elements in the basaltic and rhyolitic end-member glasses used in the mixing experiments. Concentration for major elements are given in weight percentage. Trace elements values are in ppm. For analytical conditions see section 2.3. Values of density (ρ) and viscosity (η) of the two end-members are also reported.

2.2.2 Chaotic mixing experiments

Magma mixing was induced using a chaotic mixing setup installed at the Department for Earth and Environment at the University of Munich (LMU, Germany). The setup employs the "Journal Bearing Flow" configuration used by Swanson & Ottino (1990) to investigate the

chaotic mixing of low-viscosity fluids at room temperature. This method has recently been adapted by De Campos et al. (2011) to perform mixing experiments on synthetic silicate melts at high temperatures. The experiments presented here differ significantly from the one shown by De Campos et al. (2011) in that, here, i) we study natural melt compositions, ii) we investigate the compositional variation of both major and trace elements and iii) we derive a new approach to quantify the mobility of major and trace elements during mixing. A comparison between results from this work, using natural melts, and those from De Campos et al. (2011), using synthetic melts, is presented in Section 5. The experimental apparatus consists of an outer Pt_{80}-Rh_{20} cylinder and an inner Al_2O_3 cylinder, the latter of which is off-centered with respect to the former (Fig. 1).

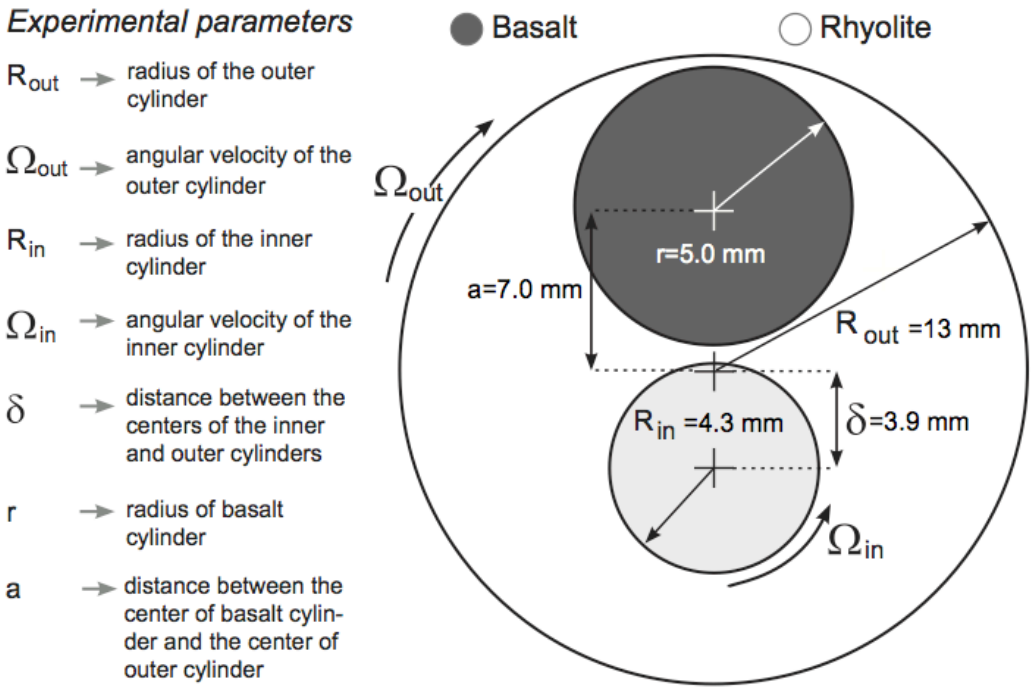

***Figure 1**: Schematic 2D section of the experimental apparatus used to perform chaotic mixing experiments. In the figure experimental parameters are also reported. Their values are as follows: R_{out}=13 mm, Ω_{out}=0.06 rpm, R_{in}=4.3 mm, Ω_{in}=0.3 rpm, δ=3.9, r=5.0 mm. Further details about the experimental setup can be found in De Campos et al. (2011).*

The outer cylinder hosts the end-member melts. The inner Al_2O_3 cylinder is sheathed by a Pt_{80}-Rh_{20} alloy foil to prevent contamination of the melt from the Al_2O_3 at high-temperature. The motions of the two cylinders are independent and their rotations at given angular velocities (Ω) induce mixing with variable degree of "chaoticity" (Fig. 1; De Campos

et al., 2011). The geometry of the system is defined by two parameters: the ratio of the radii of the two cylinders, $r=R_{in}/R_{out}=1/3$, and the eccentricity ratio to the outer cylinder $\varepsilon=\delta/R_{out}=0.3$, where δ is the distance between the centers of the inner and outer cylinders (R_{in} and R_{out}; Fig. 1). The outer cylinder was filled with the rhyolitic end-member and cooled down to room temperature to produce a glass. From this glass two cylinders were drilled out yielding two cavities: i) one cavity at the position of the inner cylinder and ii) a second cavity to insert the basaltic end-member (Fig. 1). These cylindrical cavities were produced by high-precision coring; the basalt cylinder was carefully polished to ensure a tight fit into the rhyolitic glass.

This study investigates the interaction between 80% of rhyolitic melt and 20% of basaltic melt. The experiments were performed at 1350 °C and 1400 °C with identical starting conditions, experimental protocol, and duration (i.e. 108 min; Fig. 1). The viscosity and density under experimental conditions are reported in Table 1. The viscosity ratios during the experiments were $7.8\text{x}10^3$ and $5.9\text{x}10^3$ at 1350 °C and 1400 °C, respectively. This small difference in viscosity ratios owes to the slightly different temperature-dependence of viscosity of each melt. Although the viscosity ratio is regarded as the most important parameter controlling mixing processes (e.g. Sparks and Marshall, 1986; Grasset and Albarede, 1994; Bateman, 1995; Poli et al., 1996; Perugini and Poli, 2005), the small contrast between the two temperature makes the experiments comparable, and, as discussed below, they are used here to investigate the effect of different mixing patterns on chemical exchanges.

The sample assembly was heated to experimental conditions in two phases: first, it was heated to 900 °C in 21 minutes, then it was rapidly heated to 1350 or 1400 °C in approximately 5 minutes to minimize the potential occurrence of chemical exchange before the onset of the experiment. The experimental protocol (i.e. relative number of rotation of the two cylinders) has been determined following Muzzio et al. (1992) to ensure the occurrence of chaotic dynamics. The method consists of alternating rotations of the outer and inner cylinders in the following sequence: (1) two complete rotations of the outer cylinder in 36

min; (2) six complete rotations of the inner cylinder in 18 min. These two steps were repeated once. Such experimental protocol, in conjunction with the tested viscosities, provided flow conditions with Reynolds' numbers on the order of 10^{-7} (see De Campos et al., 2011 for further detail of the experimental setup and protocol). After completion of each experiment, the furnace was switched off, allowing quenching of the experimental product at a mean rate of ca. 40 °C/min. Once at room temperature, the crucible was removed from the furnace, while leaving the inner cylinder inside the quenched-in glass product. Each experimental product was recovered by coring out a cylindrical sample with a radius of 11.0 mm. Each core was then cut into ten 4-mm thick slices perpendicular to the core's long axis and thin sections were prepared for further analyses. Two representative slices containing different mixing patterns were selected in order to perform geochemical analyses (Fig. 2).

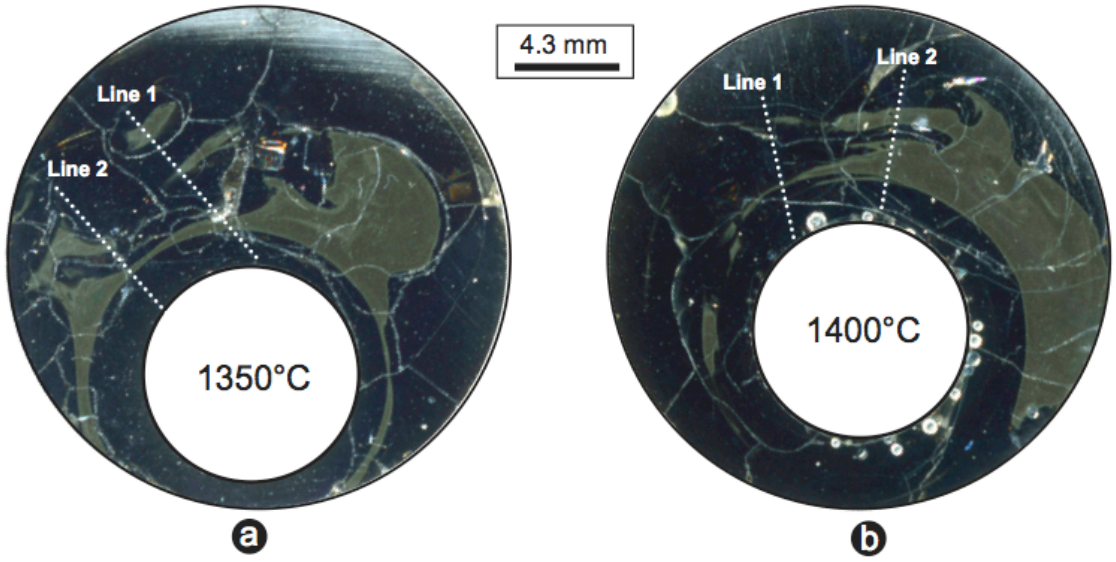

Figure 2: Optical images of two sections of experimental samples for 1350°C (a) and 1400°C (b) acquired with a flatbed optical scanner. The path of analyzed transects is indicated by dashed lines in each picture.

2.2.3 Analytical methods

The concentrations of major elements were measured with a Cameca SX100 electron micro probe analyzer (EMPA) available in the Department of Earth and Environment at the University of Munich. The chemical analyses were carried out at 15 kV acceleration voltage and 20 nA beam current. A defocused 10-µm beam was used for all elements in order to minimize alkali loss. Synthetic wollastonite (Ca, Si), periclase (Mg), hematite (Fe), corundum (Al), natural orthoclase (K), and albite (Na) were used as standards, and matrix correction was performed by PAP procedure (Pouchou and Pichoir, 1984). The precision was better than 2.5% for all analyzed elements. This standard set up was used for all analyses. Accuracy was tested by analyzing the set of standard glasses known as MPI-DING (e.g. Jochum et al., 2000) and is better than 3.0% for the analyzed elements.

Trace elements were measured by Laser Ablation Inductively Coupled Plasma Mass Spectrometer (LA-ICP-MS) microanalysis (Department of Earth Sciences, University of Perugia; see Petrelli et al., 2007 for details of the technique). The analyzed spot size had a diameter of 40 µm and spacing between consecutive points was kept at 60 µm. Here, particular attention was drawn to the following trace elements: Rb, Sr, Y, Zr, Nb, Ba, La, Ce, Pr, Nd, Sm, Eu, Gd, Dy, Yb, Th, and U. Ca was used as internal standard for the analysis. The analytical precision was better than 10% for all of these elements (Petrelli et al., 2008).

In order to adequately map the relationship between major and trace elements for each experiment, a series of 100-spot analysis was conducted along four transects (Fig. 2 and 3). During EMPA measurements, back-scattered electron images were also taken to permit structural analysis (Fig. 3).

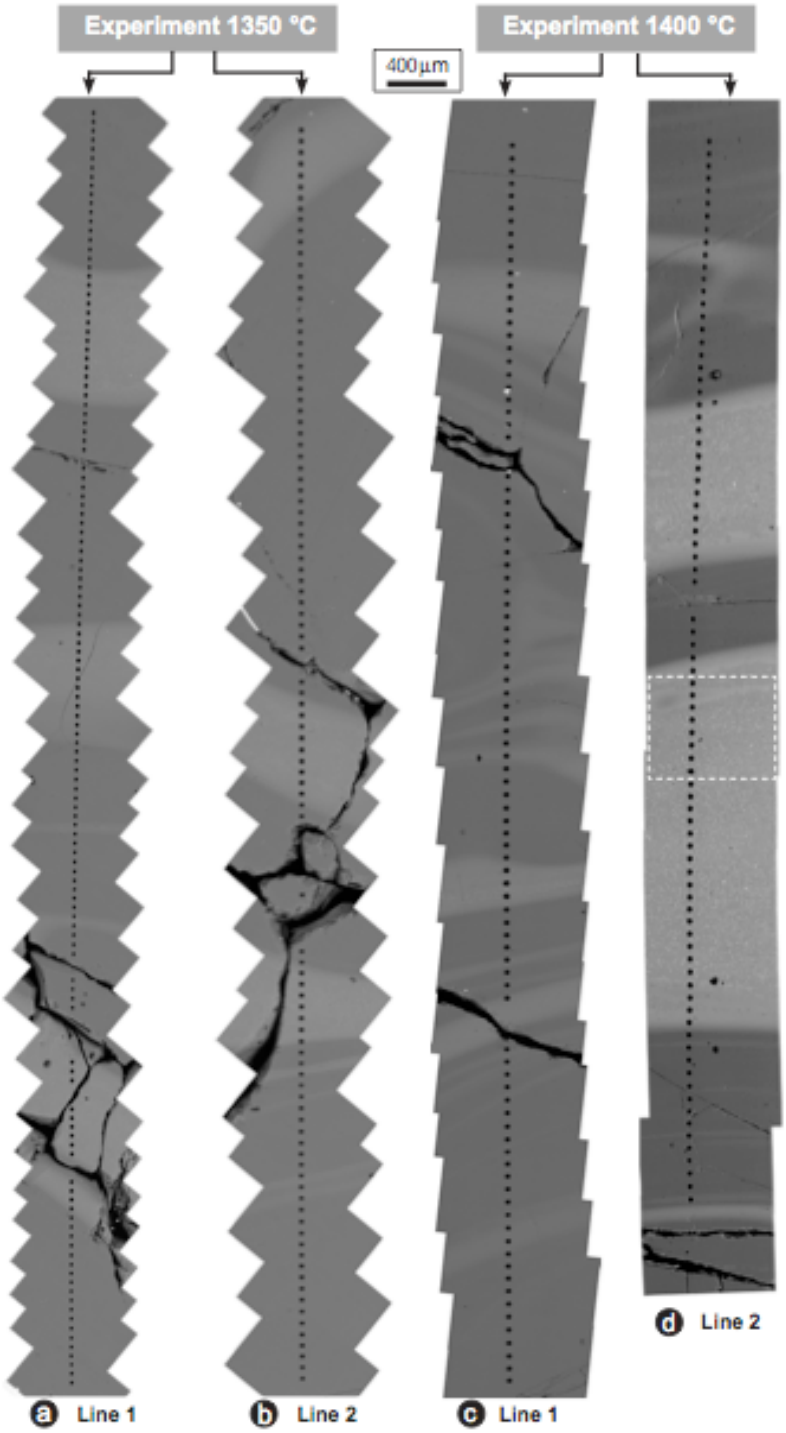

Figure 3: Back-Scattered Electron (BSE) images along the transects in which the analysis of major and trace elements have been performed. a-b) 1350° C experiment; c-d) 1400°C experiment. The black dots in the images are the craters left by the laser used for trace element analysis. The dashed square in (d) highlights portion of a filament of the most mafic melt in which oxide skeletal micro-crystals were observed. This portion is enlarged in Fig. 4.

2.3 Results

2.3.1 Optical analysis

Observations of the experimental products reveal that the basaltic liquid was dispersed within the rhyolitic liquid due to the dynamics of stretching and folding generated by the experimental protocol (Fig. 2). Back-scattered electron image analysis help visualize the chemical boundary patterns developed during mixing (Fig. 3). From these images it is clear that the basaltic liquid (light grey color) has been stretched and folded generating an intricate pattern of filaments in the rhyolitic liquid (dark grey color). The thickness of filaments is variable in different sections of the samples, as should be expected from chaotic mixing dynamics. For the product of the experiment at 1350 °C we selected two transects which contained 5-6 filaments with thicknesses ranging from 80 to 450 μm (Fig. 3a and b). For the product of the experiment at 1400 °C, we selected two transects containing 15 and 4 filaments with thicknesses ranging from 80 to 300 μm (Fig. 3c) and 80 to 1600 μm (Fig. 3d), respectively. These four different transects were chosen for further geochemical analysis.

Microscopic examination of the experimental products in back-scattered electron imaging mode reveals that the quenched-in filaments are glassy, and thus preserved original information to quantify the diffusion of elements, except for a few thicker filaments (>400 μm) of less evolved composition (i.e., towards the basaltic end-member) in which skeletal microlites (1.0-3.0 microns in thickness) are observed (Fig. 4).

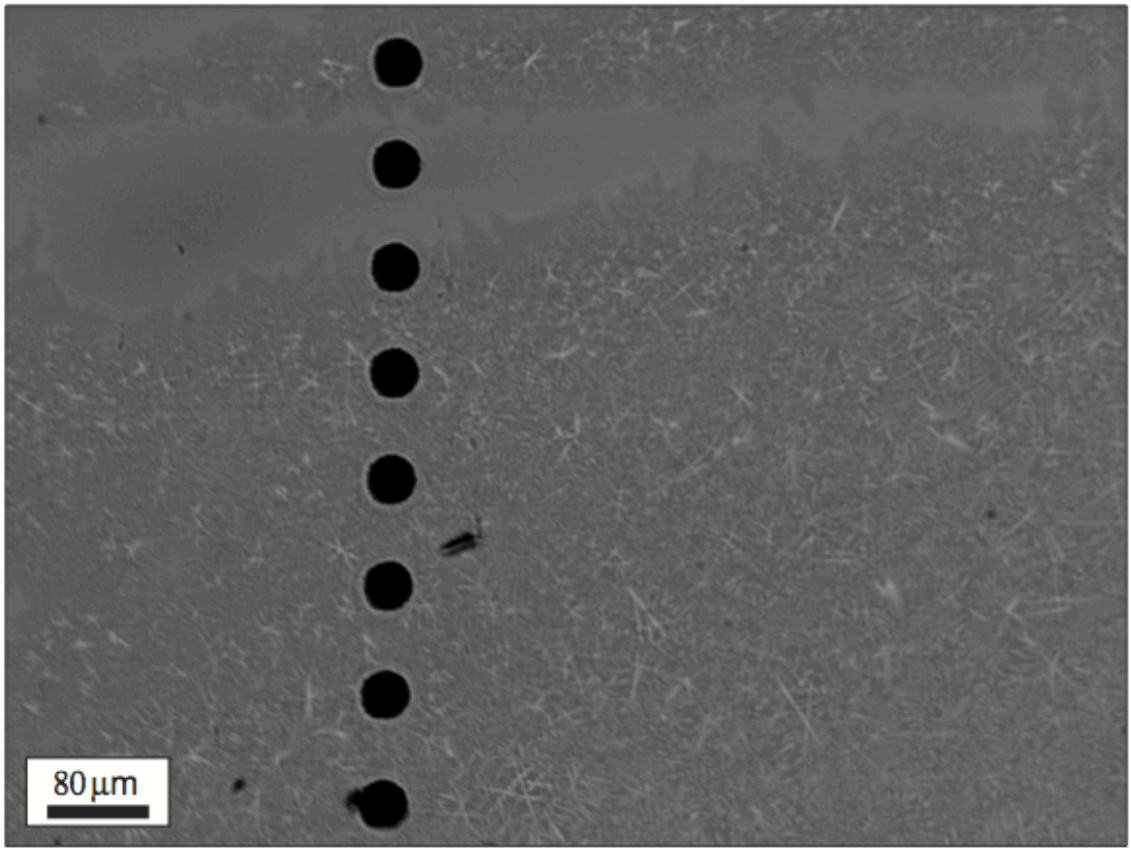

Figure 4: Enlargement of the section marked by the dashed square in Fig. 3d showing the occurrence of oxide skeletal micro-crystals in a filament constituted by the most mafic melt. That black dots in the image are the craters left by the laser used for trace element analysis.

Considering the super-liquidus temperature conditions of the experiments, we assert the presence of these microlites to a small degree of crystallization occurring during quenching, after completion of the experiments. Note that the size of these crystals is too small to be analyzed with an electron micro probe analyzer; yet, the color of the microlites (which scales with density) suggest that they are most likely iron oxides, which would explain the minor scattering in FeO_{tot} in this region (see below). Regarding the compositional variations in major and trace elements, the use of a spot size (20 µm for EMPA and 40 µm for LA-ICP-MS) far exceeding the sizes of the skeletal microlites results in the approximation of bulk compositional values. In these estimates, only FeO_{tot} appears to suffer from minor scattering, which supports our view that the microlites are likely iron oxides. Therefore, in the following sections Fe will not be taken into account. Yet, the geochemical analyses presented for the

other elements are considered to be representative of the compositional variation induced by the process of mixing of the basaltic and rhyolitic melts.

2.3.2 Geochemical variations

The variability of major and trace elements along the analyzed transects is displayed in Figure 5-6, respectively. For each element profile, the original concentrations in each end-member are displayed by two grey lines as a reference. In general, element variability exhibits an oscillatory pattern with compositional "hills and valleys" corresponding to the presence of filaments of the two melts. The steepness of compositional gradients between filaments depends on the thickness of the filaments: the larger the filament thickness, the sharper the compositional variation (compare, as an example, the variability of MgO in Figure 5l and p). In the thinner filaments, the element concentrations increase (or decrease) more progressively, forming bell-shape patterns across filaments (e.g. Fig. 5a, d and l). This is a reflection of the fact that, in addition to the physical stretching and folding mechanism at the onset of mixing, significant chemical diffusion also occurred.

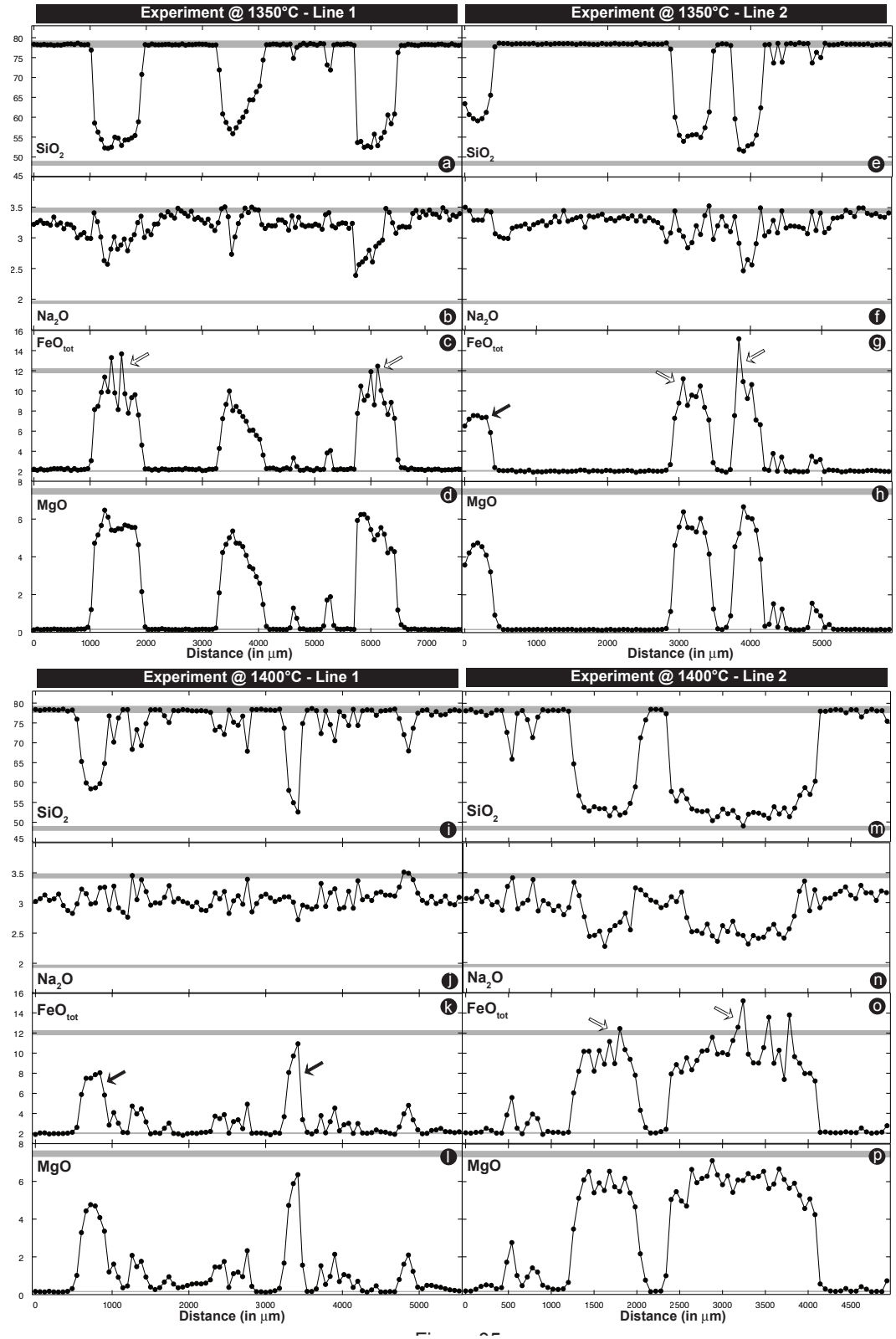

Figure 5: Variation of representative major elements across the analyzed transects (Fig. 3). Concentrations of initial basaltic and rhyolitic melts are marked in different grey shades. These are reported as a range (grey areas) to include analytical uncertainties. White arrows in the FeO_{tot} plot indicate filaments of the most mafic melt in which micro-crystals have been observed. Black arrows indicate the largest filaments of the most mafic melt in which micro-crystals have not been observed.

For the experiment conducted at 1350 °C, the relative magnitude of compositional variations in Line 1 and Line 2 appear comparable for both major and trace elements (Fig. 5 and 6). For the experiment conducted at 1400 °C, however, the mixing pattern appears to strongly influence chemical exchanges between the two melts. In particular, the transect crossing the series of multiple small-size filaments (e.g. Line 1 on Fig. 3c) shows that the compositional contrast between the two end-members is strongly reduced (Fig. 5i-l and Fig. 6i-l). In contrast, the transect crossing the large-size filaments (e.g. Line 2 on Fig. 3d) does not show the same compositional contraction after the same mixing time (Fig. 5m-p and Fig. 6m-p).

The concentration of FeO_{tot} tends to fluctuate in the large filaments containing microlites (indicated by white arrows in Fig. 5c,g and o). Note that FeO_{tot} is the only elements for which strong fluctuations are measured in the microlite-bearing filaments. Noteworthy is the fact that in microlite-free filaments (black arrows in Fig. 5g and k) the concentration of Fe does not exhibit any anomalous fluctuation compared to the other elements.

The extent of contraction of compositional variability significantly contrasts between the different elements; that is, their degree of homogenization vary as evidenced by the preservation or disappearance of heterogeneous filaments. Na_2O and K_2O (not shown) are always more homogenized than the other major elements (e.g. SiO_2 or MgO). Similar observations can be made for trace elements. For example, while some elements (e.g. Sr; Fig. 6) show large compositional differences whose extreme values fall in the fields of the initial end-members, others (e.g. Rb or Dy; Fig. 6) show a strong contraction of their compositional variability towards a hybrid concentration.

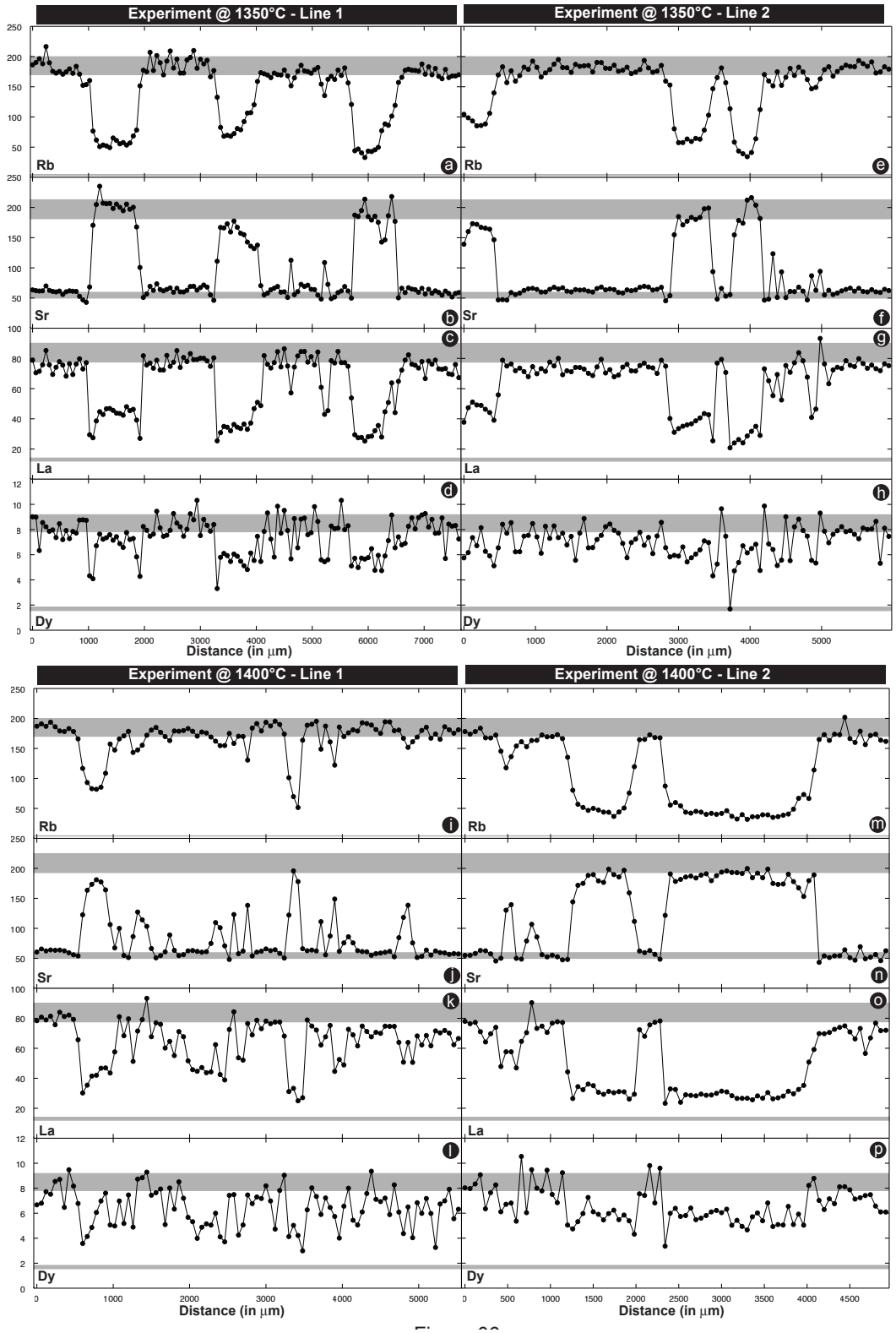

Figure 6: Variation of representative trace elements across the analyzed transects (Fig. 3). Concentrations of initial basaltic and rhyolitic melts are marked in different grey shades. These are reported as a range (grey areas) to include analytical uncertainties.

However, as for the major elements, the trace element compositional variation is modulated by the geometry of the mixing patterns.

Binary inter-elemental plots of some representative major and trace elements are displayed in Figures 7, 8 and 9.

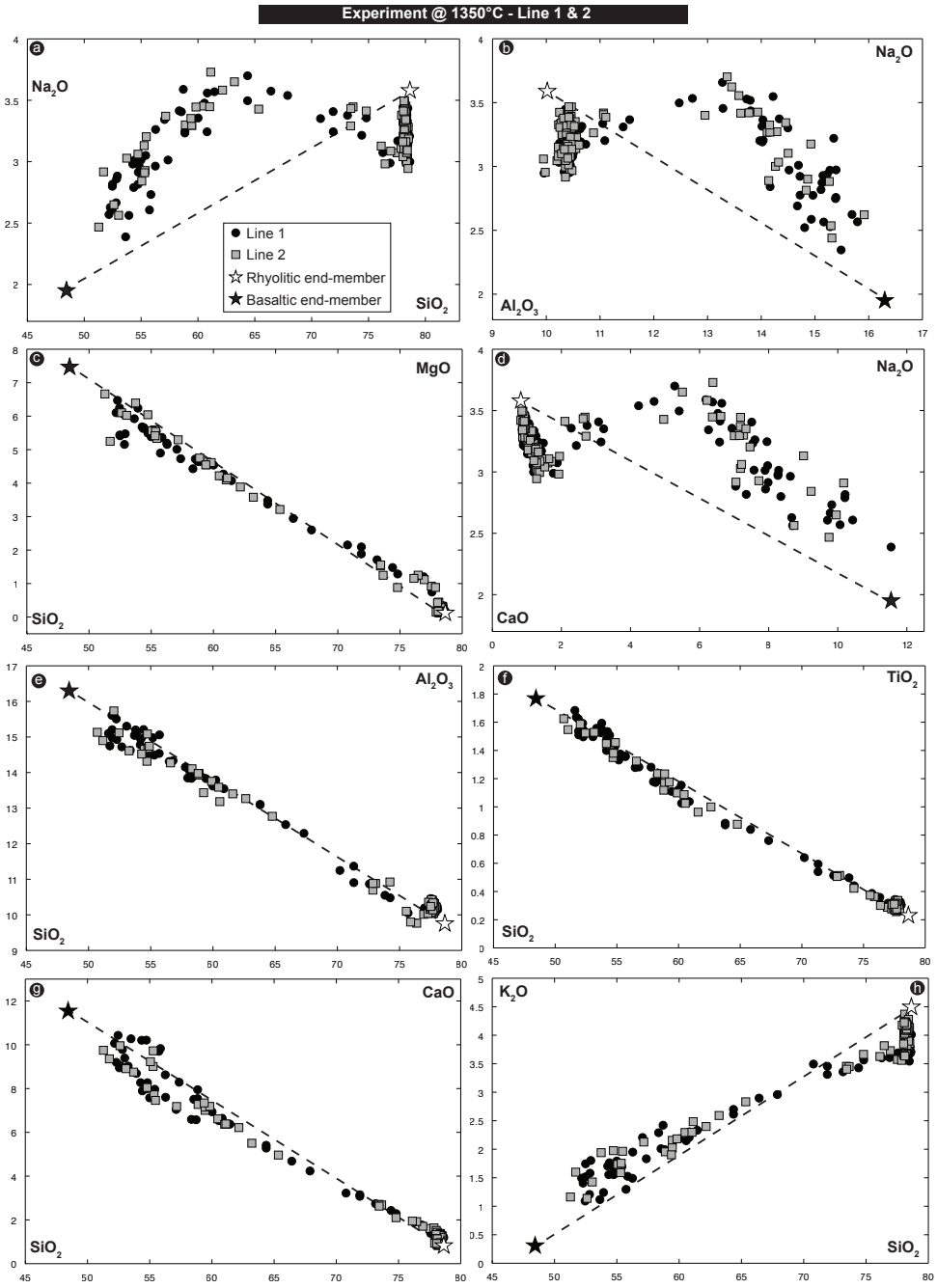

Figure 7: Representative binary plots showing the variable correlation between pairs of major elements for the transects analyzed on the 1350°C experiment. The mixing line connecting the two end-members is also reported. Initial mafic and felsic end-member compositions are reported as black and white star, respectively.

In particular, Figures 7 and 8 show the variation of major elements for the 1350 °C and 1400 °C experiment; the upper and lower panels of Figure 9 report trace element data from the 1350 °C and 1400 °C experiment, respectively. In these plots major elements tend to define linear patterns (e.g. SiO_2 vs. MgO, CaO vs. MgO). The main exceptions are Na_2O and K_2O that are not linearly correlated with any major element (Fig. 7 and 8).

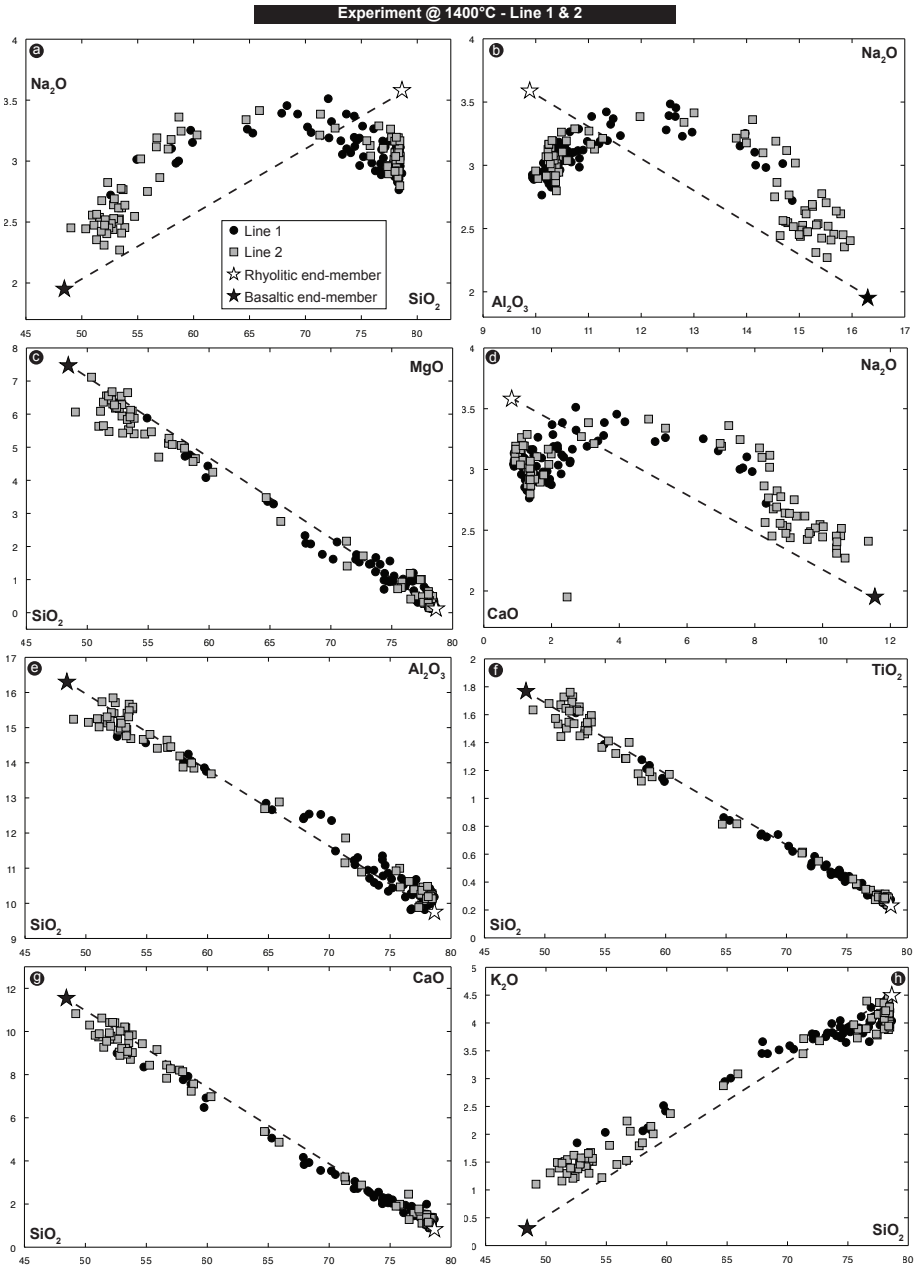

Figure 8: Representative binary plots showing the variable correlation between pairs of major elements for the transects analyzed on the 1400°C experiment. The mixing line connecting the two end-members is also reported. Initial mafic and felsic end-member compositions are reported as black and white star, respectively.

Instead, these elements define curved patterns of data points passing from the basaltic to the rhyolitic end-member. The curved pattern is more evident for Na_2O than for K_2O. Regarding trace elements, patterns in binary plots appear to be more complex. Some pairs of elements display linear relationships (e.g. La vs. Pr; Fig. 9a and g), whereas others define irregular trends with a variable degree of scattering around the simple mixing line (e.g. La vs. Rb or Ba vs. Nb; Figs. 9d and f - j and l).

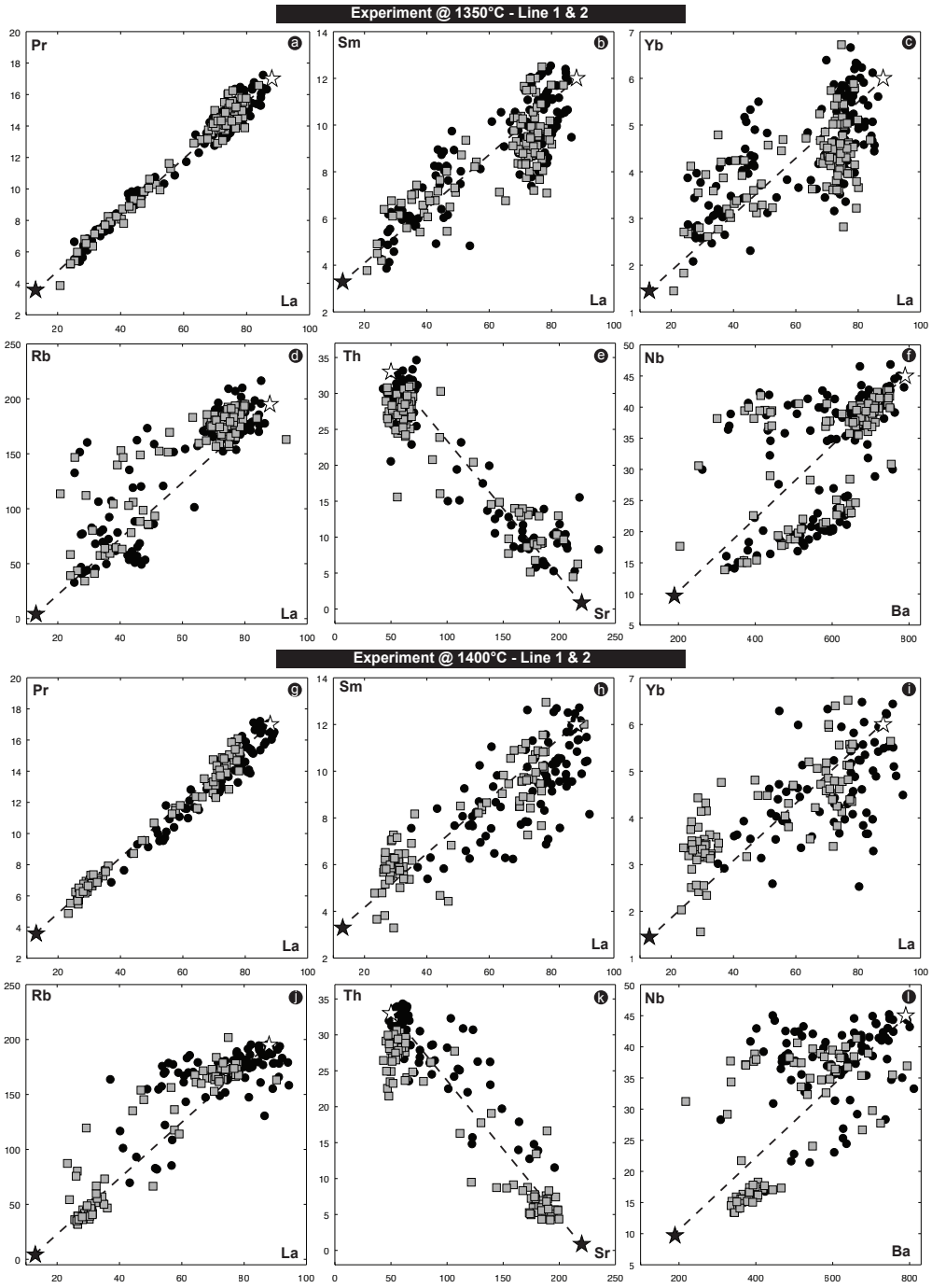

Figure 9: Representative binary plots showing the variable correlation between pairs of trace elements for the analyzed transects. The mixing line connecting the two end-members is also reported. Initial mafic and felsic end-member compositions are reported as black and white star, respectively. Concentrations are given in ppm.

These qualitative observations suggest that the mobility of the different chemical elements during the experiments was different. However, a more rigorous analysis is necessary in the attempt to quantify this process.

2.4. Concentration variance analysis

An adequate quantification of the variable mobility of chemical elements during mixing in a multi-component magma system should account for all influencing factors (e.g. the compositional and rheological dependence, the melt structure, etc.). In the fluid dynamics literature, the concentration variance is commonly used as a measure to evaluate the degree of homogenization and, hence, to quantify the mobility of components during fluid mixing (e.g. Rothstein et al., 1999; Liu and Haller, 2004). The variance of concentration for a given chemical element (C_i) is given by

$$\sigma^2(C_i) = \frac{\sum_{j=1}^{N}(C_j - \gamma_j)^2}{N} \qquad \text{[Eq. 1]}$$

where N is the number of samples, C_i is the concentration of element i and μ is the mean composition. Through time, such a value is destined to decrease, as the system progresses towards homogeneity. Variance defined by Eq. [1] depends on absolute values of chemical element concentrations. Given the wide range of concentrations for the different elements (i.e., from a few ppm to tens of percent) the variance values need to be normalized to the initial variance for comparative purposes. Therefore, in the following we refer to concentration variance (σ_n^2), or simply variance, as

$$\sigma_n^2 = \frac{\sigma^2(C_i)_t}{\sigma^2(C_i)_{t=0}} \qquad \text{[Eq. 2]}$$

where $\sigma^2(C_i)_t$ and $\sigma^2(C_i)_{t=0}$ are the concentration variance of a given chemical element (C_i) at time t (e.g. 108 minutes for our experiments) and time t=0 (i.e., the initial variance before mixing), respectively. The initial variance $\sigma^2(C_i)_{t=0}$ was calculated using the two end-member compositions reported in Table 1. This measure quantifies the degree of homogeneity of a chemical element in the mixing system. In detail, the concentration variance σ_n^2 varies between unity at t=0 (i.e., the time at which the system is most heterogeneous) and zero at t=∞ (i.e. the time at which the system is completely homogeneous).

Concentration variance σ_n^2 was calculated for major and trace elements in the two experiments and results are displayed in Figures 10 and 11.

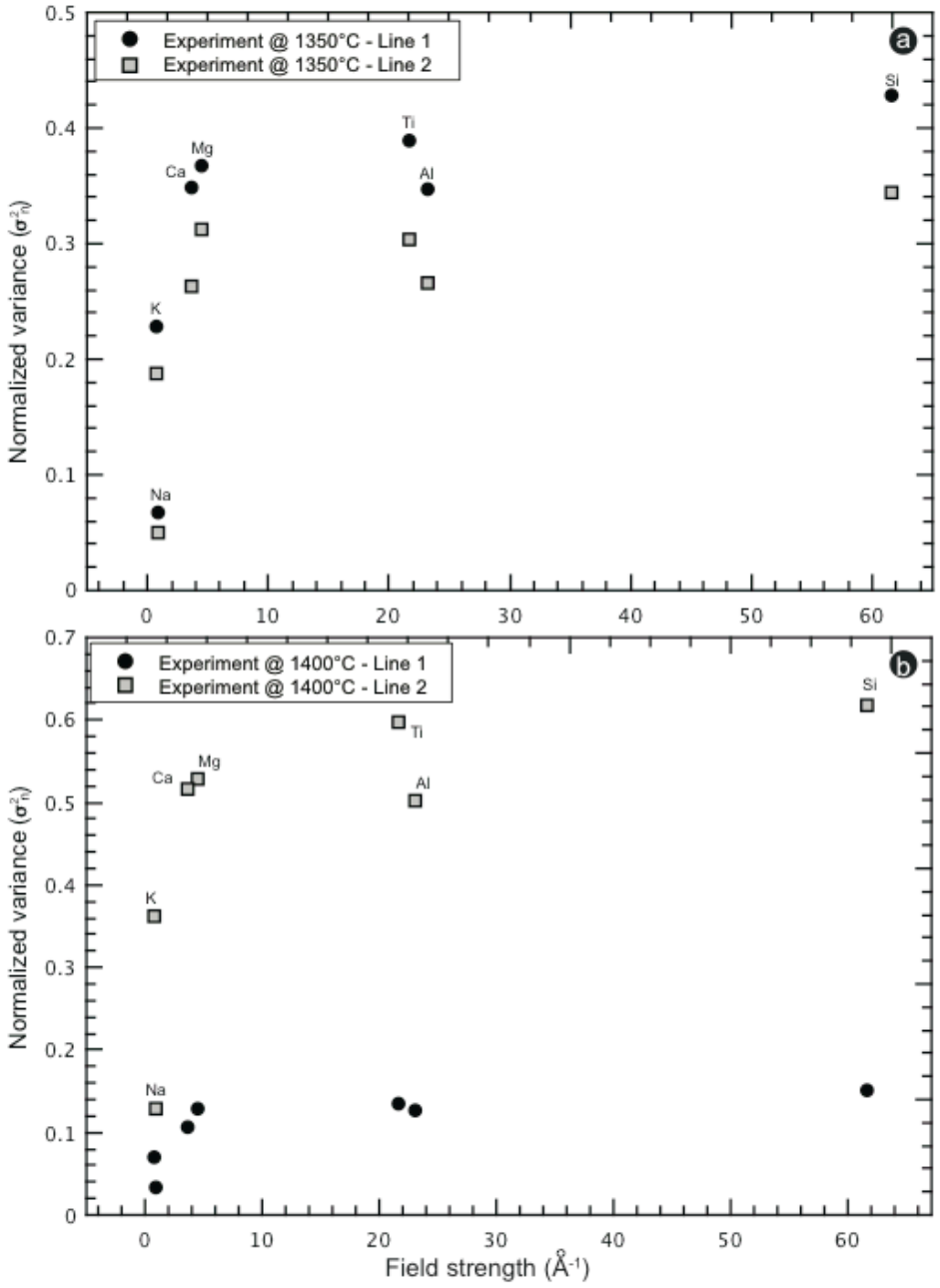

Figure 10: Variation of concentration variance σ_n^2 against field strength (Z^2/r; Z = ionic change, r = ionic radius) for major elements in the studied compositional transects.

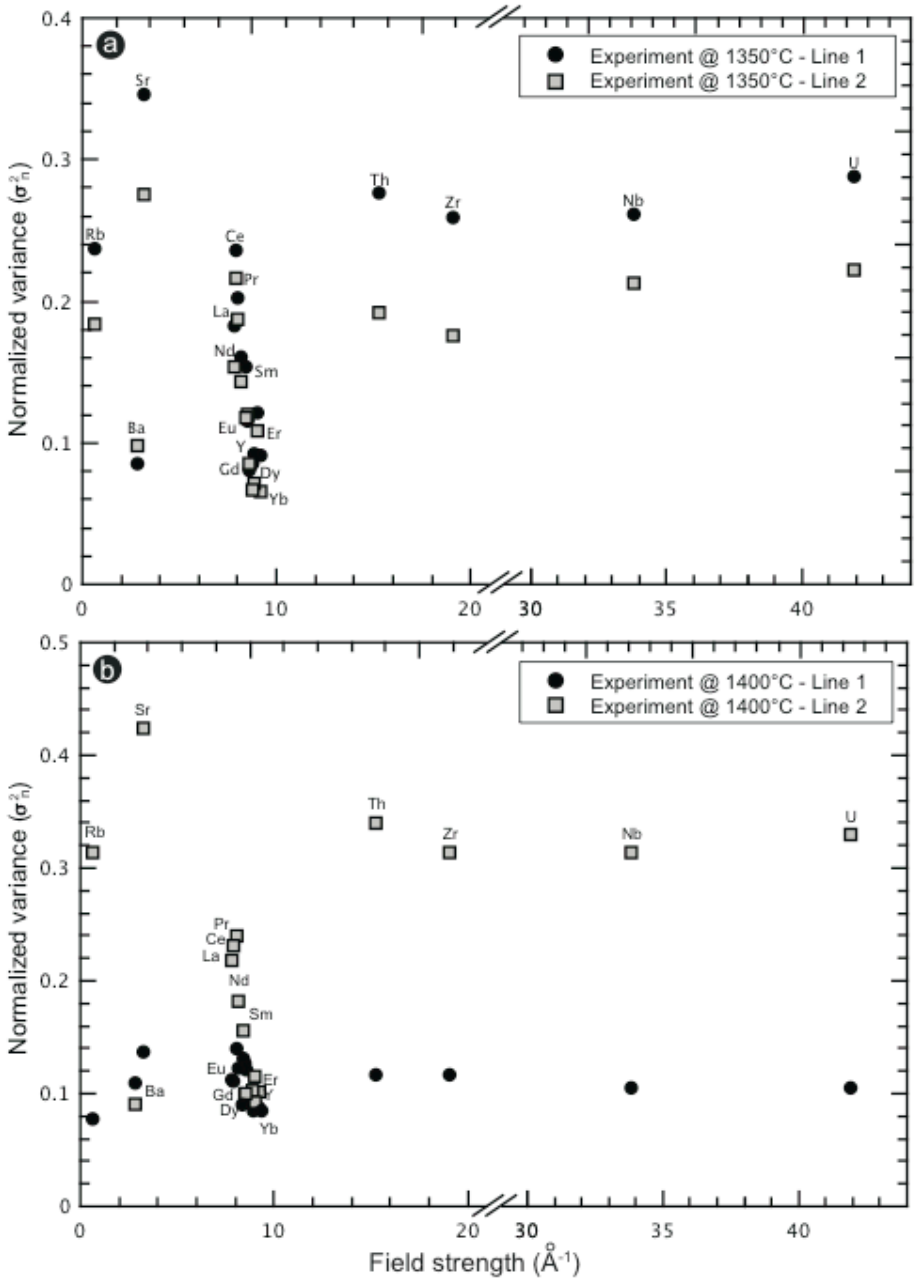

Figure 11: Variation of concentration variance σ_n^2 against field strength (Z^2/r; Z = ionic change, r = ionic radius) for trace elements in the studied compositional transects.

Figure 12 provide a zoomed-in view on the Rare Earth Elements (REE). In Figures 10-12 the value of σ_n^2 is plotted as a function of the field strength Z^2/r [calculated as the square of the nominal charge (Z), divided by the ionic radius (r)]. Field strength is used here because it has been suggested to correlate with element diffusivity in silicate melts (e.g. Mungall, 2002). The calculation of field strength requires the knowledge of the ionic radius of chemical elements

that, in turn, depends on their coordination number. Following Mungall (2002) we have used ionic radii reported in Shannon (1976) considering most cation radii for octahedral coordination, except for Si and Al assumed to be in tetrahedral coordination (Mungall, 2002).

Figures10-11 show that chemical elements have a variable mobility. In particular, the mobility of major elements does not vary systematically with field strength and increases with the following order: Si, Ti, Mg, Ca, Al, K and Na (Fig. 10). As for trace elements, the sequence of mobility is Sr, Th, U, Nb Zr, Rb Ce, Pr, La, Nd, Sm, Eu, Ba, Y, Gd, Dy, Yb (Fig. 11). The Rare Earth Elements (REEs) however show that their mobility systematically decreases with increasing field strength, with the exception of La (Fig. 12).

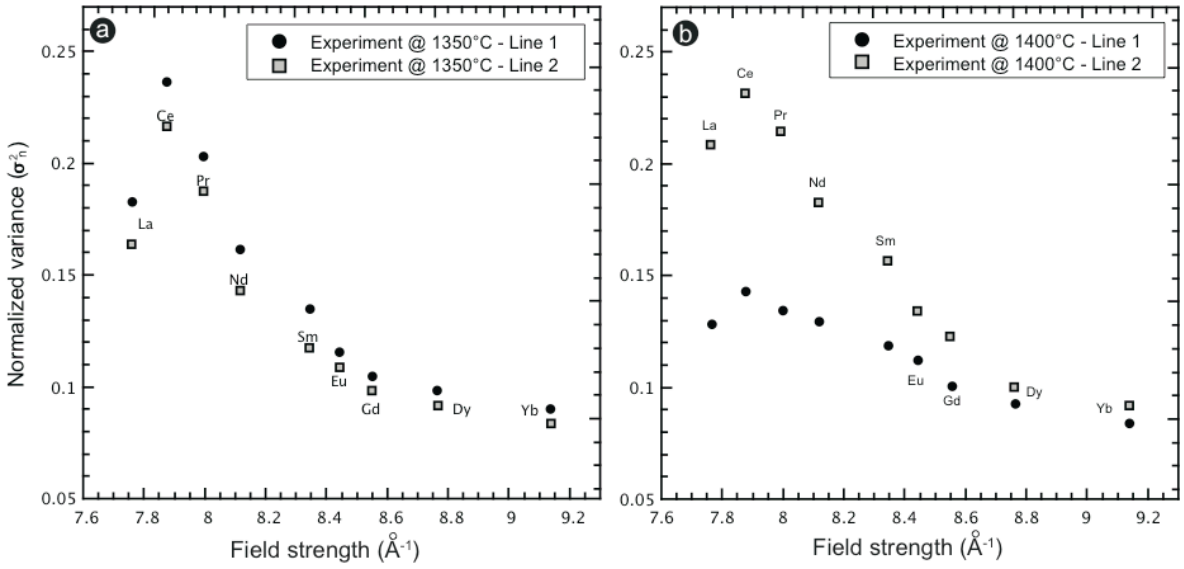

Figure 12: Variation of concentration variance σ_n^2 against field strength (Z^2/r; Z = ionic change, r = ionic radius) for Rare Earth Elements (REE) in the studied compositional transects.

Note that the order of element mobility defined above is consistently observed for all analyzed transects. The only exception is given by Line 1 of the 1400 °C experiment, for which most elements reached minimal values making the discrimination between different element mobilities rather difficult.

Despite the consistent relative behavior observed for the other three transects, however, elements have different values of σ_n^2 in each transect. This is the result of different

mixing efficiency due to a different spatial distribution of filaments (i.e. the mixing pattern): the mixing efficiency increases from Line 2 (1400 °C) to Line 1 (1400 °C); the transects of the 1350 °C experiment show mixing efficiencies intermediate between the two previous transects. Figure 13 shows the influence of averaged filaments thickness (ψ) on the overall mobility of chemical elements (i.e., the normalized variance). The parameter ψ reflects the complexity of mixing pattern and decreases as the mixing efficiency increases.

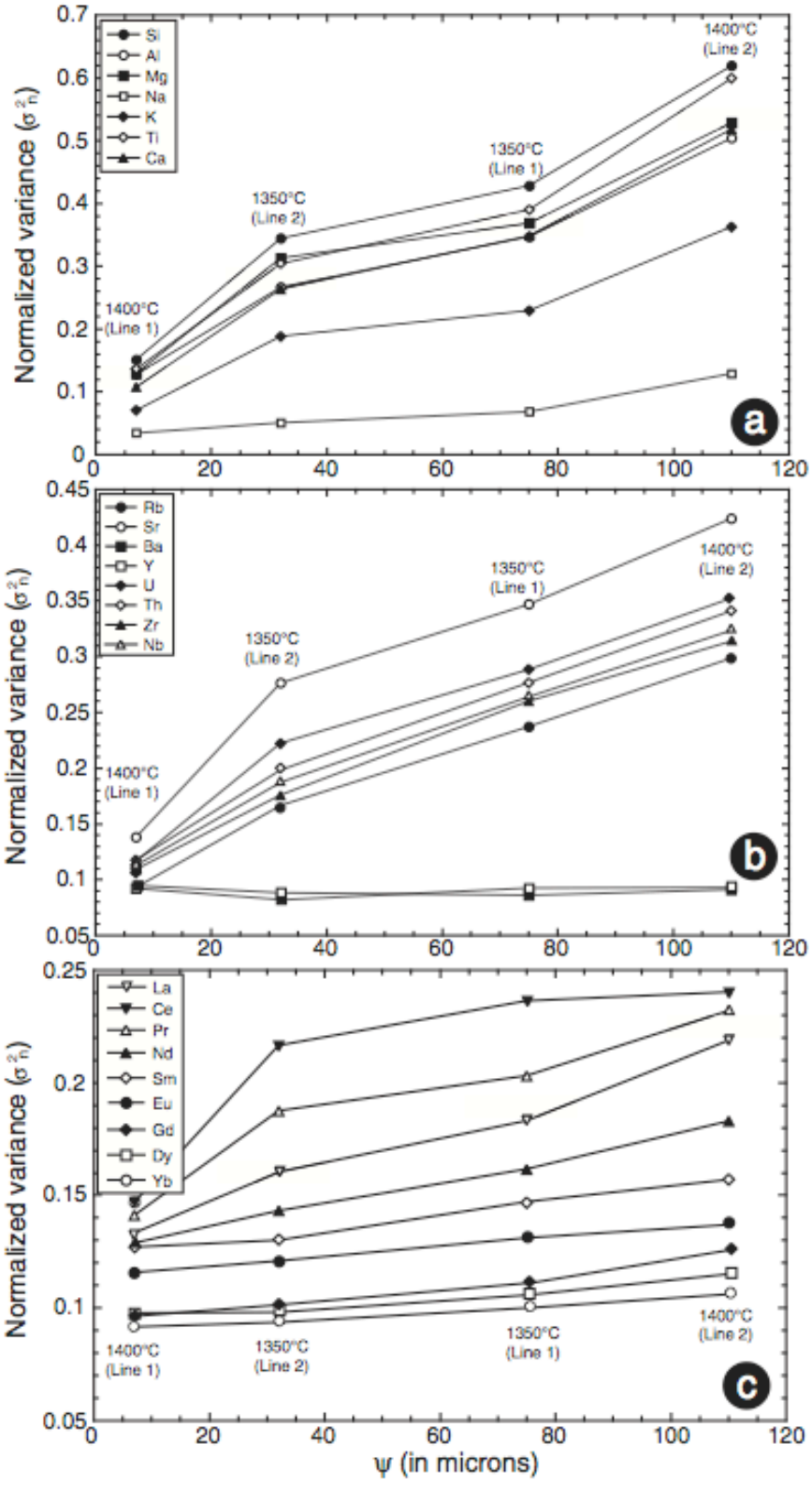

Figure 13: Variation of concentration variance with parameter ψ in the four analyzed transects for major (a) and trace elements (b and c).

The graphs show that for both major and trace elements there is a positive correlation between concentration variance and ψ indicating that the complexity of the mixing pattern, in the different regions of the same system, can strongly influence the mobility of chemical

elements. In addition, the same element is found to move with a different efficiency (i.e. different concentration variance values) in the different transects as a function of the complexity of the mixing pattern.

2.5. Discussion

The results offered by the chaotic mixing experiments on natural multi-component systems provide a very complex view on the process of mixing. As mentioned above, the different mobility of chemical elements in mixing systems is likely the main cause of poor correlations in inter-elemental binary plots (especially in the trace elements). Typically in the study of magma mixing it is assumed that correlations between pairs of chemical elements should follow straight lines. This idea is based on the classic two end-member mixing equation (e.g. Fourcade and Allegre, 1981) for which the only possible outcome is a linear correlation between the two starting end-members. However, this concept may only be valid if we were to assume that all chemical elements in a multi-component magmatic system had exactly the same mobility. Here, we have shown that this is not the case and, therefore, this assumption is not valid. Our results show that not only is the correlation between elements non-linear, but also that the degree of correlation degrades towards progressively more scattered distribution as pairs of elements with increasing different mobility are considered. Therefore, the problem cannot be solved by simply invoking non-linear mixing trends and further processes capable of producing scattering in binary plots must be taken into account. Recent studies have shown that during chaotic mixing dynamics, the coupled action of stretching and folding together with chemical diffusion are indeed able to produce an increasing degree of scattering in inter-elemental plots as the difference in mobility between pairs of elements increases (e.g. Perugini et al., 2006, 2008; De Campos et al., 2008, 2011). Such irregular correlations in inter-elemental binary plots has been observed in natural samples (Perugini et al., 2006), numerical simulations and experiments (e.g. Perugini et al., 2008; De Campos et al., 2008, 2011) and they have been ascribed to the onset of a diffusive

fractionation induced by the combined actions of chaotic flow fields and chemical diffusion. Given that our experiments were performed by coupling a chaotic flow fields and chemical diffusion processes, this process can be considered as the main cause of the differential inter-elemental correlations. Support to these considerations is given by the comparison between Figure 10 and Figure 7, and Figures 11-12 and Figure 8. For example, Figure 7 shows that good linear correlations are observed in plots such as CaO vs. MgO and SiO_2 vs. MgO, whereas non-linear and scattered correlations are seen for SiO_2 vs. Na_2O and CaO vs. Na_2O. Figure 10 indicates that those pairs of elements showing good linear correlations also have similar values of σ_n^2, i.e. they have similar mobilities. Elements with different mobilities (e.g. Si and Na, or Ca and Na) display, instead, poor linear correlations. Concerning major elements, their diffusivities (i.e. their mobility in the silicate melt) have been shown to be interdependent (e.g. Chakraborty et al., 1995; Liang et al., 1996). For example, Na content appears to be correlated with the silica content of the melt (e.g. Lundstrom, 2000) and this can also contribute in the generation of non-linear variations in binary plots.

Comparison of our experimental findings to those obtained by De Campos et al. (2011) on synthetic melt using the same experimental conditions, reveal interesting differences. Firstly, all plots shown by De Campos et al. (2011) display non-linear patterns, whereas in our experiment on natural end-members, only Na, and to some extent K, display a non-linear correlation with other major elements. Secondly the degree of homogenization of chemical elements shown in De Campos et al. (2011) is much higher that the one shown here. A possible explanation for these differences may reside in the contrasting chemical composition of the starting end-members used in each investigation. The synthetic compositions of De Campos (2011) contain a low number of major elements: Si, Al, Na and K, for the felsic end-member and Si, Al, Ca and Mg for the mafic end-member. The low number of elements and their relatively high concentrations compared to natural composition may favor the development of non-linear relationships in binary plots. In addition, the viscosity ratio

between the end-members in De Campos et al. (2011) is $1.1x10^3$, whereas in the experiments presented here it is $7.8x10^3$ and $5.9x10^3$ at 1350 °C and 1400 °C, respectively. Viscosity ratio is the most significant parameter influencing the kinetics of mixing processes (e.g. Sparks and Marshall, 1986; Grasset and Albarede, 1994; Bateman, 1995; Poli et al., 1996; Perugini and Poli, 2005): the lower the viscosity ratio, the faster the mixing and hence, homogenization. In the experiment shown here the viscosity ratio is 6-8 times larger than in De Campos et al. (2011) and this can explain the lower degree of mixing.

Observations similar to those made for major elements can also be done for trace elements for which there is a quite continuous deterioration of inter-elemental correlations at increasing differences in mobility (σ_n^2). For example, the plot La vs. Pr shows a good linear correlation (Fig. 9a-g) because these two elements have similar mobilities (Fig. 12). As the difference in mobility increases (e.g. La vs. Sm, La vs. Yb, or Ba vs. Nb) the plot becomes progressively more scattered.

As previously mentioned, physical stretching and folding followed by chemical exchanges (molecular diffusion) are the forces promoting the process of chaotic mixing (e.g. Ottino, 1989; Aref and El-Naschie, 1995; Perugini et al., 2003; Perugini et al., 2004). The fact that mixing is a chaotic process implies that the contact area between interacting magmas increases exponentially in time and, consequently, chemical diffusion becomes progressively more efficient. Chemical exchanges are subjected to the so-called "Sensitivity upon Initial Conditions" (SIC) of chaotic systems (e.g. Strogatz, 1994). Such a property, popularly know as the "butterfly effect", states that a small change at one place in a dynamic system can result in large differences to a later stage. The effect of SIC during chaotic mixing manifests itself in the fact that nearby trajectories of the flow fields diverge exponentially in time. As the initial distance between pairs of trajectories decreases, the time span at which they will start to diverge increases exponentially (e.g. Perugini et al., 2006; 2008). Chemical diffusion is the process carrying elements from a certain portion of the magmatic system to another portion,

according to a given chemical activity gradient. The distance travelled by an element depends on its mobility: the larger the mobility, the larger the distance. If two elements (*a* and *b*) have very similar mobility the distance they will travel in equal times will be about the same; on the contrary, if two elements (e.g. *a* and *c*) have different mobility, their respective travelled distances will be different. It follows that, in the same time span, volumes of melts having variable amounts of elements can be generated depending on their relative mobility. The mixing process will disperse these volumes of melts according to SIC. Since elements *a* and *b* are at about the same location, their relative distance will be maintained constant for a certain time during advection. On the contrary, at the same time, elements such as *a* and *c* will experience much more rapidly the effect of SIC because of the larger initial distance. This process is revealed by geochemical variations as a variable correlation between elements in binary plots. As an example, since *a* and *b* have similar mobility, they will tend to be well-correlated. On the contrary, at the same time, *a* and *c* will be strongly uncorrelated in binary plots because of their different mobility. These considerations can explain the observed variability in inter-elemental correlations in the studied experiments.

2.6. Conclusions and outlook

We presented the first chaotic magma mixing experiments performed using natural basaltic and rhyolitic melts. The results indicate that the mixing process, governed by the heterogeneous development of stretching and folding processes, produces portions of samples exhibiting a wide variety of flow patterns coexisting at the same time in the same system. These different patterns strongly modulate the chemical exchanges between the two melts leading to sample segments having extremely variable degrees of homogenization. We quantified the mobility of both major and trace elements considering the concentration variance of elements. We have shown that elements spread and homogenize in the mixing system with different efficiencies and, therefore, the attainment of the hybrid compositions requires different times for the different elements. The methodological approach introduced

here can in principle be used in the study of natural outcrops for a variety of purposes, ranging from the estimate of time-scales of magma mixing to the impact of the development of chaotic mixing processes in the petrological study of the compositional variability of natural rock samples.

In conclusion, despite the limitations still persisting in the application of laboratory experiments to natural systems, the findings of this study surmise that the proposed novel approach represents an important step towards a more complete understanding of the complexity of magma mixing in nature. However, further efforts and investigations such as a study on the time scale of chemical exchange during mixing are required before application of the proposed method to nature.

Chapter 3

TIME EVOLUTION OF CHEMICAL EXCHANGES DURING MIXING OF RHYOLITIC AND BASALTIC MELTS

Summary

We present the first set of chaotic mixing experiments performed using natural basaltic and rhyolitic melts. The mixing process is triggered by a recently developed apparatus that generates chaotic streamlines in the melts, mimicking the development of magma mixing in nature. The study of the interplay of physical dynamics and chemical exchanges between melts is carried out performing time series mixing experiments under controlled chaotic dynamic conditions. The variation of major and trace elements is studied in detail by electron microprobe (EMPA) and Laser Ablation ICP-MS (LA-ICP-MS).

The mobility of each element during mixing is estimated by calculating the decrease of concentration variance in time. Both major and trace element variances decay exponentially, with the value of exponent of the exponential function quantifying the element mobility. Our results confirm and quantify how different chemical elements homogenize in the melt at differing rates. The differential mobility of elements in the mixing system is considered to be responsible for the highly variable degree of correlation (linear, non-linear, or scattered) of chemical elements in many published inter-elemental plots. Elements with similar mobility tend to be linearly correlated whereas, as the difference in mobility increases, the plots become progressively more non-linear and/or scattered.

The results from this study indicate that the decay of concentration variance is in fact a robust tool for obtaining new insights into chemical exchanges during mixing of silicate melts. Concentration variance is (in a single measure) an expression of the influence of all possible factors (e.g. viscosity, composition, fluid-dynamic regime) controlling the mobility of chemical elements and thus can be an additional petrologic tool to address the great complexity characterizing magma mixing processes.

3.1. Introduction

Magma mixing is a petrologic phenomenon which plays a key role in modulating the compositional variability of igneous rocks in both intrusive and extrusive environments (e.g. Anderson 1976, 1982; Wiebe 1994; Bateman 1995; De Rosa et al. 1996; Perugini and Poli 2005; Kratzmann et al. 2009). Evidence of this process is present in the rocks as variable structures including enclaves, filament-like patterns, synplutonic dykes, basic septa, and minerals displaying a variety of textures due to the physicochemical disequilibrium occurring when magmas with different composition and temperature come into contact (e.g. Hibbard et al. 1981; 1995; Wada 1995; Didier and Barbarin 1991; Flinders and Clemens 1996; Perugini et al. 2002; Perugini et al. 2003). The occurrence of these structures is influenced strongly by the dynamics arising during the mixing process (e.g. Flinders and Clemens 1996; Poli and Perugini 2002; Perugini et al. 2003) and their interpretation requires detailed analytical and experimental studies.

Studies focused on numerical and experimental investigation of mixing dynamics (e.g. Perugini et al. 2003; Perugini et al. 2008; De Campos et al. 2008, 2011; Petrelli et al. 2011) have highlighted a great complexity of this process, whose evolution is governed by a continuous interplay between physical dispersion of melts and chemical exchanges. One of the most striking results arising from these studies is that, during mixing, chemical elements experience a diffusive fractionation process due to the development in time of chaotic mixing dynamics (Perugini et al. 2006, 2008). This process is considered the source of the strong deviations of many chemical elements from the linear variations in inter-elemental plots that would otherwise be expected based on a conceptual model classically adopted in the geochemical modeling of magma mixing processes (e.g. Fourcade and Allegre 1981). The false assumption of evidence for a linear trend poses problems in the study of rocks generated by magma mixing because it may lead to an erroneous interpretation and reconstruction of the mixing end-members with important consequences on the reconstruction of the geochemical features of source regions and associated geological and geodynamic interpretations.

Recently, in order to shed new light on the complexity of magma mixing processes, a new experimental apparatus has been developed which is able to perform experiments using high viscosity silicate melts at high temperature (De Campos et al. 2011; Perugini et al. 2012). This device has been used to study the mixing process between "low-complexity" synthetic silicate melts composed of a few chemical elements enabling the study of the modulation of chaotic dynamics on the geochemical evolution of the mixing system.

In order to increase our understanding about magma mixing processes and their impact on the geochemical evolution of silicate melts we present here the first set of experiments performed using natural basaltic and rhyolitic melts. In particular, the study of the interplay of physical dynamics and chemical exchanges between these two melts is carried out using time series mixing experiments performed under controlled chaotic dynamical conditions. The variation of major and trace elements is studied in detail by electron microprobe (EMPA) and Laser Ablation ICP-MS (LA-ICP-MS) and the time-evolution of chemical exchanges during mixing is investigated. Using the concentration variance as a proxy to measure the rate of chemical element homogenization in time, a model to quantify chemical element mobility during chaotic mixing of natural silicate melts is proposed.

3.2. End-members and experimental setup

3.2.1 End-member selection and preparation

Experiments were performed using natural samples from Bruneau Jarbidge eruptive center (Snake River Plain). Specifically, the basaltic and rhyolitic compositions belong to the Mary's Creek basalt and the Cougar Point Tuff (CPT) rhyolite (unit V), respectively (Bonnichsen 1982; Cathey and Nash 2009).

Rock powders from both end-members were melted and homogenized using a concentric cylinder geometry (Dingwell 1986). The melts were placed in a $Pt_{80}Rh_{20}$ crucible (5.0 cm long, 2.5 cm inner diameter, 0.1 cm wall thickness) and stirred with a $Pt_{80}Rh_{20}$ spindle for 72 hours at 1600°C for the rhyolite and 6 hours for the basalts. This procedure yielded, upon cooling of the samples, homogeneous, bubble-free glasses that were used in the chaotic

mixing experiments. The compositions of the starting basaltic and rhyolitic end-members are given in Tab. 1.

	Basalt	Rhyolite
SiO_2	48.44	78.64
Al_2O_3	16.30	9.75
TiO_2	1.77	0.23
FeO_{tot}	12.20	1.83
MgO	7.47	0.12
CaO	11.54	0.82
MnO	0.28	bdl
Na_2O	1.95	3.45
K_2O	0.31	4.50
P_2O_5	0.43	bdl
V	261	7
Ga	15	39
Rb	4	195
Sr	220	50
Y	18	47
Zr	112	360
Nb	10	45
Cs	7.3	0.5
Ba	190	790
La	13	88
Ce	27	175
Pr	3.6	16.0
Nd	14	58
Sm	3.3	12.0
Eu	2.0	0.5
Gd	1.3	10.0
Tb	0.5	1.6
Dy	1.7	8.5
Ho	0.7	1.9
Er	2.0	5.0
Tm	0.2	0.9
Yb	1.5	6.0
Lu	0.2	0.8
Hf	2.6	11.0
Ta	0.8	3.7
Pb	2.0	11.0
Th	0.9	33.0
U	0.2	7.5
η (log Pas)	0.86	4.75
ρ (g/cm^3)	2.98	2.33

Table 1: Concentrations of major and trace elements in the basaltic and rhyolitic end-member glasses used in the mixing experiments. Concentrations for major elements are given in weight percentage. Trace elements values are in ppm. For analytical conditions see section 2.3. Values of density (ρ) and viscosity (η) of the two end-members are also reported.

3.2.2 Experiments

Magma mixing experiments were performed using the chaotic mixing device installed at the Department for Earth and Enviromental Sciences (LMU, Germany). This experimental apparatus consists of an outer and an inner cylinder, which is located off-center (Fig. 1).

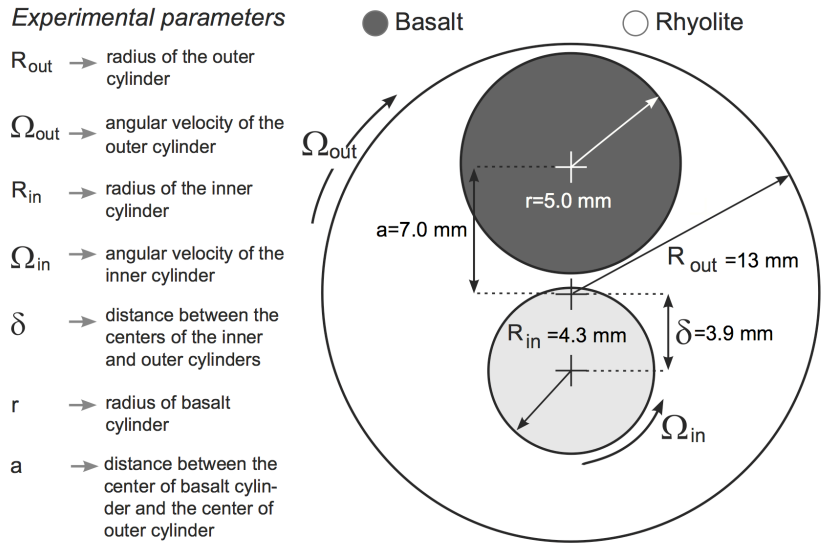

Figure 1: Schematic 2D section of the experimental apparatus used to perform chaotic mixing experiments. In the figure experimental parameters are also reported. Their values are as follows: R_{out}=13 mm, Ω_{out}=0.06 rpm, R_{in}=4.3 mm, Ω_{in}=0.3 rpm, δ=3.9, r=0.5 mm. Further details about the experimental setup can be found in De Campos et al. (2011).

The outer cylinder hosts the end-member melts. Both cylinders are fabricated from a Pt_{80}-Rh_{20} alloy to resist high-temperature contamination of natural compositions and maintain experimental geometry. The motions of the two cylinders are independent and their rotation with given angular velocities generates chaotic streamlines (De Campos et al. 2011; Perugini et al. 2012; Morgavi et al. 2012). The outer cylinder was filled with the rhyolitic end-member at high temperature and cooled down to room temperature to produce a glass. From this glass two cylinders were drilled out, one at the position of the inner cylinder, and a second one at the initial position of the basaltic end-member (Fig. 1). The experimental protocol (i.e. the relative number of rotations of the two cylinders) has been chosen to ensure the occurrence of chaotic dynamics within the entire experimental sample. The protocol consists of alternating rotations of the outer and inner cylinders in the following sequence: (1) two complete rotations of the outer cylinder in 35 min; (2) six complete rotations of the inner cylinder in 18 min. Such an experimental protocol, in conjunction with the tested viscosities (Tab. 1), provided flow conditions with Reynolds number on the order of 10^{-7} (see De Campos et al. 2011 and Perugini et al. 2012 for further detail of the experimental setup and protocol). Three

experiments were performed at 1350 °C with identical starting conditions (Fig. 1). Durations of experiments were 53, 106, and 212 min, corresponding to the application of one, two and four experimental protocols. In the following we refer to those experiments as Exp.1, Exp. 2 and Exp. 3. Initial proportions of end-members were: rhyolite 80% and basalt 20%. Viscosity ratio during experiments was 7.8×10^3. After the complete mixing protocol was finished, the experiment was terminated by switching off the power supply of the furnace, allowing the melt to cool to room temperature at a quench rate of ca. 80°C/min. Each crucible with the experimental charge was recovered from the gas-mixing furnace by disconnecting the motor from the inner cylinder and extracting the outer cylinder from the bottom of the oven with the spindle (inner cylinder) still inside the sample. Each sample was recovered by coring out a cylinder with a radius of 11 mm from the crucible (outer cylinder). Each core was then sectioned perpendicular to its long axis into slices (ca. 4.0 mm in thickness) for further analyses. One representative slice was selected for each experiment and used for the analysis of the variability of major and trace elements (Fig. 2).

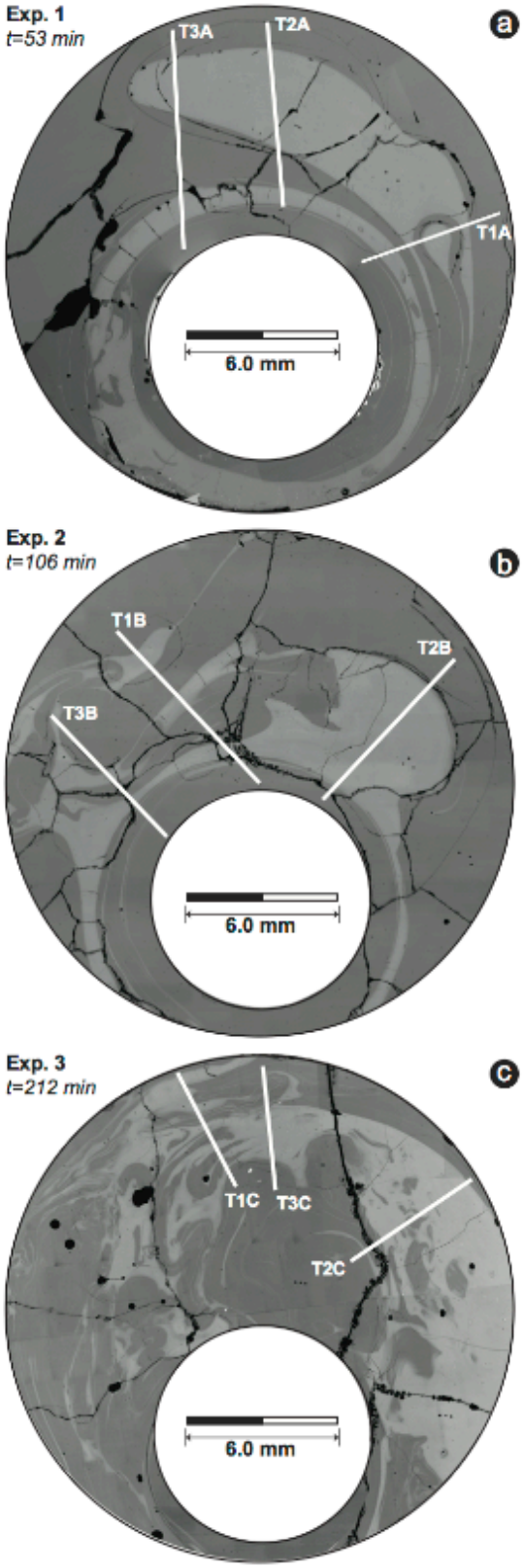

Figure 2: Representative BSE images of the three chaotic mixing experiments at different mixing times (t): a) Exp. A, t=53 min, b) Exp. B, t=106 min), c) Exp. C, t=212 min. On the images are also marked the transects (T) along which geochemical analyses of major and trace elements have been performed.

3.2.3 Analytical methods

Concentrations of major elements were measured with a Cameca SX100 (Earth and Environment, LMU-Munich). The electron microprobe operating conditions were 15 kV acceleration voltage and 20 nA beam current. A defocused 10-μm beam was used for all elements in order to avoid alkali loss. Synthetic wollastonite (Ca, Si), periclase (Mg), hematite (Fe), corundum (Al), natural orthoclase (K), and albite (Na) were used as standards, and matrix correction is performed by PAP procedure (Pouchou and Pichoir 1984). Standard deviations were lower than 2.5% for all analyzed elements.

Trace elements were measured at the University of Frankfurt by Laser Ablation ICP-MS microanalysis (Institut für Geowissenschaften Facheinheit Mineralogie Petrologie und Geochemie). Spot size used was 40 μm with spacing between consecutive data points of 40 μm. The use of this spot size allowed us to appreciate in details the compositional variability in the experiments studied.

On each experiment, the compositional variability in the mixing system was studied along three different compositional transects (T) measuring both major and trace elements (Fig. 2a-c). The three transects were chosen to cover different segments of the mixing pattern characterized by variable amounts of filaments of the two melts to characterize at best each sample (see below). The number of analyzed data points (N) was (Fig. 2): Exp. A (T_{1A}, N=90; T_{2A}, N=115; T_{3A}, N=142), Exp. B (T_{1B}, N=126; T_{2B}, N=90; T_{3B}, N=121), Exp. C (T_{1C}, N=81; T_{2C}, N=98; T_{3C}, N=83). Hence, a total of 955 data points constitute the database of geochemical analyses used in this work.

3. Results

3.1 Optical analysis

Representative slices for each experiment are displayed in the Back-Scattered-Electron (BSE) images of Fig. 2a-c. The figures show that the basaltic end-member melt was dispersed within the rhyolitic melt via the onset of stretching and folding dynamics, triggered by the

applied experimental protocol. In the following we refer to the least evolved and most evolved melts as mafic and felsic, respectively. After 53 min (Fig. 2a) the basaltic melt (light grey color) was stretched and folded generating a pattern of filament-like morphologies in the rhyolitic melt (dark grey color). In detail, around the inner cylinder, a filament of mafic melt is visible. The top part of the sample shows a lobate blob of the mafic melt, which is connected with this filament in the bottom part of the sample. On the right side of the experiment a small volume of felsic melt, containing a drop-like morphology of mafic melt, infiltrated within the above-mentioned blob of mafic material. The 106 min experiment (Exp. 2) shows a clear evolution of the mixing pattern (Fig. 2b). The mafic melt appears much more deformed than in the previous sample (Fig. 2a) and shows a larger number of stretched and folded filaments both around the inner cylinder and on the left side of the sample. The right side of the sample shows that the lobate blob of mafic melt evolved towards a sub-circular morphology in which, from the left side, the felsic magma tends to penetrate. After 212 min (Fig. 2c) the experimental sample (Exp. 3) shows a dramatic evolution of the mixing pattern. The filament-like structures are strongly deformed and an intricate lamellar pattern consisting of alternate filaments of mafic and felsic melt is produced. This is mostly evident in the left part of the sample. On the right side the blob-like structure of mafic melt is no longer recognizable and that volume of mafic melt contains filaments and small deformed blobs of the felsic magma that, during the evolution of the mixing process, penetrated and intimately mixed with it.

3.3.2 Geochemical variations

The variability of major and trace elements along the three representative transects (T1A, T1B, T1C; Fig. 2) at different mixing times is displayed in Fig. 3 and 4, respectively.

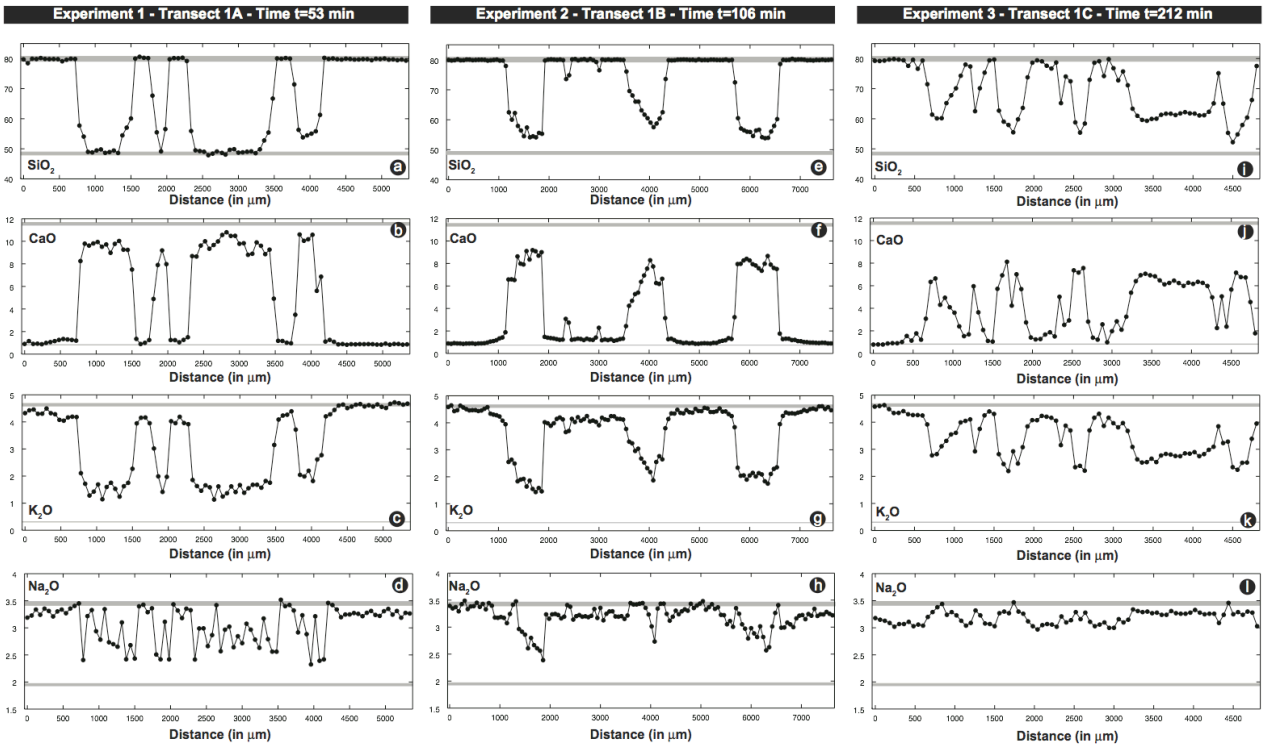

Figure 3: Variation of some major elements along three representative transects reported in Fig. 2. Concentrations of initial basaltic and rhyolitic melts are marked in different grey shades. These are reported as a range (grey areas) to include analytical uncertainties.

In Fig. 3 and 4 element concentrations for both the end-members are also marked in order to better resolve the time evolution of mixing. In general, element variability exhibits an oscillatory pattern corresponding to the alternating occurrence of filaments of the two melts. Element concentrations increase (or decrease) continuously passing from one filament to the other defining smooth patterns. This indicates that, in addition to the stretching and folding mechanism responsible for mechanical mixing (or mingling), also chemical diffusion occurred among filaments. Filaments have different thicknesses as indicated by the different widths of the compositional fluctuations (Figs. 3 and 4).

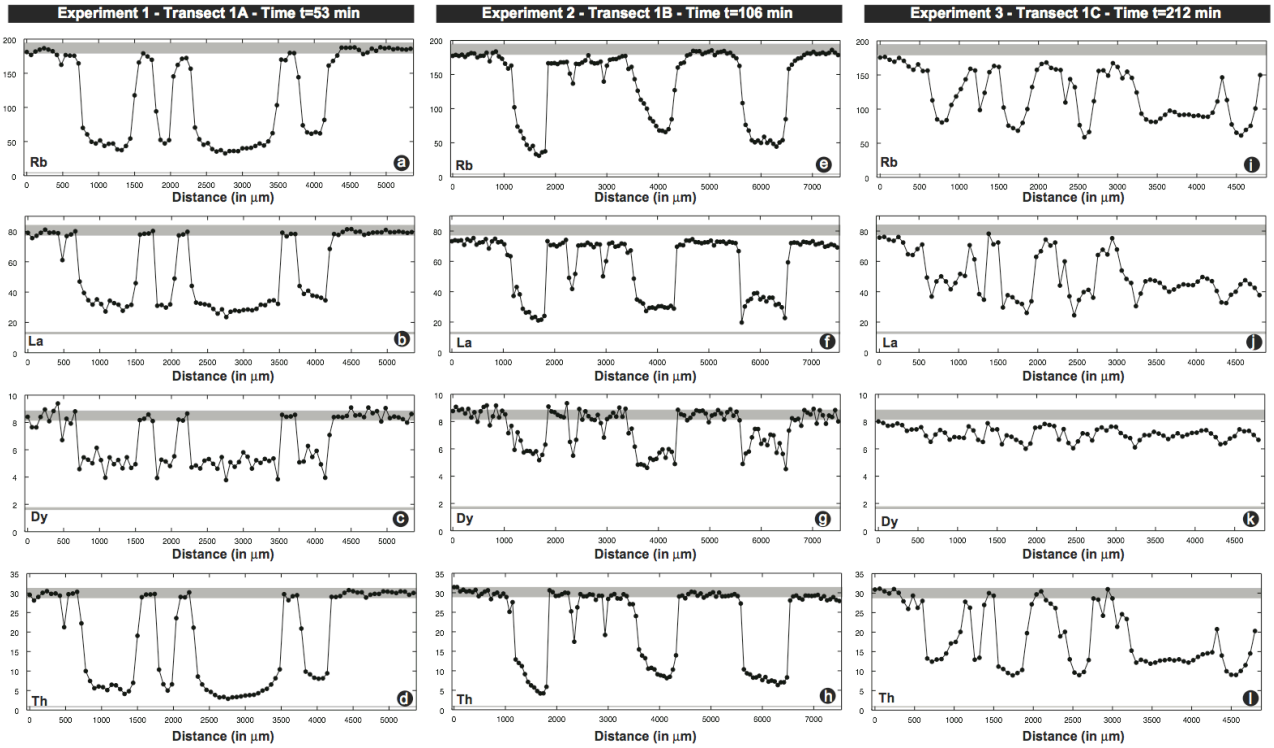

Figure 4: Variation of some trace elements along three representative transects reported in Fig. 2. Concentrations of initial basaltic and rhyolitic melts are marked in different grey shades. These are reported as a range (grey areas) to include analytical uncertainties.

It is interesting to note that for most elements, after 53 min (Fig. 3a-d and 4a-d), only a few filaments of the mafic melt still exhibit the initial composition. The only exception is SiO_2 that, for the thickest filaments, maintains the original mafic composition. This effect is strongly amplified in the 106 min and 212 min experiments (Fig. 3 and 4) where no trace of the starting mafic melt is identified along the analyzed transects. Some elements, for example Na_2O (Fig. 3) and Dy (Fig. 4), show that compositional fluctuations are strongly contracted towards an almost homogeneous composition as the mixing time increases.

To better visualize the evolution in time of compositional fields Figs. 5 and 6 display binary inter-elemental plots of some representative major and trace elements measured on transects T1A, T1B, T1C, for the three experiments (Fig. 2).

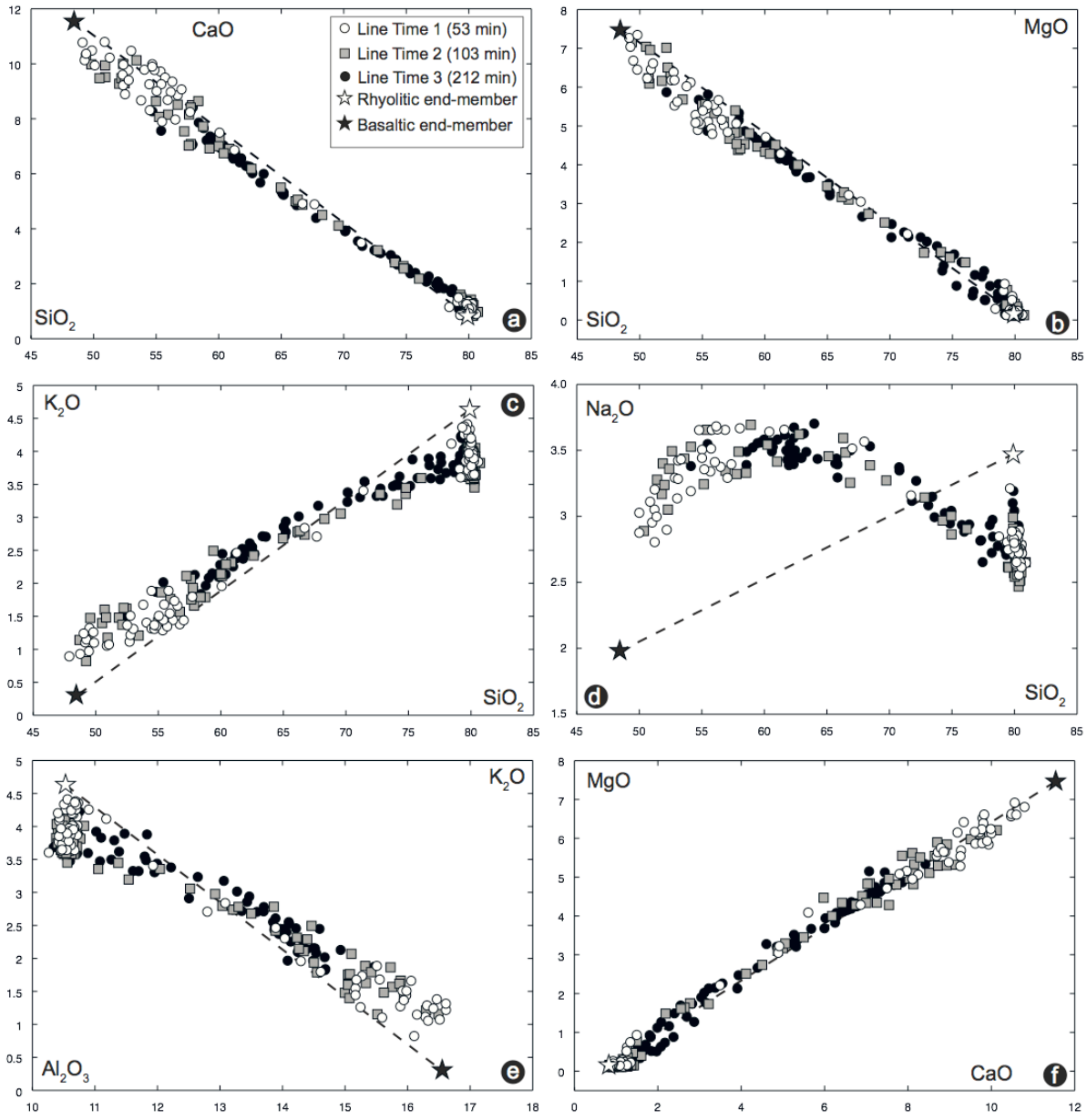

Figure 5: Representative binary plots showing the variable correlation between pairs of major elements for the transects shown in Fig. 3 and 4. The mixing line connecting the two end-members is also reported. Initial mafic and felsic end-member compositions are reported as black and white star, respectively.

For all binary plots the geochemical evolution is marked by a continuous narrowing of the compositional variability in time. In these plots major elements tend to define linear patterns (e.g. SiO_2 vs.CaO, SiO_2 vs. MgO, CaO vs. MgO; Figs. 5a, b, and f). The major exception is provided by Na_2O (and to same extent K_2O) that is not linearly correlated with any major element (e.g. Fig. 5d). Instead, this element defines "S" shaped patterns passing from the basaltic to the rhyolitic end-member. Regarding trace elements, inter-elemental plots are in general more complex. Some pairs of elements display linear relationships (e.g. Zr vs.

Nb, Th vs. Hf; Fig. 6a and b), whereas others define curved trends with a variable (generally high) scattering of data points (e.g. Sm vs. Rb or Th vs. Ba; Figs. 6d and e). Note that the considerations made above for transects T1A, T1B, and T1C are also valid for all the other analyzed transects.

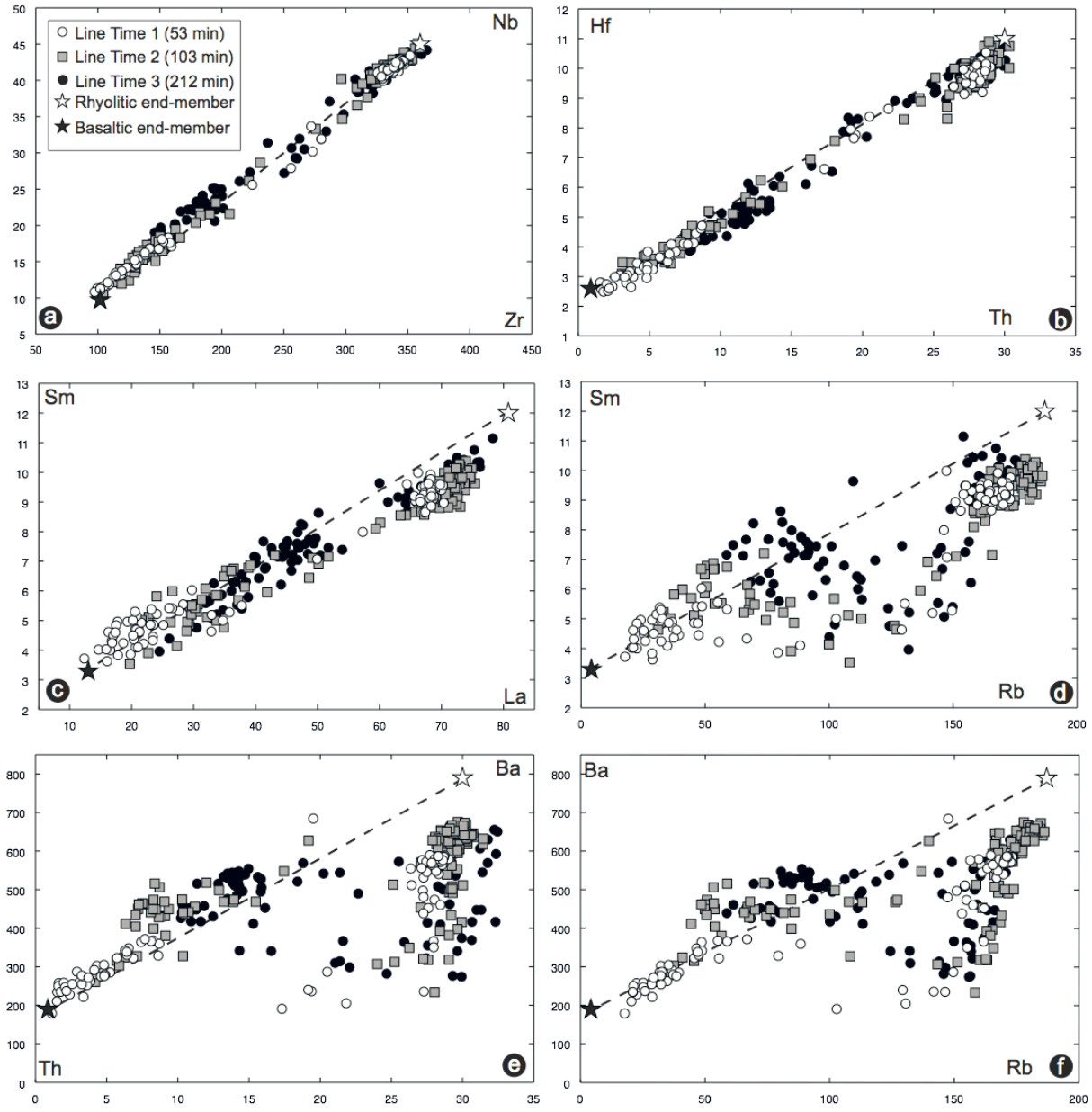

Figure 6: Representative binary plots showing the variable correlation between pairs of trace elements for the transects shown in Fig. 3 and 4. The mixing line connecting the two end-members is also reported. Initial mafic and felsic end-member compositions are reported as black and white star, respectively.

The evolution of the compositional variability during the mixing process outlined above indicates that while some elements are linearly correlated in inter-elemental plots, others strongly deviate from this simple pattern. In addition, the general picture emerges that the rate of homogenization of the different chemical elements is different: some elements display a strongly reduced compositional variability, whereas others still show well detected compositional fluctuations - in the same system and at the same time (see e.g. Fig. 3 and 4). Although these qualitative observations may help in identifying the rate of homogenization of elements during the development of the mixing processes, a quantitative analysis is necessary to establish firm constraints. We develop such an approach in the following section.

3.4. Discussion

3.4.1. Validation of the two end-member mixing model

A typical model, which is considered valid when dealing with mixing processes, is that linear correlations must be observed in any inter-elemental binary diagram, irrespective of the chosen pairs of elements. This idea comes from the so-called two end-member mixing model

$$C_H = C_F x + C_M (1 - x) \qquad \text{(Eq. 1)}$$

where C_H, C_F and C_M are the concentrations of the hybrid, most evolved (rhyolitic) and least evolved (basaltic) magma, respectively, and x is the initial fraction of the rhyolitic end-member. This equation predicts linear variations in inter-elemental plots.

From the above discussion it is clear that, although a two end-member mixing process characterized the experiments, inter-elemental plots for many elements substantially deviate from the linear correlations predicted by Eq. 1.

A quantitative evaluation of the deviation of our experimental system from the classical concept of two end-members mixing can be performed using the so-called “mixing test” proposed by Fourcade and Allegre (1981). This test is commonly utilised to assess the occurrence of magma mixing processes in petrologic research (e.g. Janoušek et al. 2000;

Solgadi et al. 2007). The mixing test is performed by plotting the difference in all chemical elements between the rhyolitic and the basaltic end-member (i.e. C_F-C_M) vs. the difference in all chemical elements of a supposed hybrid composition and the basaltic end-member (i.e. C_F-C_M). Linear interpolation of data points gives a twofold information: i) the correlation coefficient (r^2), whose value indicates whether the supposed hybrid sample can be regarded as the product of mixing - i.e. the larger the r^2 value, the stronger the evidence that the sample has a hybrid composition; ii) the slope of the linear fitting (x) which gives the initial proportion of the rhyolitic end-member in the mixture. The mixing test equation is derived from Eq. 1, by rearranging variables is such a way that:

$$C_H - C_M = x(C_F - C_M) \qquad \text{(Eq. 2)}$$

Plotting C_F-C_M vs. C_H-C_M and performing a linear interpolation of data gives the parameters of interest (i.e. r^2 and x). As reported above, application of this test requires the choice of a sample, which is supposed to have attained the hybrid composition. Where the composition of the two original end-members and their relative proportions in the mixture are known, the theoretical hybrid composition for each element can be calculated by applying Eq. 1. Then, from the available datasets, samples displaying the hybrid composition for a given element were selected and a graph of C_F-C_M vs. C_H-C_M was drawn. As an example, these calculations are shown in Fig. 7 and 8 considering the compositional variability along transect T1C, i.e. the compositions generated for the longest mixing time (Fig. 2).

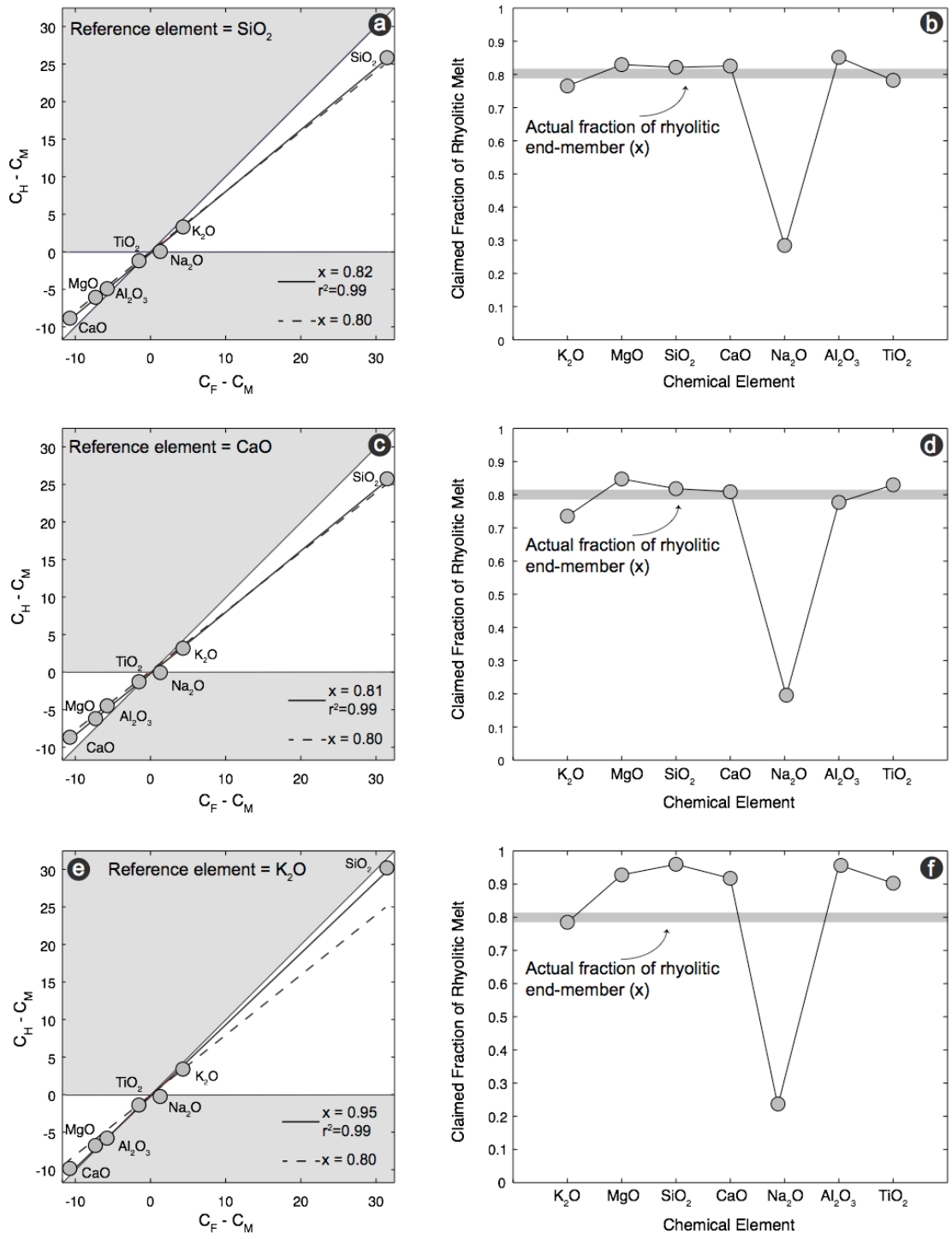

Figure 7: (a-c-e) representative plots resulting from the application of the "mixing test" (Fourcade and Allegre, 1981) considering as reference the hybrid concentrations of SiO_2, CaO and K_2O for the transect T1C of the 212 min experiment (Exp. C); (b-d-f) plots displaying the fraction of rhyolitic end-member claimed by each element (see text for details).

This choice is motivated by the fact that the longer the mixing time, the higher the probability is to find elements with the hybrid composition. Plots resulting from the application of the mixing test are displayed on the left panels of Fig. 7 and 8, respectively.

Note that on C_F-C_M vs. C_H-C_M diagrams only a portion of the plot can be populated by chemical elements for a two end-member mixing process; this portion, represented in the white colour in Figure 7 and 8, is bounded by the lines with slope x=1.0 (i.e. the system is totally constituted by the rhyolitic end-member) and x=0.0 (i.e. the system is totally constituted by the basaltic end-member). As for major elements (Fig. 7), these graphs indicate that all elements fall in the region associated with a two end-member mixing process and that correlation coefficients (r^2) are all very high. At first sight this result may indicate that the selected samples have reached the hybrid compositions for all analysed chemical elements. However, more detailed observations indicate that the estimated proportion of the rhyolitic end-member (i.e. the slope x of the linear interpolation) is, in some cases, incorrect. The right side of Fig. 7 displays plots in which the fraction of rhyolitic end-member claimed by each element is reported. In other words, the value of x calculated for each element from the plots on the left side is reported as a "spider diagram" on the right side. Consider, for example, the plot in Fig. 7b drawn considering SiO_2 as the reference hybrid composition. The plot shows that most of the other elements point correctly to the initial fraction of rhyolitic end-member, with the important exception of Na_2O, for which is inferred a fraction of the rhyolitic end-member of 30%; this value deviates by ca. 50% from the real initial fraction. A similar discussion can be made for the plot in Fig. 7d where the reference element is CaO. In this case, in addition to Na_2O, also K_2O displays a deviation from the initial fraction of rhyolite by about 10%. The plot drawn considering K_2O as the reference element (Fig. 7f) displays strong deviations for most elements. In particular, the largest deviations are observed for Na_2O (ca. 60%), SiO_2 and Al_2O_3 (ca. 15%), and CaO, TiO_2 and MgO (ca. 10%).

The plots for trace elements are presented in Fig. 8 highlight larger deviations from the initial proportion of rhyolitic melt compared to major elements, with most elements claiming for erroneous initial fractions of rhyolite. For example, if Rb or Th is chosen as reference element for the hybrid composition (Fig. 8b and f), all the other trace elements strongly deviate from the actual initial fraction 80% of rhyolitic end-member, with variations in the

range of ca. 60% to 10 %. These variations correspond to r^2 values in the plots of Fig. 8a and e of 0.59 and 0.51, respectively. It is interesting to note that, when La is used as the reference element, the plot in Fig. 8c shows a very good correlation coefficient. However, this good correlation is only apparent because on the plot in Fig. 8d most elements claim for initial fractions of rhyolite that deviate by 10-20%.

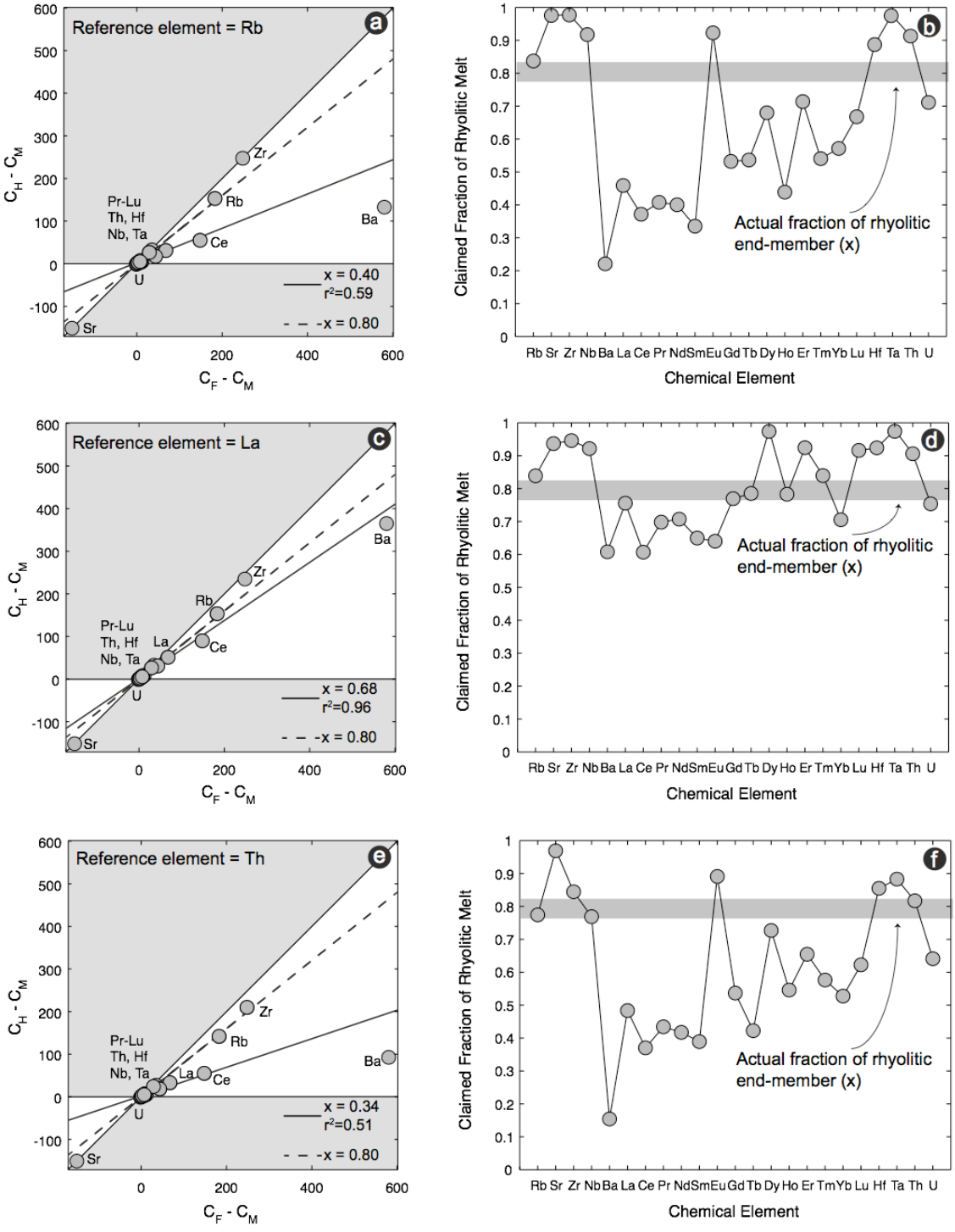

Figure 8: (a-c-e) representative plots resulting from the application of the "mixing test" (Fourcade and Allegre, 1981) considering as reference the hybrid concentrations of Rb, La and Th for the transect T1C of the 212 min experiment (Exp. C); (b-d-f) plots displaying the fraction of rhyolitic end-member claimed by each element (see text for details).

The reason for this is that trace elements are present in very different abundances in the original end-members with concentrations ranging from a few to several hundred ppm. The presence of elements with high concentrations (e.g. Sr, Zr or Ba) exerts a strong influence on the goodness of linear correlation between C_F-C_M vs. C_H-C_M (e.g. Fig. 8c) and in particular it leads to a strong increase of the r^2 value resulting from the linear fitting. This feature is often called the "King Kong" effect (Makridakis et al. 1998) and it is known to produce spurious correlations during linear fitting procedures.

A further issue related to the application of the mixing test is that, for both major and trace elements, elements showing the largest deviations in the plot of Fig. 7 and 8, are also the same elements that in the binary plots of Fig. 5 and 6 are associated with non-linear and scattered patterns of data points.

These results indicate that a two end-member mixing conceptual model fails in explaining the compositional variability triggered by the onset of chaotic mixing dynamics in the experimental samples and that additional processes need to be considered to explain the observed geochemical evolution of the mixing process.

3.4.2 Quantification of element mobility during mixing

The variable correlation of chemical elements in binary plots in magma mixing systems has been already observed in natural rock samples (Perugini et al. 2006), numerical simulations and experiments (e.g. Perugini et al. 2008; De Campos et al. 2011) and it has been related to the on-set of a diffusive fractionation process triggered by the combined action of chaotic flow fields and chemical diffusion. Such a process would produce a different rate of homogenization of chemical elements and a variable scattering in inter-elemental binary plots due to the different mobility of chemical elements (e.g. Perugini et al. 2006, 2008; De

Campos et al. 2004, 2008, 2011; Morgavi et al. 2012). In order to test this hypothesis, a rigorous analysis of element mobility is necessary.

The quantification of element mobility during magma mixing must include all possible factors influencing element mobility (e.g. compositional and rheological variations within the system, fully multicomponent melt thermodynamics, and a complete description of the strain history). As all of these data are never available for a given mixing system, another way must be found to normalize out the effects of absolute diffusive and convective histories.

A quantity commonly used in the fluid dynamics literature (e.g. Liu et al. 2004; Rothstein et al. 1999) to evaluate the degree of homogenization of fluid mixtures is the concentration variance (σ^2). The variance of concentration for a given chemical element (C_i) is given by

$$\sigma^2(C_i) = \frac{\sum_{i=1}^{N}(C_i - \mu_i)^2}{N} \qquad \text{[Eq. 3]}$$

where N is the number of samples, C_i is the concentration of element i and μ is the mean composition. Such a measure decreases with mixing time as the system approaches homogeneity. Variance defined by Eq. [3] depends on absolute values of concentrations of chemical elements. Given the different range of concentrations of elements in the experimental sample (Tab. 1), variance values must be normalized to the initial variance of each element for comparative purposes. Therefore, in the following we refer to concentration variance, or simply variance, considering the following quantity

$$\sigma_n^2 = \frac{\sigma^2(C_i)_t}{\sigma^2(C_i)_{t=0}} \qquad \text{[Eq. 4]}$$

where $\sigma^2(C_i)_t$ and $\sigma^2(C_i)_{t=0}$ is the concentration variance of a given chemical element (C_i) calculated after the experimental time t (i.e. 53, 106 or 212 min) and time t=0 (i.e. the initial variance before the mixing starts), respectively.

The physico-chemical meaning of this measure is illustrated schematically in Fig. 9.

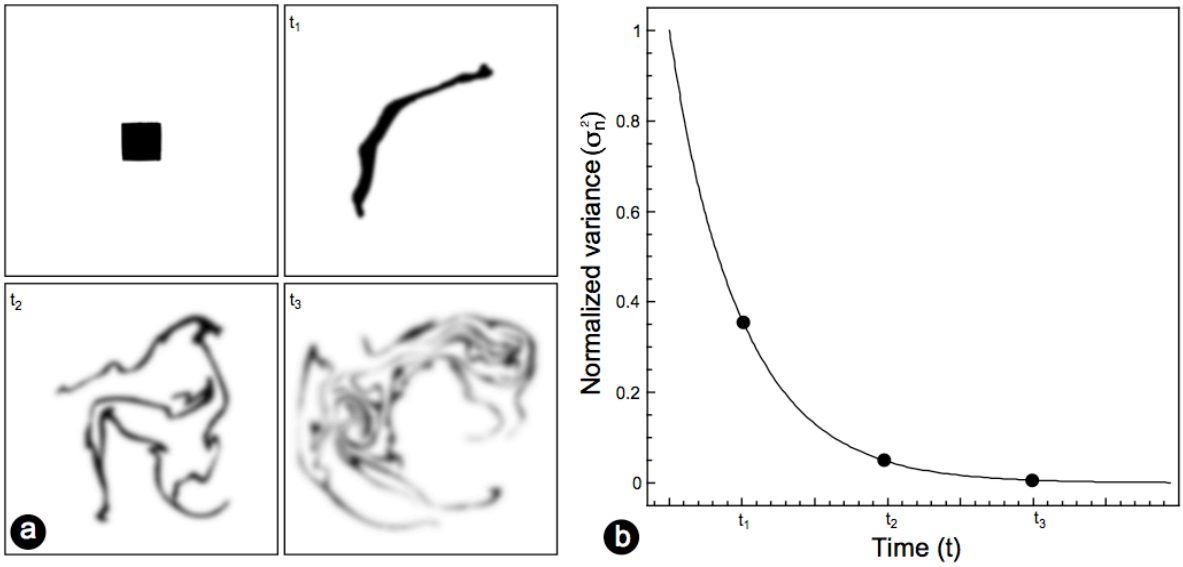

Figure 9: a) Hypothetic evolution in time of a mixing system in which a black colored blob of fluid is mixed with a white colored fluid via stretching and folding processes and chemical diffusion. b) Representative relaxation of concentration variance (σ_n^2) in time (t) for the mixing process shown in (a).

In particular, Fig. 9a shows the hypothetic evolution in time of a mixing system in which a black blob of fluid is mixed with a white fluid via stretching and folding plus chemical diffusion. As the black blob is stretched and folded in time, chemical diffusion becomes progressively more efficient due to the generation of new interfacial areas. Consequently, the system is progressively more homogeneous and, hence, concentration variance (σ_n^2) is expected to decay in time. This is shown in Fig. 9b where σ_n^2 is plotted against mixing time (*t*). σ_n^2 decays quickly during the first stages of mixing and then shows a relaxation towards $\sigma_n^2 = 0$ for long mixing times, indicating that the system is approaching homogeneity.

Concentration variance (σ_n^2) was calculated for all analyzed chemical elements at the three mixing times (i.e. 53, 106, and 212 min). In detail, σ_n^2 for each element was calculated for the three transect (T1-T3) in each experiment and the three values were than averaged to obtain a single value of σ_n^2, which is representative of the degree of homogenization of a

given element in the mixing system. Results are displayed in Fig. 10a and b for some representative major and trace elements, respectively.

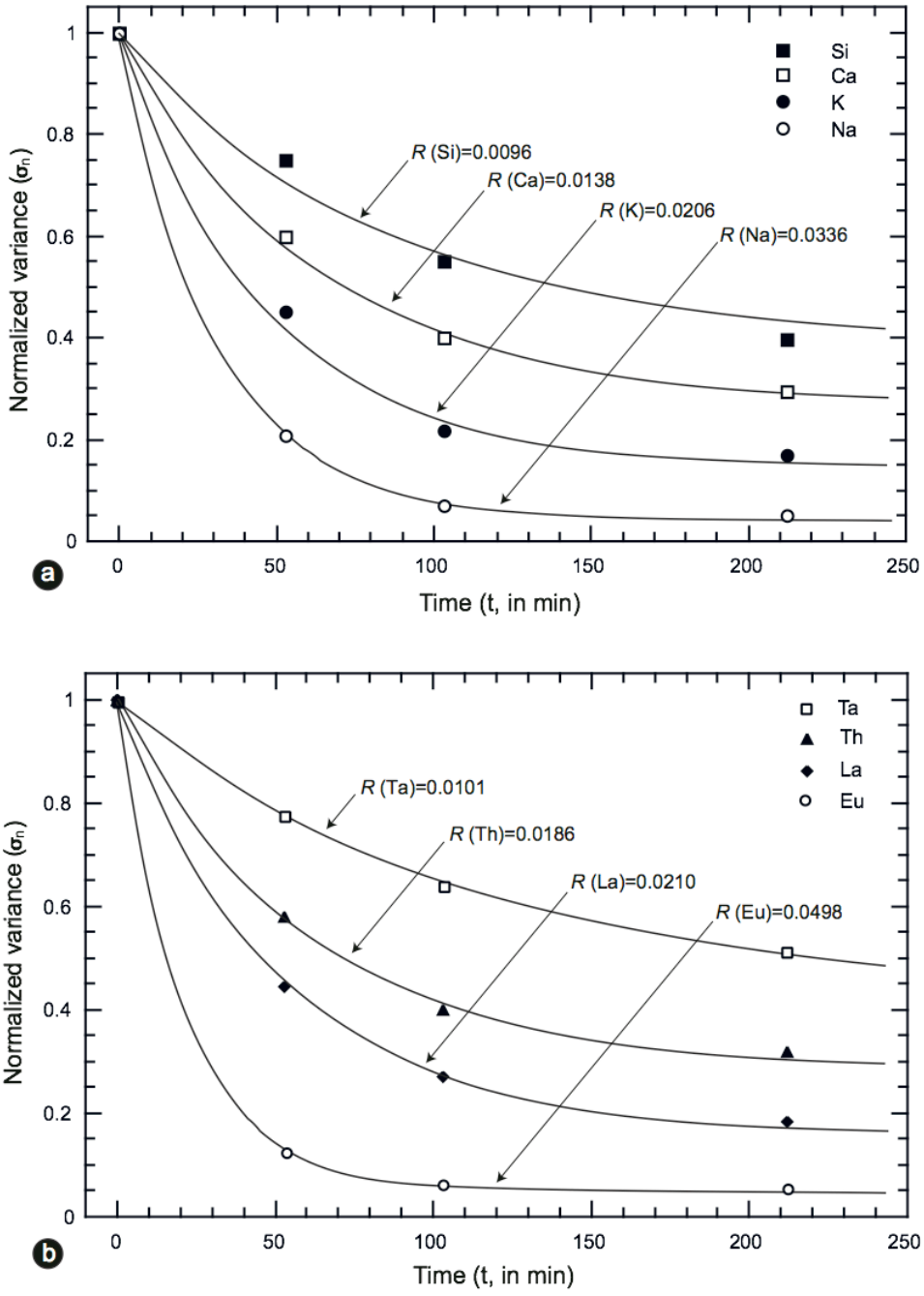

Figure 10: Relaxation of concentration variance (RCV) for some representative major (a) and trace (b) elements fitted using Eq. [5]. The Relaxation of Concentration Variance, RCV, (i.e. parameter R of the fitting in Eq. [5]) is also reported in the graphs for each element.

It can be seen hat σ_n^2 decreases in time, as would be expected from the time evolution of a mixing process progressing towards homogeneity. The plots show that the decay of concentration is very rapid at the start of the mixing process. Illustrating this is the fact that,

depending on the considered chemical element, σ_n^2 decreases by ca. 20-85% after just 53 minutes of mixing, and it continues decaying to 40-95% after 212 minutes (Fig. 10). σ_n^2, therefore, relaxes towards zero as mixing proceeds in time, indicating that the system is approaching homogeneity.

An important result emerging from the plots in Fig. 10 is the fact that the rate of decay of concentration variance ($\sigma^2{}_n$) is different for the different chemical elements. For example, considering the major elements displayed in Fig. 10a, the rate of decay increases from SiO_2 to Na_2O. Analogous discussion can be made for the trace elements shown in Fig. 10b where the rate of decay $\sigma^2{}_n$ increases from Ta to Eu.

A number of studies (e.g. Rothstein et al. 1999; Mathew et al. 2007) have highlighted that the decay of concentration variance during mixing of fluids can be fitted by an exponential function such as

$$\sigma_n^2(C_i) = C_0 \cdot \exp(-Rt) + C_1 \qquad \text{[Eq. 5]}$$

where C_0, R and C_1 are fitting parameters and t is the mixing time. In order to quantify the rate of decay of concentration variance of the different chemical elements in the experimental samples, Eq. [5] was used to fit the change in time of $\sigma^2{}_n$ for all analyzed elements. Fitting examples are reported for the elements displayed in Fig. 10a and b. Correlation coefficients of the fitting (i.e. r^2 values) are always better that 0.98, supporting the idea that concentration decay followed exponential trends. From Eq. [5] it is clear that the rate of concentration decay is governed by the parameter R. We call this parameter "Relaxation of Concentration Variance" (RCV) and we use it as a measure of element mobility during mixing.

The graph of Fig. 11 shows estimated values of RCV for all analyzed chemical elements plotted against their ionic radius. Among major elements, Na displays the highest mobility followed by K, Al, Ca, Mg, Ti and Si. As for trace elements, the order of mobility is: Eu, Gd, Tb, Yb, Dy, Sr, Sm, Ba, Y, Ce, Er, La, Tm, Nd, Th, Hf, Rb, Pr, U, Nb, Zr, Ta. It is interesting to compare the mobility of elements in Fig. 11 with the binary correlation plots

shown in Fig. 5 and 6. Elements with similar RCV values are well correlated; as the difference in RCV values between elements increases, also the quality of the correlation in binary plots deteriorates progressively (compare Fig. 11 and Fig. 5 and 6).

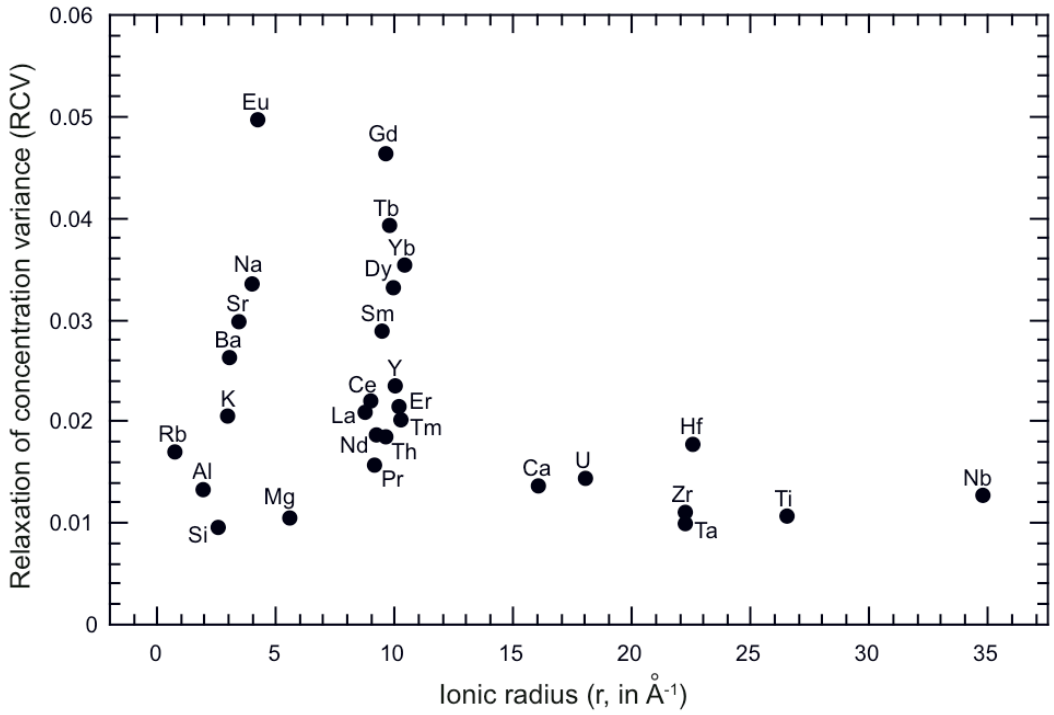

Figure 11: Estimated values of Relaxation of Concentration Variance (RCV) for all analyzed chemical elements plotted against their ionic radius. Ionic radius data from Shannon (1976).

3.4.3 Causes of the differential mobility of chemical elements during mixing

Stretching and folding dynamics during magma mixing and the onset of chemical exchanges (molecular diffusion) are the forces promoting the chaotic mixing process (e.g. Ottino 1989; Aref and El Naschie 1995; Perugini et al. 2003; Perugini and Poli 2004). The fact that mixing is a chaotic process implies that contact area between interacting melts increases exponentially in time and, consequently, chemical exchanges increase progressively. Chemical exchanges are subjected to the so-called "Sensitivity to Initial Conditions" (SIC) of chaotic systems (e.g. Strogatz 1994). The effect of SIC during chaotic mixing manifests itself in the fact that nearby trajectories of the flow fields diverge exponentially in time. As the initial distance between pairs of trajectories decreases, the time span at which they will start to diverge increases exponentially. Chemical diffusion is a flux

responding to the force resulting from chemical potential gradients that moves elements from a certain volume of the magmatic system to another volume, according to a given concentration gradient. The distance travelled by an element depends on its mobility (e.g. diffusion coefficient; *D*): the larger the *D*, the larger the distance. If two elements (*a* and *b*) have very similar values of D , then the distance they will travel in equal times will be about the same; on the contrary, if two elements (e.g. *a* and *c*) have significantly different values of *D* then their respective travelled distances will be substantially different. It follows that, in the same time span, volumes of melts having variable amounts of elements can be generated depending on their relative mobility. The mixing process will disperse these volumes of melts according to SIC. Since elements *a* and *b* are at about the same location, their relative distance will be maintained constant for a certain time during advection. On the contrary, at the same time, elements such as *a* and *c* will experience much more rapidly the effect of SIC because of the larger initial distance. This process is revealed by geochemical variations as a variable correlation between elements in binary plots. As an example, since *a* and *b* have similar *D* values, they will tend to be well correlated in binary plots. On the contrary, at the same time, *a* and *c* will be strongly uncorrelated in binary plots because of their different *D* values. These observations can explain the variable degree of correlation seen in the binary plot of Fig. 5 and 6 in the light of the different element mobility shown in Fig. 11. In particular, it can be said, for example, that among major elements, Na_2O vs. SiO_2 have a different mobility because the relative binary plot shows a curved and scattered pattern (Fig. 5d), whereas CaO and MgO have similar mobilities (i.e. the plot shows a good linear correlation; e.g. Fig. 5f). Similar considerations can be made for trace elements. As an example, since Rb and Ba have a different mobility (Fig. 11), the relative binary plot (Fig. 6f) displays non-linear and scattered patterns. On the contrary, being Zr and Nb characterized by a similar mobility, the Zr-Nb plot shows a linear array of data points.

Results presented in Fig. 11 are worth discussing in the light of literature data on diffusion coefficients, commonly used to quantify the mobility of elements in magmatic

systems. In doing this we need to keep into account that there are virtually no published data of diffusion coefficients for the melts studied in this work and, at most, the comparison can be qualitative. In addition, the comparison here is mostly between diffusivities measured for single homogeneous compositions (i.e. literature data) and strongly heterogeneous compositions generate by a mixing process (i.e. this work). Nevertheless, we believe that such a comparison can be instructive.

Regarding major elements it has been shown (e.g. Baker 1990, 1991) that alkalis (i.e. Na and K) can have much larger diffusion coefficients relative to the other major elements. Our results shown that this is indeed the case because Na and K display the largest RCV values. Regarding the other major elements, they display a quite restricted variation of RCV indicating a similar mobility during the mixing process (Fig. 11). This is in keeping with results reported in the literature (e.g. Baker 1990, 1991) where diffusivities for these elements display quite similar values.

Regarding trace elements, systematic studies of most elements are few (Nakamura and Kushiro (1998); Mungall et al. 1999; Behrens and Hahn (2009). Nakamura and Kushiro (1998) determined trace elements diffusivities for synthetic diopsidic and jadeitic melts. Behrens and Hahn (2009) used trachytic and phonolitic potassium-rich melts. Both studies highlighted that Rb, Sr and Ba have the highest diffusivities, followed by the groups of REEs. This is partially in agreement with results presented in Fig. 11. In detail, Fig. 11 shows that Sr and Ba are among the elements having the largest values of RCV, but Rb has a lower RCV. This latter has an RCV value similar to Hf and Th. Nb, Ta, Zr and U display similar mobilities, whereas Hf and Th shows a larger value of RCV. It is worth noting that from results reported by Nakamura and Kushiro (1998) U and Th have the highest diffusivities for a jadeitic melt, which is contrary to what we obtained from our analysis. These elements have not been reported by Behrens and Hahn (2009). A convergence of our results with those reported by Nakamura and Kushiro (1998) and Behrens and Hahn (2009) regards the elements Nb, Ta, Zr, and Hf. In the plot of Fig. 11 they have the lowest RCV values. This is in

agreement with both Nakamura and Kushiro (1998) and Behrens and Hahn (2009) who have shown that these elements are the slowest diffusing species. Regarding REEs, our results indicate that they are divided into two groups with the light REEs having lower mobilities than the heavy REEs. This result appears in accordance with data from Nakamura and Kushiro (1998) and Behrens and Hahn (2009), where REEs diffusivities tend to decrease from light to heavy REEs. A further issue regards the behavior of Eu. Under reducing conditions Eu is present mostly in the divalent state while the other REEs are present only in the trivalent state. Nakamura and Kushiro (1998) and Behrens and Hahn (2009) have shown that in reducing conditions Eu can have diffusivities that are up to two orders of magnitude higher than the other REEs. This result can explain the larger RCV for Eu relative to the other REEs.

Therefore, whereas for some elements there is a similarity between RCV and diffusion coefficient, for many other elements such a similarity is lacking. We believe that these discrepancies are due to the fact that diffusion coefficients measured for single melts cannot be used directly to study mixing processes, where different melts interact in a complex way. Hence, our results supports the fact that, in the context of mixing, the use of RCV values has advantages over simply considering the diffusion coefficient as the measure quantifying the ability of chemical elements to diffuse in the magmatic system. To reiterate, the RVC parameter incorporates in a single measure a number of variables including: 1) the possible element fractionation due to partitioning into two structurally different melts (e.g. Watson 1976), 2) the compositional dependence of diffusivities (e.g. Zhang 2008), 3) the modulation of diffusivity by fluid-dynamics (e.g. Perugini et al. 2006) and 4) up- and downhill diffusion patterns (e.g. Watson and Jurewicz 1984).

We note however, that although the RCV parameter incorporates all those parameters, we do not know how these parameters interact and what their relative roles are. . Further theoretical and experimental efforts are needed before these relationships can be understood. Practically speaking, we propose the preferential use of RCV values to study the compositional variations during mixing of multicomponent silicate melts. This approach

could be a possible solution until a unifying model, incorporating all these parameters, is available.

3.4.4. Relative mobility of chemical elements in time & conclusion and outlook

An interesting feature emerging from the exponential decay of concentration variance is the relative variation of variance ($\Delta\sigma_n^2$) of couples of chemical elements in time. Consider, as an example, the graph in Fig. 12a, where the exponential relaxation of concentration variance for two chemical elements (A and B), having different mobility in the mixing system, is shown.

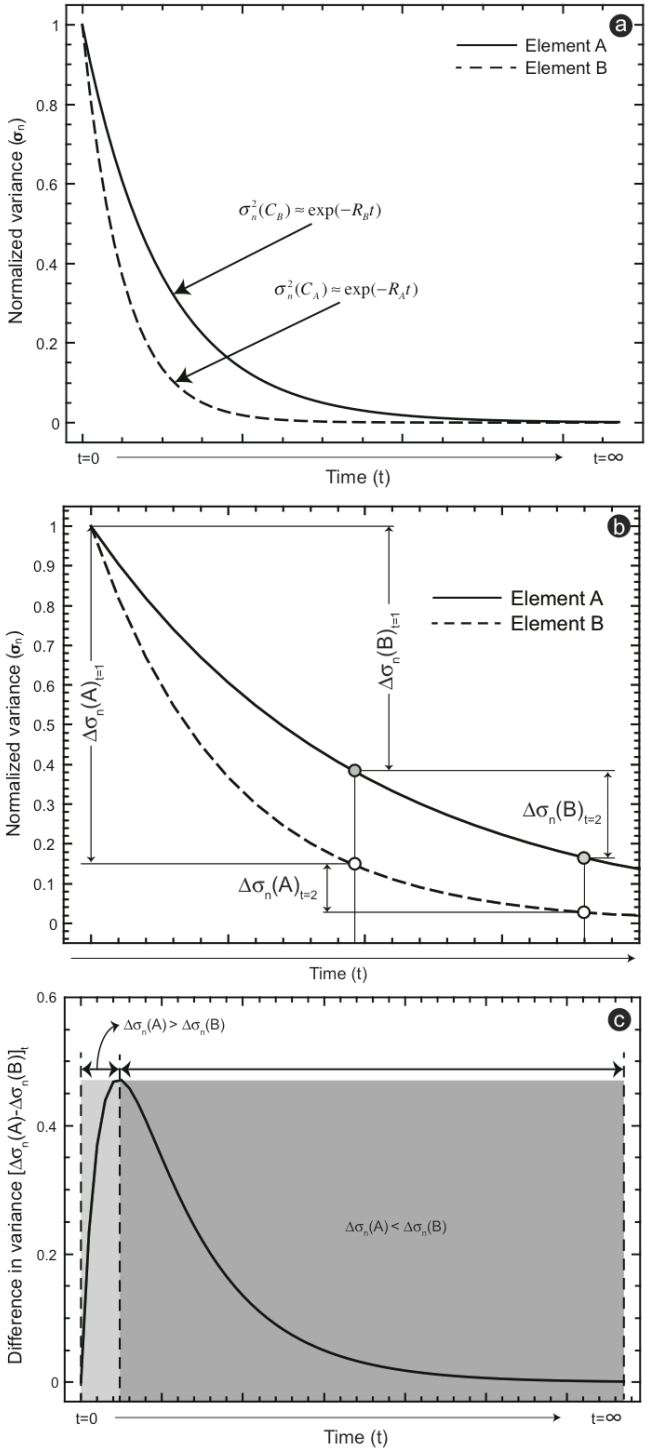

Figure 12: (a) Exponential decay of the concentration variance σ_n^2 *for two hypothetical chemical elements (A and B) having different mobilities. The equation of exponential decay is reported for each element. (b) Enlargement of the plot in (a) showing the different variation in concentration variance* $\Delta\sigma_n^2$ *for the two elements considered s at different mixing time (t). (c) Variation of the difference between the two exponential functions shown in (a)* $\left[\Delta\sigma_n^2(A) - \Delta\sigma_n^2(B)\right]_t$ *against mixing time (t). The graph is divided in two regions where* $\Delta\sigma_n^2(A)_{t=1} > \Delta\sigma_n^2(B)_{t=1}$ *(light gray) and* $\Delta\sigma_n^2(A)_{t=2} < \Delta\sigma_n^2(B)_{t=2}$ *(dark gray).*

The plot of Fig. 12b shows an enlargement of the plot of Fig. 12a. At a given mixing time (e.g. t=1) the two elements (A and B) will have experienced a decay of concentration variance and their $\Delta\sigma_n^2$ values [$\Delta\sigma_n^2(A)_{t=1}$ and $\Delta\sigma_n^2(B)_{t=1}$] will be different. In particular, given that element A has a larger mobility than element B, $\Delta\sigma_n^2(A)_{t=1} > \Delta\sigma_n^2(B)_{t=1}$ (Fig. 12b). This inequality, however, will not hold at all times during the mixing process. Indeed, after a certain time (e.g. t=2) this relationship will be inverted and $\Delta\sigma_n^2(A)_{t=2} < \Delta\sigma_n^2(B)_{t=2}$ (Fig. 12b). This happens because the exponential functions defining the decay of σ_n^2 for the two elements diverge from the beginning of mixing [i.e. $\Delta\sigma_n^2(A)_{t=1} > \Delta\sigma_n^2(B)_{t=1}$], but are destined to converge towards zero in the long mixing time [i.e. $\Delta\sigma_n^2(A)_{t=2} < \Delta\sigma_n^2(B)_{t=2}$]. In the limit of t=∞, the system will be completely homogeneous (i.e. the two exponential functions will both converge to zero) and no difference will exist between the concentration variance of the two elements. This evolution can be visualized in the plot of Fig. 12c, where the difference between the two exponential functions shown in Fig. 12a (i.e. $\left[\Delta\sigma_n^2(A) - \Delta\sigma_n^2(B)\right]_t$) is reported against the mixing time (t). The plot shows a curve increasing during the first stages of mixing, reaching a maximum, and subsequently relaxing to zero for the longest mixing time. This curve divides the plot in two fields. On the left side of the curve, $\Delta\sigma_n^2(A)_{t=1} > \Delta\sigma_n^2(B)_{t=1}$, whereas the right side $\Delta\sigma_n^2(A)_{t=2} < \Delta\sigma_n^2(B)_{t=2}$. The maximum of the curve is the threshold time at which there is a shift between the two kinematic regimes.

This variation of concentration variance in time has important consequences because it highlights the evolution of the compositional heterogeneity in time and its possible impact on the understanding of igneous rocks generated by magma mixing processes. In particular, from the plots of Fig. 10 and 12 it is clear that the probability of retrieving on a given outcrop the compositional heterogeneity produced by mixing for the fastest elements is much lower compared to low mobility ones. In fact, while for the fastest elements the variation of concentration variance ($\Delta\sigma_n^2$) is very large as soon as the mixing process starts and quickly

relaxes to zero, the slower elements in the same time span may still show large $\Delta\sigma_n^2$ values, provided that the system in temporally situated on the left side of Fig. 12c. This means that after a given time only the "residual" compositional heterogeneity associated with the slowest elements might be observable in the mixing system. Observation of the plot in Fig. 11 and the binary plots in Fig. 5 and 6 indicate that, when the slowest mobility elements are compared, they tend to display linear correlations. This might lead one to think that the classic two end-member mixing model can be revived and applied in the study of magma mixing processes. This is however only partially true because although this conceptual model might be valid for those elements, it would likely lead to fallacious interpretations for others. The first pitfall is the temptation to reconstruct of the starting composition of the end-member melts that participated to the mixing process. In fact, this could be done in principle only for a limited range of chemical elements, provided that the two end-member compositions are still recognizable in the mixing system. As we have shown here, the mafic melt tends to disappear from the mixing system as soon the mixing process starts, strongly undermining the possibility to reconstruct its original composition. In addition, also assuming that the two starting composition are still preserved the question arises as to what criteria to use to identify the starting composition of the initial end-members for the high mobility elements. As shown above, indeed, these elements are very likely to produce hybrid compositions in short mixing time. This means that our ability to the recover their concentrations in the starting end-members is strongly hindered. In fact, we will never know whether the homogeneous composition observed for those elements in the mixed system is the result of complete homogenization due to mixing or the two initial melts actually had the same concentrations for those elements. This may lead to an erroneous definition of end-members and can prevent proper interpretation with deep consequences. Indeed, mafic and felsic end-members are typically used to infer the type of source region in the Earth mantle and crust, respectively. In turn, this information may be used to investigate, for instance, crustal structuring processes or

crust-mantle interaction in different geodynamic setting. Thus, an erroneous interpretation and reconstruction of end-members can produce incorrect geological and geodynamic interpretations. Thus, a careful examination of the compositional variability of igneous rocks suspected to have undergone magma mixing processes is needed before making direct inferences about source regions of magmas from the composition of the apparent end-members. This is a major challenge for future petrologic research because it requires an approach combining detailed determination of the compositional variability on natural rock samples, numerical modeling, and experimental research. In particular, efforts should be made to perform experiments constrained as much as possible by the topological properties of mixing structures observed in igneous rocks and geochemical data on natural samples. Therefore it will be very important to investigate the morphochemistry of patters produce by mixing.

Chapter 4

MORPHOCHEMISTRY OF PATTERNS PRODUCED BY MIXING OF RHYOLITIC AND BASALTIC MELTS

Summary

In this work we present the results of time series experiments performed by mixing basaltic and rhyolitic melts at high temperature using a device recently developed to trigger chaotic dynamics in a mixing system. The morphology of mixing patterns is quantified at different times by measuring their fractal dimension and a linear relationship is derived between mixing time and morphological complexity. The complexity of mixing patterns is also compared to the degree of homogenization of chemical elements during mixing and empirical relationships are established between the fractal dimension and the temporal variation of concentration variance of elements.

New concepts and tools to study the magma mixing process unfold from the experimental results presented in this work: i) the mixing patterns are fractals and they can be quantified by measuring their fractal dimension representing a further step in the quantification of the magma mixing process; ii) the relationship between the fractal dimension of the mixing patterns and mixing time is linear and has important volcanological implications as the analyses of the morphology of mixing patterns in volcanic rocks can be complemented by experiments to build a new chronometer to estimate the mixing-to-eruption time; iii) the relationships between the fractal dimension of mixing patterns and concentration variance represent the first morphochemical study in igneous petrology bringing with it the potential to infer the relative mobility of chemical elements during the time progression of mixing by analyzing the morphology of mixing patterns in the rocks.

1. Introduction

Magma mixing is widely recognized to be a ubiquitous petrologic process in the evolution of the Earth system (e.g. Anderson, 1982, Abe, 1997) and a major process in generating the diversity of igneous rocks (e.g. Bateman, 1995; Bergantz, 2000; Perugini et al., 2006; Slaby et al., 2011). In addition, the injection of mafic magmas into felsic magma chambers is regarded as a key process that can trigger highly explosive volcanic eruptions (e.g. Sparks et al., 1977; Murphy, 1998; Leonard et al., 2002; Martin et al., 2008; Perugini et al., 2010). An understanding of the details of magma mixing, therefore, is of primary importance for petrology and volcanology, with direct implications for the interpretation of the compositional variability of igneous rocks as well as in hazard assessment in active volcanic areas.

Some of the most striking evidence of magma mixing in igneous rocks is the occurrence of textural heterogeneity, and the processes responsible have been discussed extensively (e.g. Eichelberger, 1975; Anderson, 1976; Bacon, 1986; Snyder, 2000; Perugini and Poli, 2005; Perugini and Poli, 2012). This heterogeneity includes enclaves, banding, and "streaky" structures (e.g. Didier and Barbarin, 1991; Wada, 1995; De Rosa et al., 1996; Ventura, 1998; Smith; 2000; De Rosa et al., 2002; Perugini and Poli, 2002; Perugini et al., 2007). Recent studies on the mineralogical and geochemical features of mixed rocks (e.g. Hibbard et al., 1981; 1995; Wallace and Bergantz, 2002; Costa and Chakraborty, 2004; Perugini et al., 2005; Slaby et al., 2010; 2011), as well as those focused on quantitative analyses of morphologies related to textural heterogeneity (e.g. Wada, 1995; De Rosa et al., 2002; Perugini and Poli, 2002; Perugini et al., 2002; 2004) have highlighted the dominant role played by chaotic mixing dynamics in producing the substantial complexity of geochemical variations and textural patterns found in the resultant rocks (e.g. Flinders and Clemens, 1996; De Campos et al., 2011; Morgavi et al., 2012; Perugini et al., 2012). Despite significant attention in the past, however, few works have focused on the understanding of the relationship between the morphology of the mixing patterns and the geochemical variability

of the system (e.g. De Rosa et al., 2002; Perugini et al., 2004). There is a paucity of data concerning the link between the complexity of mixing patterns and the compositional heterogeneity triggered by the mutual dispersion of melts with different initial compositions. Yet this aspect appears particularly relevant in the light of recent results obtained from natural samples, numerical simulations and experiments that indicate a key role being played by chaotic mixing processes in generating scale-invariant mixing patterns (i.e. fractals) propagating from the meter to the micrometer length scale in the magmatic mass (e.g. Perugini et al., 2003; Perugini et al., 2008; De Campos et al., 2008, 2011; Petrelli et al., 2011; Morgavi et al., 2012). The generation of such structures implies the development of large contact interfaces between interacting melts through which chemical exchanges are strongly amplified leading to highly variable degrees of homogenization depending on the different mobility of chemical elements and thermal and rheological properties of interacting melts (e.g. Perugini et al., 2006; 2008; De Campos et al., 2011; Perugini et al., 2012; Perugini and Poli, 2012; Morgavi et al., 2012). In addition, preliminary results indicate that the study of the time evolution of compositional exchanges between magmas can be effectively modeled, leading to the prospect that the record of magma mixing processes may serve as chronometers to estimate the time interval between mixing and eruption (Perugini et al., 2010).

Here we present the results of new time series magma mixing experiments performed using basaltic and rhyolitic melts. The mixing process is triggered by a recently developed experimental apparatus generating chaotic dynamics in the system, a process amply recorded in natural outcrops (e.g. Flinders and Clemens, 1996; De Rosa et al., 2002; Perugini et al., 2006). The morphology of mixing patterns at different times is quantified by measuring their fractal dimension and an empirical relationship between mixing time and morphological complexity is derived. The complexity of mixing patterns is also compared to the degree of homogenization of chemical elements during mixing and empirical relationships are established between the fractal dimension and the variation of concentration variance of chemical elements in time. The petrologic and volcanologic implications are discussed.

2. Magma mixing experiments

2.1 End-member selection and preparation

Experiments were performed using natural basaltic and rhyolitic compositions from the Bruneau Jarbidge eruptive center (Snake River Plain). The basalt and rhyolite belong to the Mary's Creek and Cougar Point Tuff (CPT; unit V) outcrops, respectively (Bonnichsen, 1982; Cathey and Nash, 2009). The basalt end-member was collected from a lava flow having a thickness of 2-4 meters and showing columnar jointing. The sample consists of a microcrystalline groundmass mostly constituted by plagioclase, in which phenocrysts of plagioclase, clinopyroxene and olivine are present. The rhyolite end-member was collected from an ignimbrite deposit (cooling unit V; Bonnichsen, 1982) with thickness of 10-20 meters. The sample has a glassy groundmass with a few amounts (less than 5%) of phenocrysts of quartz, plagioclase, and sanidine.

Powders from end-members were melted and homogenized using a concentric cylinder viscometer geometry (Dingwell, 1986). The melts were stirred in a $Pt_{80}Rh_{20}$ crucible for 72 hours at 1600°C for the rhyolite and 6 hours for the basalt. This procedure yielded, after quenching of the samples in air, homogeneous bubble- and crystal-free glasses that were used as starting materials in the chaotic mixing experiments. The major element compositions of the starting basaltic and rhyolitic end-members are given in Tab. 1. Further details about the preparation of end-member glasses are given in Morgavi et al. (2012).

	Basalt	Rhyolite
SiO_2	48.44	78.64
Al_2O_3	16.30	9.75
TiO_2	1.77	0.23
FeO_{tot}	12.20	1.83
MgO	7.47	0.12
CaO	11.54	0.82
MnO	0.28	bdl
Na_2O	1.95	3.45
K_2O	0.31	4.50
P_2O_5	0.43	bdl
Total	100.68	99.34
η (log Pas)	0.86	4.75
ρ (g/cm^3)	2.98	2.33

Table 1: Concentrations of major elements in the basaltic and rhyolitic end-member glasses used in the mixing experiments. Concentrations are given in weight percentage. For analytical conditions see section 3.2. Values of density (ρ) and viscosity (η) of the two end-members are also reported.
Further details about the preparation of end-member glasses are given in Morgavi et al. (2012).

2.2 Experiments

Mixing experiments were performed using the chaotic mixing device installed at Department for Earth and Environmental Sciences, Ludwig-Maximilians University, Germany (LMU). This device consists of an outer cylinder as well as an inner cylinder, the latter of which is located off-center (Fig. 1).

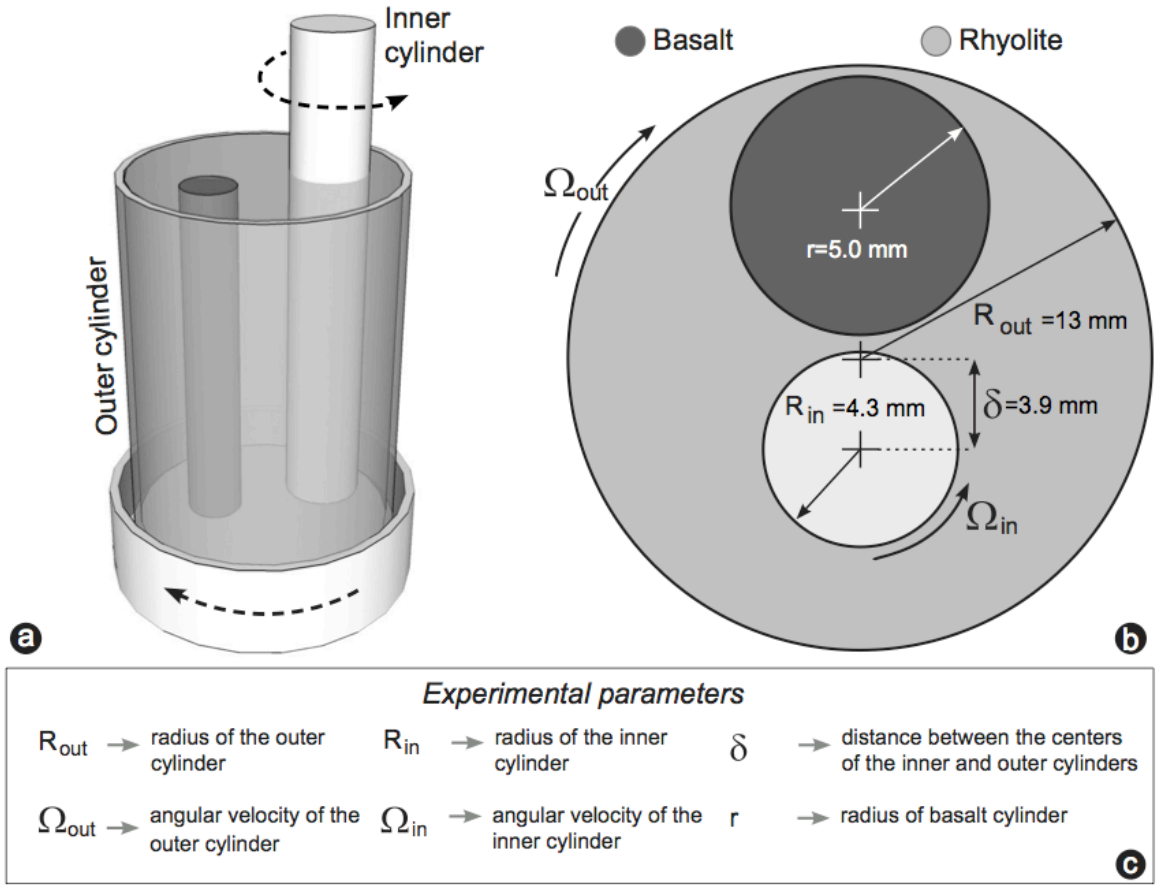

Figure 1: (a) schematic 3D-model and (b) 2D section of the experimental apparatus used to perform chaotic mixing experiments. In the figure experimental parameters are also reported (c). Their values are as follows: R_{out}=13 mm, Ω_{out}=0.06 rpm, R_{in}=4.3 mm, Ω_{in}=0.3 rpm, d=3.9, r=5.0 mm. Further details about the experimental setup can be found in Morgavi et al. (2012).

Both cylinders are fabricated from a $Pt_{80}Rh_{20}$ alloy. As illustrated in De Campos et al. (2011) and Perugini et al. (2012) the independent rotation of the two cylinders generates chaotic streamlines. The choice of triggering the mixing process by chaotic dynamics was motivated by the fact that the study of natural examples has led to the inference that the magma mixing process can be defined as a chaotic process (e.g. Flinders and Clemens 1996; De Rosa et al. 2002; Poli and Perugini 2002; Perugini et al. 2003, 2006). The experimental system used here contains all the essential physical ingredients to replicate the magma mixing process.

The outer cylinder of the experimental system (Fig. 1) was filled with the rhyolitic end-member and cooled down to room temperature to produce a glass. From this glass body two cylinders were drilled out, one at the position of the inner cylinder, and a second one at the initial position of the basaltic end-member (Fig. 1). The experimental protocol (i.e. relative number of rotation of the two cylinders) was chosen to ensure the occurrence of chaotic dynamics within the entire experimental sample. The protocol consists of alternating rotations of the outer and inner cylinders in the following sequence: (1) two complete rotations of the outer cylinder in 35 min; (2) six complete rotations of the inner cylinder in 18 min. The Reynolds number during experiments was the order of 10^{-7} (see De Campos et al., 2011 and Perugini et al., 2012 for further detail about the experimental setup and protocol). Three experiments were performed at 1350 °C with identical starting conditions (Fig. 1). Durations of experiments were 53, 106, and 212 min, corresponding to the application of one, two and four experimental protocols. Below we refer to those experiments as Exp.1, Exp. 2 and Exp. 3. Initial proportions of end-members were: rhyolite 80% and basalt 20% by volume. The viscosity ratio during experiments was calculated to be 7.8×10^3. After the application of the mixing protocol, the experiment was terminated allowing the melt to cool to room temperature. Samples were recovered by coring out a cylinder with a radius of 11.0 mm from the crucible (outer cylinder). Each core was then sectioned perpendicular to its long axis

into slices (ca. 4.0 mm in thickness) for further analyses. One representative slice was selected for each experiment (Fig. 2) and used for the analyses.

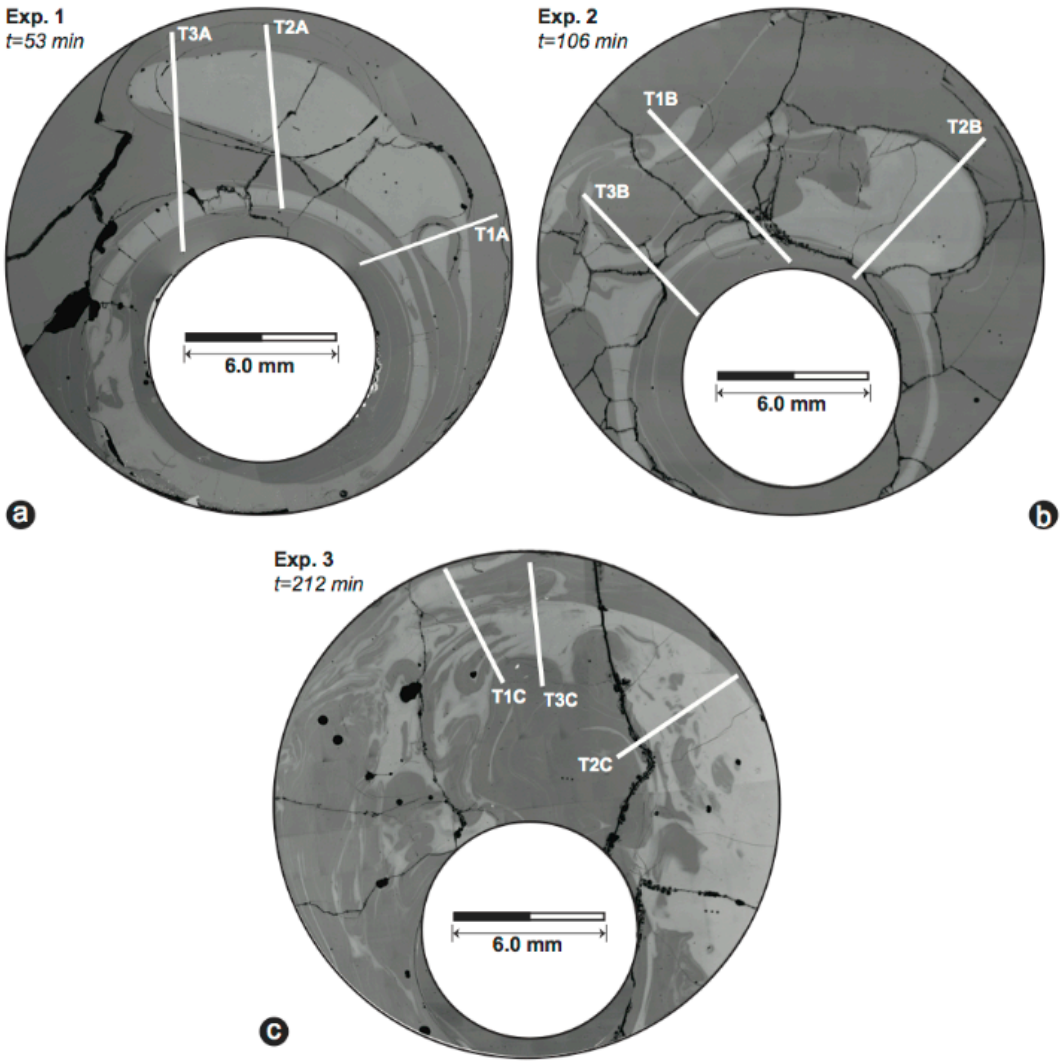

Figure 2: Representative BSE images of the three chaotic mixing experiments at different mixing times (t): a) Exp. A, t=53 min, b) Exp. B, t=106 min), c) Exp. C, t=212 min. On the images are also marked the transects (T) along which geochemical analyses of major and trace elements have been performed.

3. Analysis of mixing patterns

3.1 Optical analysis

Fig. 2a-c shows Back-Scattered-Electron (BSE) images for each the three experiments. These images show that the basaltic end-member melt was dispersed within the rhyolitic one by stretching and folding dynamics triggered by the chaotic mixing protocol. In the following we refer to the least evolved and most evolved melts as mafic and felsic, respectively. After 53 min (Fig. 2a) the basaltic melt (light grey color) generated a filament-

like pattern in the rhyolitic melt (dark grey color) around the inner cylinder. The top part of the sample shows an ellipsoidal blob of the mafic melt, which is connected with this filament in the lower part of the image. On the right side of the experiment a small volume of felsic melt, containing a drop-like morphology of mafic melt, infiltrated within the blob of mafic material. The 106 min experiment (Exp. 2) shows an evolution of the mixing pattern (Fig. 2b) towards a higher mixing intensity. The mafic melt is much more deformed and shows a larger number of stretched and folded filaments both around the inner cylinder and on the left side of the image. The right side of the sample shows that the ellipsoidal blob of mafic melt evolved towards a sub-circular morphology in which, from the left side, the felsic magma infiltrates. After 212 min (Fig. 2c; Exp. 3) filament-like structures are strongly deformed and an intricate lamellar pattern consisting of alternate filaments of mafic and felsic melts is visible. This mostly occurs in the left part of the sample. On the right side of the sample the mafic melt incorporated filaments and small blobs of the felsic magma.

3.2 Geochemical analysis

Concentrations of major elements were measured with a Cameca SX100 (Earth and Environment, LMU-Munich). The electron microprobe operating conditions were 15 kV acceleration voltage and 20 nA beam current. A defocused 10-µm beam was used for all elements in order to minimize alkali loss. Synthetic wollastonite (Ca, Si), periclase (Mg), hematite (Fe), corundum (Al), natural orthoclase (K), and albite (Na) were used as standards, and a matrix correction was performed by PAP procedure (Pouchou and Pichoir, 1984). Standard deviations were lower than 2.5% for all analyzed elements.

On each experiment, the compositional variability was studied along three different compositional transects (T) (Fig. 2a-c). The three transects were chosen to cover different segments of the mixing pattern characterized by variable amounts of filaments of the two melts to characterize at best each sample (see below). The number of analyzed data points (N)

was (Fig. 2): Exp. 1 (T_{1A}, N=90; T_{2A}, N=115; T_{3A}, N=142), Exp. 2 (T_{1B}, N=126; T_{2B}, N=90; T_{3B}, N=121), Exp. 3 (T_{1C}, N=81; T_{2C}, N=98; T_{3C}, N=83).

The compositional variability along three representative transects (T_{1A}, T_{1B}, T_{1C}; Fig. 2) at different mixing times is presented in Fig. 3.

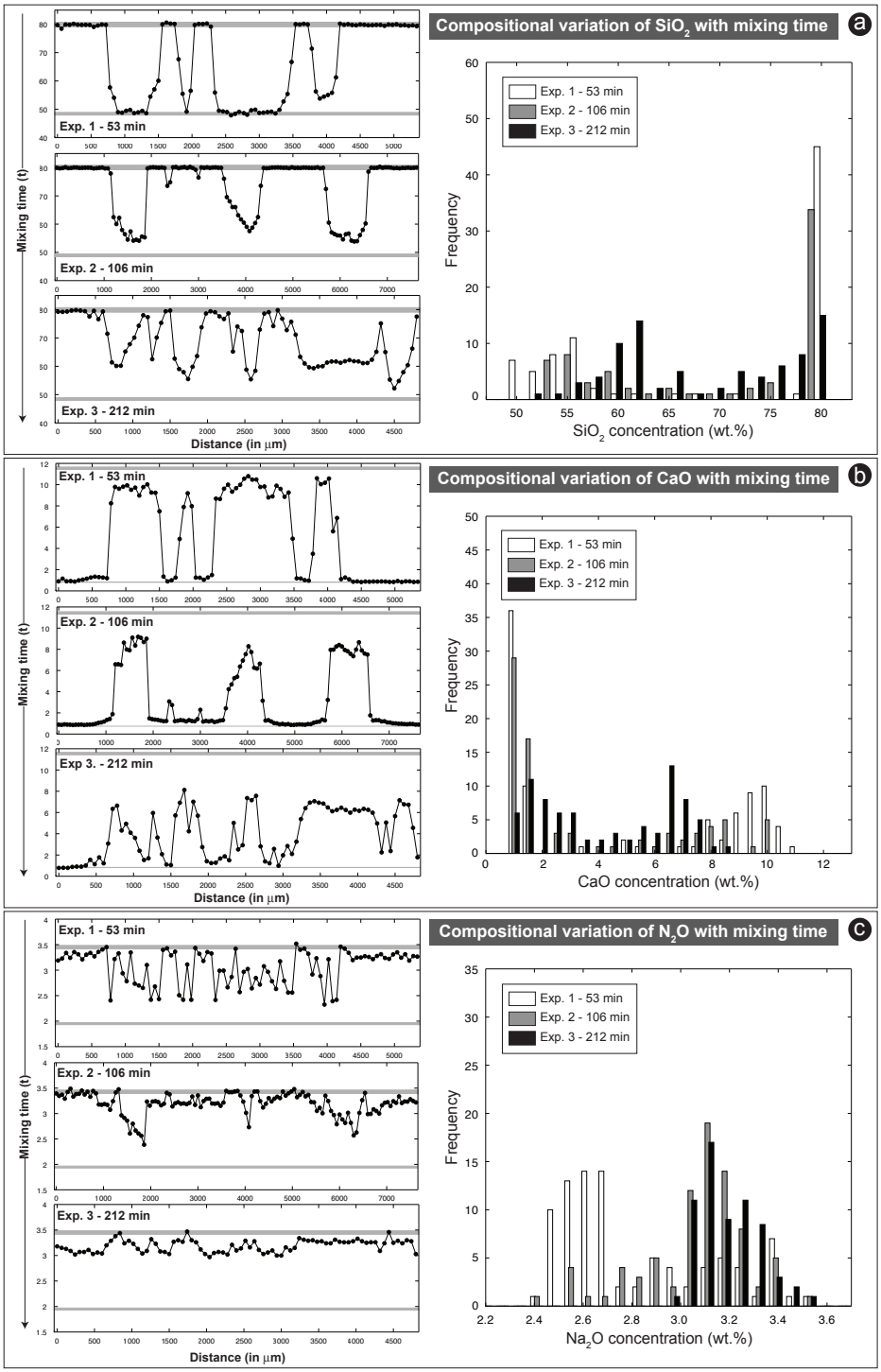

Figure 3: Compositional variation along three representative transects and on compositional histograms at different mixing times for representative major elements: (a) SiO_2, (b) CaO, and (c) Na_2O. In the left panels concentrations of initial basaltic and rhyolitic melts are marked in different grey shades. These are reported as a range (grey areas) to include analytical uncertainties.

In Fig. 3 are also marked element concentrations for both the end-members to better decipher the time evolution of mixing. In general, element variability exhibits an oscillatory pattern corresponding to the alternating occurrence of filaments of the two melts. Element concentrations increase (or decrease) continuously passing from one filament to the other defining smooth patterns. This indicates that, in addition to the stretching and folding mechanism responsible for mechanical mixing, also chemical diffusion occurred among filaments. Filaments have different thicknesses as indicated by the different widths of the compositional fluctuations (Fig. 3).

The compositional variations displayed on the left panels of Fig. 3 also indicate that the degree of homogenization of chemical elements is different. This is evident from the comparison between the variability in concentration for SiO_2, CaO and Na_2O. In particular, passing from SiO_2 to Na_2O it is clear that the compositional variability decreases progressively (Fig. 3). As shown by Morgavi et al. (2012) this feature is related to the different mobility of chemical elements during the mixing process that produces different degrees of hybridization at the same time and in the same mixing system.

To better appreciate this feature, the right panels of Fig. 3 display compositional histograms obtained plotting together the compositional variability of the aforementioned elements at the three different mixing times. As shown by Perugini et al. (2004; 2008) compositional histograms for a mixing system evolve in time from the original end-member compositions (i.e. the compositional histogram is constituted by two populations of concentrations corresponding to the two initial end-members) to a bell-shape whose maximum corresponds to the hybrid composition. If the mixing process is eventually completed (i.e. a homogeneous volume of melt with the hybrid composition is generated) the compositional spectrum collapses to a single population whose concentration coincides with the hybrid composition. The histograms of Fig. 3 display that, as mixing process evolves in time, the compositional variability narrows differently for the different elements. In particular, Na_2O displays an evolution towards a bell-shape pattern indicating a higher degree of

homogeneity compared to SiO_2 and CaO that, at the same time, still show a broader range of compositions.

Since the study of the relationships between the time-evolution of complexity of the mixing patterns and compositional variability in the experimental systems is the main goal of this work, a rigorous quantification of the degree of compositional variability in the mixing system for the different elements is necessary.

A quantity commonly used in the fluid dynamics literature (e.g. Liu et al., 2004; Rothstein et al., 1999) and recently employed in the study of magma mixing (e.g. Perugini et al., 2012; Morgavi et al., 2012) to evaluate the degree of homogenization of fluid mixtures is the concentration variance (σ^2). The variance of concentration for a given chemical element (C_i) is given by

$$\sigma^2(C_i) = \frac{\sum_{i=1}^{N}(C_i - \mu_i)^2}{N} \qquad \text{[Eq. 1]}$$

where N is the number of samples, C_i is the concentration of element i and μ is the mean composition. Such a measure decreases with mixing time as the system approaches homogeneity. Variance defined by Eq. [1] depends on absolute values of concentrations of chemical elements. Given the different range of concentrations of elements in the experimental sample (Tab. 1), variance values must be normalized to the initial variance of each element for comparative purposes. Therefore, in the following we refer to concentration variance, or simply variance, considering the following quantity

$$\sigma_n^2 = \frac{\sigma^2(C_i)_t}{\sigma^2(C_i)_{t=0}} \qquad \text{[Eq. 2]}$$

where $\sigma^2(C_i)_t$ and $\sigma^2(C_i)_{t=0}$ is the concentration variance of a given chemical element (C_i) calculated after the experimental time t (i.e. 53, 106 or 212 min) and time t=0 (i.e. the initial variance before the mixing starts), respectively.

Concentration variance (σ^2_n) was calculated for chemical elements at the three mixing times (i.e. 53, 106, and 212 min). In detail, σ^2_n for each element was calculated for the three transect (T1-T3) in each experiment and the three values were than averaged to obtain a single value of σ^2_n, which is representative of the degree of homogenization of a given element in the mixing system. Tab. 2 shows the values of σ^2_n at the different mixing times and indicated that concentration variance decreases progressively in time, as should be expected by the evolution of a mixing process. σ^2_n values also indicates that the time variation in concentration variance is different for the different elements. In particular, the rate of decay of σ^2_n increases in the following sequence: SiO_2, TiO_2, Al_2O_3, MgO, CaO, FeO_{tot}, K_2O and Na_2O indicating that moving from SiO_2 to Na_2O the rate of homogenization of chemical elements increases (Morgavi et al., 2012).

	Exp. 1	**Exp. 2**	**Exp. 3**
t (in min)	53	106	212
D_{box}	1.15	1.47	1.68
		σ^2_n	
SiO_2	0.81	0.46	0.40
Al_2O_3	0.69	0.40	0.34
TiO_2	0.76	0.44	0.36
FeO	0.58	0.30	0.28
MgO	0.75	0.43	0.34
CaO	0.66	0.35	0.29
Na_2O	0.21	0.07	0.05
K_2O	0.45	0.22	0.17
	a	b	c
SiO_2	0.20	7	0.46
Al_2O_3	0.29	33	0.26
TiO_2	0.23	11	0.37
FeO	0.25	195	0.18
MgO	0.21	11	0.38
CaO	0.25	45	0.24
Na_2O	0.06	193024	0.08
K_2O	0.18	1117	0.14

Table 2: Summary of the different parameters characterizing the mixing patterns. Values of fractal dimension (D_{box}), concentration variance (σ^2_n) and fitting parameters (a, b, and c) of the curves shown in Fig. 7, are reported.

3.3 Fractal analysis of mixing patterns

Recent works indicate that the time evolution of magma mixing processes generates fractal morphologies (e.g. Wada, 1995; De Rosa et al., 2002; Perugini et al., 2003). This is the

result of the development of chaotic dynamics during mixing, the latter governed by the stretching and folding of the magmas involved in the process (e.g. Flinders and Clemens, 1996; Perugini et al., 2003; 2006). Given that the experiments presented in this work were performed under chaotic dynamic condition, we used fractal statistics to quantify the complexity of mixing patterns.

One of the most used techniques to measure the fractal dimension on digital images is known as the "box-counting" method. Before applying this technique, BSE images (Fig. 2) need to be converted to binary (black and white) images. This is done by thresholding grayscale images, to produce pictures in which the mafic and felsic melts appear in black and white colors, respectively (Fig. 4a-c). The interface between mafic and felsic magmas is then replaced by a black line (Fig. 4d-f). These operations were performed using the ImageJ software (Abramoff et al., 2004).

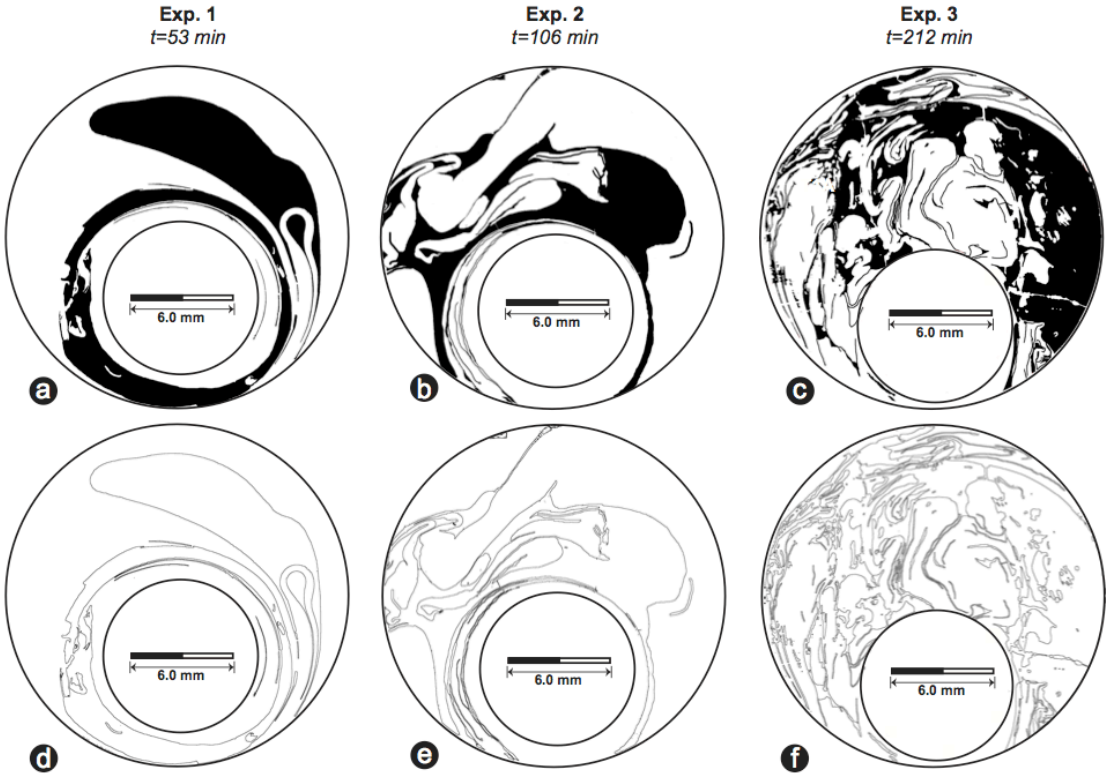

Figure 4: Black and white segmented images of the mixing patterns for the experiments performed at different mixing time: (a) 53 min, (b) 106 min, and (c) 212 min. (d-f) contact interfaces between the two melts traced from the binary images shown in (a-c). See text for details.

The images containing the interface between the two melts were used to measure the fractal dimension of the mixing patterns using the box-counting technique. This technique has been proved to be a robust tool to quantify mixing patterns in both plutonic and volcanic rocks (e.g. Wada, 1995; Perugini et al., 2003; Perugini and Poli, 2005). With the box-counting technique a square mesh of size (r) is laid over the image and the number of boxes (N_r) containing the black pixels belonging to the interface between the two melts is counted (e.g. Mandelbrot, 1982). As an example, Fig. 5a-c reports some steps of the application of the box-counting method to the mixing pattern produced after a time of 212 min. Mandelbrot (1982) showed that, for fractal patterns, the following relationship is satisfied:

$$N_r = r^{-D_{box}} \qquad \text{[Eq. 3]}$$

Using logarithms, [Eq. 3] can be also written as

$$\log(N_r) = -D_{box} \cdot \log(r) \qquad \text{[Eq. 4]}$$

[Eq. 4] shows that, in order to classify a structure as a fractal, data must lay on a straight line in the log-log plot, where the fractal dimension (D_{box}) is estimated as the slope resulting from the linear interpolation of the log(r) vs. log(N_r) graph.

Fig. 5d shows the variation of the number of boxes (N_r) containing the black pixels belonging to the interface between the two melts against the box size (r), whereas the graph in Fig. 5e displays the corresponding log-log plot. It is shown that data points follow a linear distribution indicating that interfaces are fractals. Measurements of fractal dimension of the mixing patterns were performed using the software MorphoUt 1.0: this software has been extensively tested on structures with known fractal dimension and results are found to be very accurate (Perugini, 2002).

The uncertainty of D_{box} due to the reduction of the original grayscale images to black and white images has been checked by performing several measurements of fractal dimension on binary images of the same structure obtained at different threshold levels. Results indicate that for a large range of threshold levels (from 45 to 180, in grey values), the fractal dimension of the interface between magmas shows little variations leading to fractal

dimension estimates with an error better than 0.5%. This happens because the color contrast between the mafic and felsic magmas is strong enough and allows us to separate very well the interface for a large range of threshold values. Values of fractal dimension of the mixing patterns were measured in the range of threshold values where D_{box} shows little variations. In particular, the values of fractal dimensions for the 53, 106, and 212 min experiments are 1.15, 1.47, and 1.68 (Tab. 2).

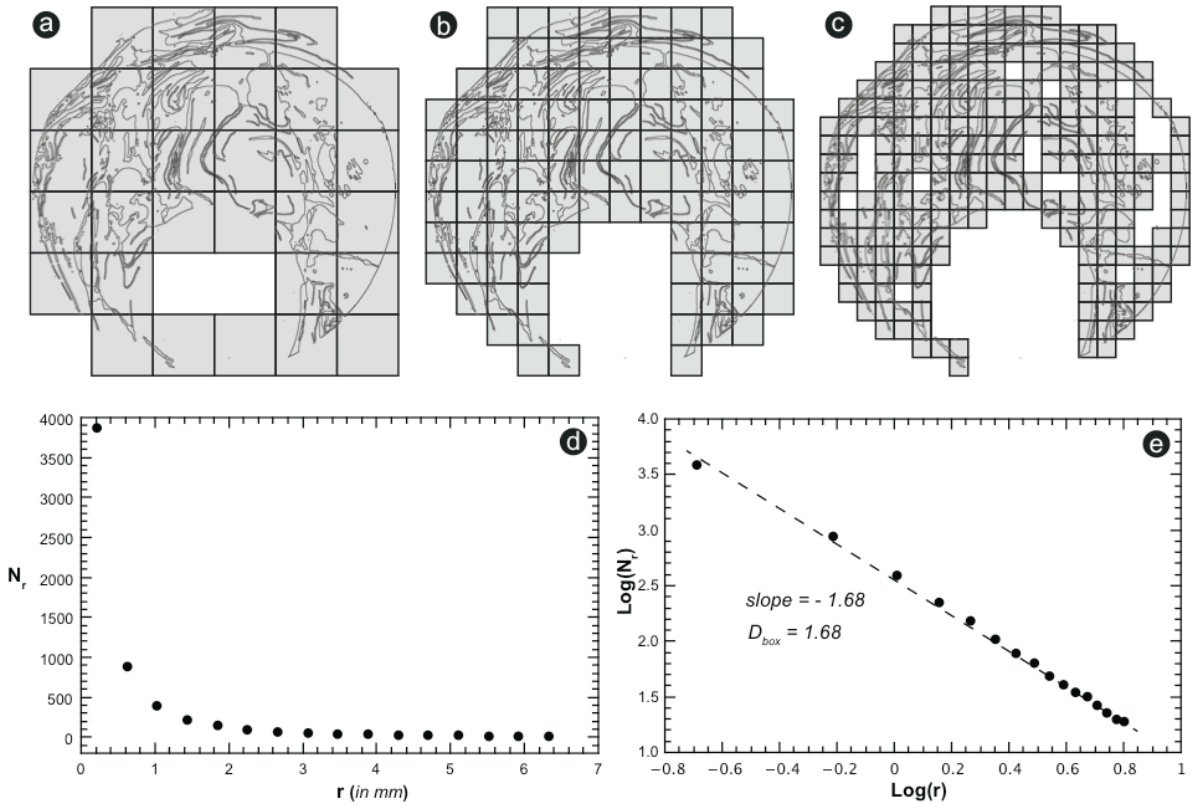

Figure 5: (a-c) Graphical representation of the application of the box-counting technique on the mixing pattern produced after an experimental time of 212 min. A mesh of different sizes (r) is placed over the image and the number of boxes (N_r) containing a part of the interface between the two melts is counted; (d) plot of r against N_r for the mixing pattern shown in Fig. 2c; (e) log-log plot of r against N_r for the mixing pattern shown in Fig. 2c showing the linear relationship between these two parameters and, hence, the fractal nature of the mixing pattern. The estimated value of the slope from linear regression, and the corresponding value of fractal dimension (D_{box}), is also reported in the graph.

4. Discussion

Fig. 6 displays the variation of fractal dimension (D_{box}) of mixing patterns with time (t). The graph shows a linear increase of D_{box} with t indicating that, as is also evident

from optical observations, the complexity of the mixing patterns increases with the repetition in time of stretching and folding dynamics.

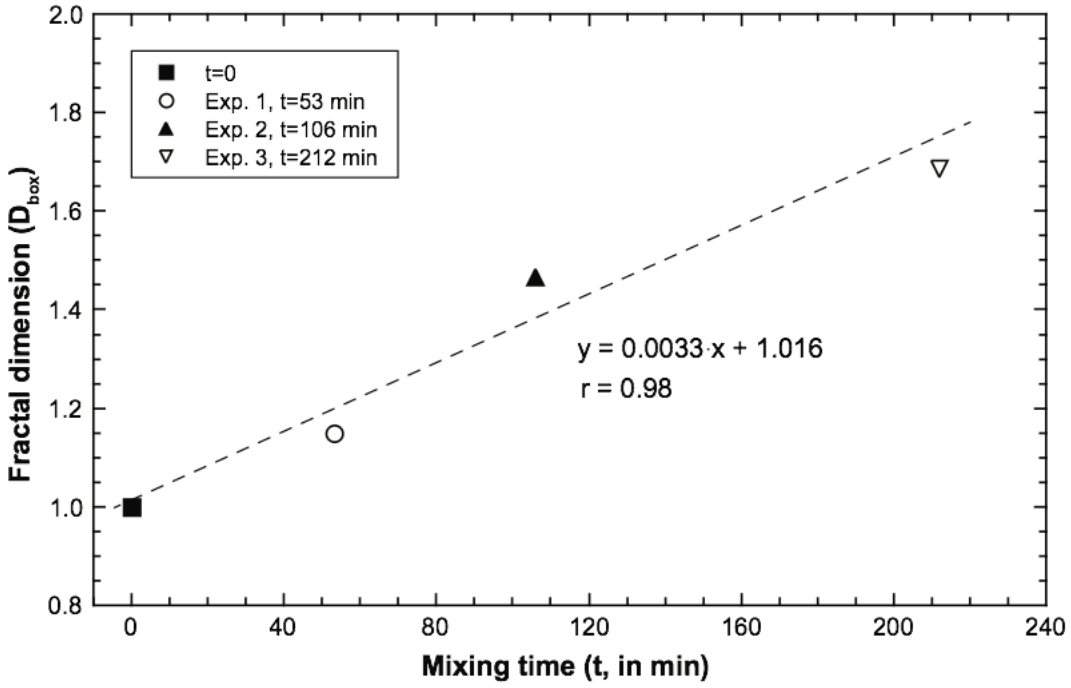

Figure 6: Empirical relationship between the fractal dimension of mixing patterns (D_{box}) and mixing time. The equation of the line corresponding to the linear fitting of data and the relative correlation coefficient are also reported in the graph.

The stretching and folding mechanisms and the increasing length contact interfaces between the melts imply that a broad distribution of length-scales develops on these interfaces. The increase of D_{box} is a direct consequence of the repetition in time of the stretching and folding mechanism. In fact, D_{box} is the exponent of the power law relation linking the number of grids containing contact interfaces (N_r) and the grid resolution r [Eq. 3]. The rate at which N_r increases with increasing resolution (i.e. for smaller r) indicates the amount of space that is filled by the contact interfaces between the two melts. Straight, circular, or otherwise regular lines are such that $N_r \sim r^{-1}$. However, for contact interfaces in fully chaotic systems, as the experiments presented here, $N(r, t)$ tends to a r^{-2} scaling as the mixing time advances (Fung and Vassilicos, 1991; Toussaint and Carriere; 1999; Ott and Antonsen, 1999). This r^{-2} scaling tendency reflects the space-filling nature of the contact interfaces in globally chaotic flows. At transient times, i.e. during the time evolution of the

mixing process, the scaling of $N(r, t)$ is well approximated by $N_r \sim r^{-Dbox}$ where D_{box} takes values between 1 and 2 and, in fact, increases with time towards 2 (e.g. Fung and Vassilicos, 1991; Ott and Antonsen, 1999). Note that before the starting of the experiment the morphology of the basalt-rhyolite interface is a hollow cylinder corresponding, on a 2D section, to a circle (Fig. 1). By definition a circle is a regular Euclidean shape whose dimension corresponds to unity (D_{box}=1.0, i.e. $N_r \sim r^{-1}$; Fig. 6; e.g. Mandelbrot, 1982). Through the repetition of the process of stretching and folding, the basaltic melt is continuously deformed into the rhyolitic one developing into complex patterns having a fractal morphology. In two dimensions, such as the experimental sections analyzed here, the basaltic melt is forced by chaotic flow fields to fill all the available space (i.e. it is dispersed across the whole 2D section) through the generation of lamellar structures (filaments). These filaments increase in number and become thinner with the time progression of mixing (Fig. 2). This implies that the contact interfaces between the basaltic and rhyolitic melts tend to fill the 2D section with scale-invariant (fractal) patterns. As the mixing pattern increases in complexity its fractal dimension (D_{box}) must increase towards the value of D_{box}=2.0 (i.e. $N_r \sim r^{-2}$) because this limit value represents the dimension of a 2D-plane according to Euclidean geometry. However, this is only true if we consider the physical dispersion of the two melts, without considering the onset of chemical exchanges by diffusion. From our experiments it is evident that not only such chemical exchanges occurred, but they occurred with different intensities due to the different mobility of the analyzed chemical elements (e.g. Fig. 3).

During mixing each chemical element is characterized by a concentration field C, which is strictly related to the geometrical configuration of the two melts in contact. The evolution of a concentration field obeys the advection-diffusion equation (e.g. Ottino, 1989; Aref and El-Naschie, 1995):

$$\partial_t C = k\nabla^2 C - v \cdot \nabla C \qquad \text{[Eq. 5]}$$

for the time-evolution of a distribution of concentration $C(x, t)$, being advected by a velocity field $v(x,t)$, and diffused with diffusivity k. In general terms, the advection term tends to create

sharp gradients of C, whilst the diffusion term tends to wipe out gradients. The evolution of the concentration field is thus given by a delicate balance of advection and diffusion.

At the beginning of the mixing process the advection term (i.e. the physical dispersion of the two melts) dominates the evolution of the concentration field. Chaotic advection transforms the initial configuration of the two melts (Fig. 1) and the width of filaments decreases exponentially with time, until an equilibrium scale is reached, at which the effect of diffusion starts to be significant. This scale is called the Batchelor scale (e.g. Ottino, 1989; Aref and El-Naschie, 1995) and is defined as

$$w_B = \sqrt{\frac{k}{\lambda}} \qquad \text{[Eq. 6]}$$

where λ is the Lyapunov exponent and k is the diffusivity. In the context of chaotic mixing, the Lyapunov exponent is a measure of the mean stretching rate experienced by each parcel of melt and is, therefore, an estimate of the physical dispersion of the two melts (e.g. Ottino, 1989). For globally chaotic systems, as the mixing experiments shows here, $\lambda>0$ on average. In other words, this means that the basaltic magma will, in time, be stretched attaining a filament-like morphology by a stretching rate that is proportional to e^{λ} (e.g. Gouillart et al., 2011, Petrelli et al., 2011). In the experiments presented in this work λ is constant because the experimental mixing protocol is simply repeated in time with the same relative rotations and velocity of the outer and inner cylinders and, hence, there is no variation of flow fields (see section 2.2). Considering the meaning of λ, therefore, the Batchelor scale defined by [Eq. 6] measures the balance between stretching and diffusion on the evolution of the concentration field. The Batchelor scale is the smallest length scale that can be observed in the concentration field, since diffusion smears out quickly any finer detail.

When filaments of the basaltic melt approach the Batchelor scale, diffusion begins to decrease significantly the contrast of concentration between the mafic filaments and the surrounding felsic melt. The resolution of the advection–diffusion equation [Eq. 5] shows that after filaments reached the Batchelor scale, the decrease of the concentration variability in the

mixing system due to diffusion is exponential, resulting in rapid homogenization with the surrounding fluid (e.g. Liu et al., 2004; Rothstein et al., 1999).

As discussed above, the concentration variance (σ^2_n) for the analyzed chemical elements is a measure of the compositional variability of each element during the time progression of mixing. It is therefore important to test whether a relationship exists between the complexity of the mixing pattern and σ^2_n. This is shown in the plot of Fig. 7 where the concentration variance (σ^2_n) of each element is plotted as a function of the fractal dimension (D_{box}) of the mixing pattern at different times.

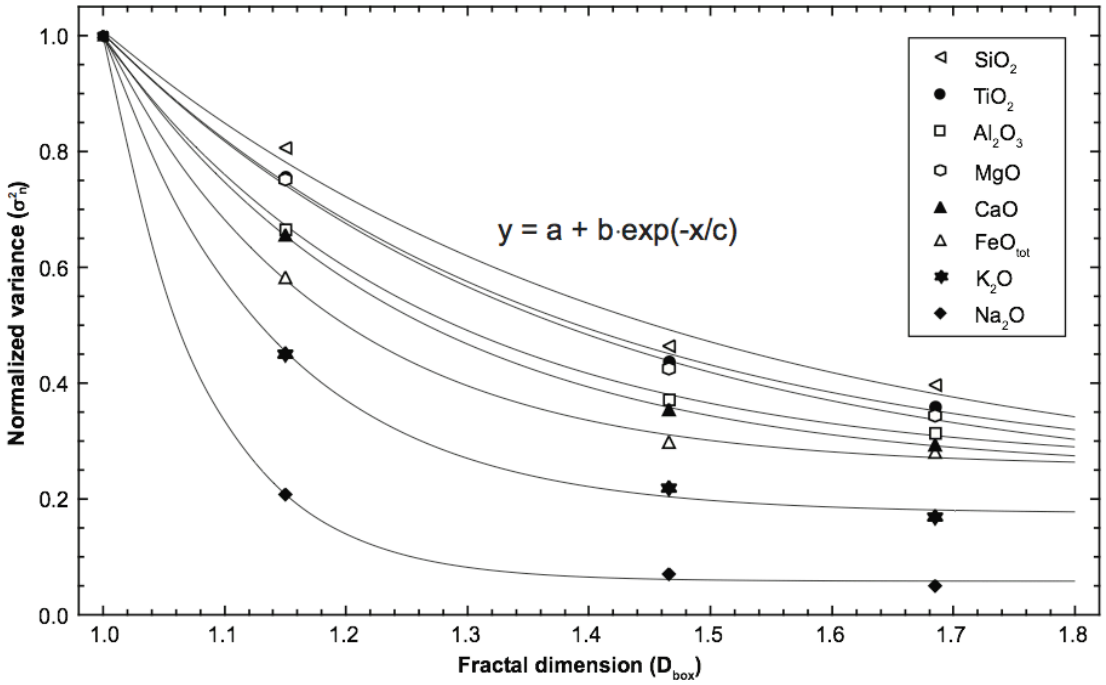

Figure 7: Variation of concentration variance (σ^2_n) of major elements at different mixing times as a function of fractal dimension (D_{box}) of mixing patterns (Fig. 2). The general exponential relationship used to fit data is also reported in the graph; values of fitting parameters (a, b and c) for each chemical element are given in Tab. 2.

The graph shows that, according to the previous discussion, σ^2_n displays an exponential variation with the morphological complexity of the mixing pattern. An important result emerging from Fig. 7 is that the different chemical elements show different exponential relationships with D_{box}. Given that the average stretching rate (λ) was constant during the time evolution of the mixing process, from [Eq. 6] it is clear that the Batchelor scale (w_B) mostly

depends upon the square root of the diffusion coefficient of the different chemical elements. The larger the value of *k*, the lower the compositional variability (σ^2_n) for a given chemical element. In other words, the Batchelor scale (i.e. the length scale at which the diffusion process starts to dominate the mixing process) must have been different for the different elements. In detail, for the fastest elements, such as Na_2O or K_2O, the length scale at which diffusion started to dominate during mixing must have been larger than for the slower elements (such as SiO_2 or TiO_2). Accordingly, from the graph of Fig. 7 is emerges that, during mixing between the basaltic and rhyolitic melts used in our experiments, w_B increases in the following order: SiO_2, TiO_2, Al_2O_3, MgO, CaO, FeO_{tot}, K_2O and Na_2O.

The exponential relationships shown in Fig. 7 have been fitted by the exponential function reported in the graph and the fitting parameters are reported in Tab. 2. These empirical relationships quantify the compositional variability (i.e. σ^2_n) that is expected for the different chemical elements during the time evolution of chaotic mixing processes considering the relative role played by advection (stretching and folding) and diffusion.

5. Conclusions and Outlook

In this work we have presented a new methodological approach to better understand the complexity of magma mixing processes combining experimental works, fractal analysis, and geochemical investigations. We have shown that, through this approach, it is possible to follow the time evolution of mixing processes between basaltic and rhyolitic melts by taking into account both the advection of the two melts via stretching and folding dynamics and chemical exchanges. These are the two fundamental factors influencing the mixing process.

Several new concepts and tools to study magma mixing processes unfold from the results presented in this work:

- The mixing patterns emerging by mixing basaltic and rhyolitic melts are fractal and they can be quantified by measuring their fractal dimension using the box-counting technique. These features were already successfully tested through the study of natural

samples and numerical simulations for mixing patterns generated by interaction of end-member melts with lower compositional differences (e.g. Perugini et al., 2002; 2003). Our results extend the range of compositions over which fractal patterns can be generated to the basalt-rhyolite end-member couple and represent a further step in the quantification of the magma mixing process starting from the morphological analyses of mixing patterns.

- There is a linear relationship between the fractal dimension (D_{box}) of the mixing patterns and mixing time. Although a positive correlation between these two variables is intuitive, we have shown that now this correlation can be established by deriving empirical relationships through experiments performed with natural silicate melts. This kind of empirical relationships may permit access to one of the most important issues regarding igneous systems: the estimation of time scales of magma mixing processes. This is a potentially new field of research that may have deep volcanological implications. For example, analyses of the morphology of mixing patterns on volcanic rocks could be complemented by experiments performed with the end-members recognized on outcrops. This would allow defining empirical relationships between D_{box} and mixing time and this may represent a new chronometer to estimate the mixing-to-eruption time. This is a fundamental issue in volcanology because the mixing process is believed to represent the triggering factor of many highly explosive volcanic eruptions (e.g. Sparks et al., 1977; Murphy, 1998; Leonard et al., 2002; Martin et al., 2008).
- The relationships presented in Fig. 7 between the complexity of mixing patterns and concentration variance represent, to the best of our knowledge, the first morphochemical study in igneous systems and may have important petrologic consequences. In particular, starting from the morphological quantification of magma mixing textures it is possible to make inferences about the compositional variability that should be expected on rock suites and the relative mobility of chemical elements.

Recent works highlighted that this is an essential feature to be taken into account in the modeling of rocks generated by magma mixing because during this process complex diffusive fractionation processes of chemical elements are triggered (e.g. Perugini et al., 2006; 2008; De Campos et al., 2011; Perugini et al, 2012; Morgavi et al., 2012). These processes are responsible for significant deviation of samples from the classic linear model of two end-member mixing model, commonly invoked when dealing with magma mixing processes. Noteworthy is the fact that these processes are only recognizable if petrological studies are carried out combining detailed textural analyses of mixing patterns, precise microanalytical investigations of the compositional variability and accurate numerical models. The use of conventional whole rock analyses would not allow us to reach such a level of understanding of the complexity of the mixing process. In fact, the small-scale variability generated by the mixing process would not be revealed by whole rock analyses in which element concentrations are averaged, resulting in a loss of valuable information. Therefore, the approach used in our work may be an additional tool towards the goal of understanding the complexity of one of the most important petrologic processes.

Chapter 5

Outlook

5.1 Outlook

The conceptual model proposed in this three-year scientific investigation, combining experimental works, quantification of the mixing patterns and geochemical analyses may provide a useful tool to directly decipher the complexity of magma mixing processes and their time evolution. Further work, however, is needed to understand whether the physical and chemical relationships derived in our study can be extended to other mixing systems, i.e., those characterized by different end-member pairs with different geochemical and rheological contrasts.

In particular, further investigations are required before we can fully apply the proposed method to address the complexity of natural systems. Among the most important points are:

- The application of compositional variability to estimate the timing of mixing processes in volcanic rocks requires time-series experiments to calibrate the decay of concentration variance for each element in a multi-component system. These can be obtained for different fluid dynamic regimes and different pairs of end-members using the approach introduced in this work.
- To better understand the complexity of a magmatic mixing system, the quantification of the mixing efficiency cannot be simply based on the chemical analysis of a few areas or transects. This is particularly important in the light of the strong modulation of the mixing process both in space and time that generates extremely variable mixing geometries and variable dynamics.
- The evolution of magma mixing processes in space and time generates a self-similar (i.e. fractal) distribution of the mixing patterns and compositional fields. The fractality of the process implies, in principle, that the chemical signature of a mixing system is scale-invariant and that experimental findings may be directly applicable to natural scenarios operating at larger scales. Therefore it becomes

imperative to compare topologically equivalent mixing patterns in order to avoid problems associated with the representativeness of sample sections.

- We demonstrated that the patterns generated by the mixing process are extremely complex and consist of alternate filaments of the two magmas propagating from the centimeter to the micron length scale, but we were only able to quantify the mixing structure in two dimensions. A further development of this work will be to acquire morphologialcal data in 3D on both natural and experimental samples, this kind of information is essential because will allow us to visualize and quantify the complexity of the mixing process in the three spatial dimensions without incurring in stereological aberrations which are typically associated with the study of 2D sections. For this purpose we are already planning to use synchrotron X-ray computed microtomography (micro-CT). This method, never used before for analysis of magma mixing structure, will be an extraordinary tool to better understand the complex physical and chemical interaction of magmas and will provide unprecedented information on this important igneous process.
- A needed parallel goal is to increase the precision and accuracy of geochemical analyses in order to measure even the smallest compositional heterogeneities on natural rocks and experimental samples. This would allow us to analyse and quantify the effects of mixing even at longer mixing times, an information that is currently inaccessible. Without this approach a complete understanding of the importance of magma mixing and its impact on the production of compositional heterogeneity in the system Earth will remain elusive.

5.2 Acknowledgements

Vorrei ringraziare il Dr. Diego Perugini che ha avuto il gravoso ruolo di seguire questo studente lungo questi tre anni di studi e di vita. Diego per me sei e rimarrai per sempre un esempio di vita, di coerenza e onestà; da te ho imparato che prima di essere un buon scienziato bisogna essere un uomo onesto e corretto. Probabilmente non sarò mai in grado di ripagare tutto ciò che hai fatto per me, ma spero un giorno di poter trasferire ad uno studente tutti i tuoi insegnamenti.

Per me sarà sempre un vanto e un orgoglio poter dire sono stato uno studente del Dr. Perugini. Grazie di cuore

I owe Prof. Don Dingwell a great debt of gratitude, for all his encouragement and advice during this project, thanks Don you were right; great things can come from this Department. For their advice, inspiration and help with the completing of this work I would like to acknoledge Prof. Cristina De Campos and Dr. Werner Ertel-Ingrisch without you two the world would be more grey. It is also a pleasure to acknowledge Yan Lavallèe for his encouragement during the time of my Ph.D.

A mia madre e mio padre cosi diversi ma cosi uguali nell' immenso amore che mi hanno sempre dato vi voglio un gran bene continuate a essere cosi.

A mio fratello per avermi trasmesso la passione per le moto che è la cosa che mi fa sognare nei giorni tristi. A mia sorella perchè è semplicemente la migliore sorella che si possa avere: „ a lè neanche la fantasia più sfrenata può creare una persona come te."

A Simone D'antuono e Vincenzo Marotta con i quali ho condiviso un anno di vita a Napoli che non potrò mai dimenticare, ragazzi non basterebbe un libro per raccontare le mille avventure passate insieme.

Al mio caro amico Fabio Arzilli grazie per il tempo passato qui a Monaco, per le lunghe chiaccherate su skype e per le grandi risate a parlare della figura mitologica del De Grisogono sei proprio Massimo Troisi e con questo ho detto tutto.

A Oryaelle in the crazy llife of Munich your friendship help me to go on, thanks

Oriella you could be the only one to study Mars because you are the closest thing to it, you are a star my frined bisou.

Vorrei ringraziare Stefano, Grazio, Teresa e Antonietta, in questi tre anni grazie a voi mi sono sentito meno solo e' proprio bello far parte della grande famiglia della Gelateria ADRIA siete speciali.

A Ylenia per avermi fatto ridere a crepa pelle e per avermi sollevato quando ero a terra grande Yle.

A Laura per i fantastici giri in motorino a Barcellona e le meravigliose passeggiate in moto per le alpi sei meravigliosa.

A big thanks to Heintz Tschinkel sometime you are lucky and you meet great people that live their life with passion. I am so happy to have meet you Heintz thanks for all the chat and the cappuccino in front of the beautifull DUCATI 750 SS.

Il piu' grande ringraziamento va a te Racheline per essermi stata a finco in tutti questi anni per avermi insegnato molto e per aver condiviso i momenti belli e i momenti brutti di questa strana ma meravigliosa vita. Sono stati sei anni bellissimi non li dimentichero' mai grazie per essermi stata accanto.

I thank D. Müller for his technical support during the microprobe analysis. M. Petrelli and Dr. Hans-Michael Seitz for the LA-ICP-MS measurements; H.W. Lohringer is thanked for the preparation of microprobe samples. A big thanks to all the people in the department of Mineralogy, petrology and geochemistry(LMU) work with you it has been a great pleasure.

I gratefully acknowledge F. Lechner, M. Troisi, Roberto Benigni, Antonio de Curtis and Paolo Villaggio for providing inspiration during the writing of this paper. This Ph.D. research was funded by the ICDP program number DFG- Project DI 431/31-1 and Di 431/31-2, AOBJ: 564369

5.3 References

Abe, Y., (1997). Thermal and chemical evolution of the terrestrial magma ocean. Phys. Earth Planet. Int. 100, 27-39.

Abramoff, M.D., Magalhaes, P.J., Ram, S.J., 2004. Image Processing with ImageJ. Biophoton. Int. 11, 36-42.

Anderson AT (1976) Magma mixing: Petrological process and volcanological tool. J Volcanol Geotherm Res. 1: 3-33

Anderson, D. L., (1982). Isotopic evolution of the mantle: the role of magma mixing. Earth Planet. Sci. Lett. 57, 1-12.

Aref H, El-Naschie M S (1995) Chaos Applied to Fluid Mixing. Pergamon Press Reprinted from Chaos Solitions and Fractals 4(6)

Bacon, C.R., (1986). Magmatic inclusions in silicic and intermediate volcanic rocks. J. Geophys. Res. 91, 6091-6112.

Baker D (1991). Interdiffusion of hydrous dacitic and rhyolitic melts and the efficacy of rhyolite contamination of dacitic enclaves. Contrib Mineral Petrol 106: 462-473

Baker, D.R., (1990). Chemical Interdiffusion of Dacite and Rhyolite - Anhydrous Measurements at 1 Atm and 10 Kbar, Application of Transition-State Theory, and Diffusion in Zoned Magma Chambers. Contrib. Mineral. Petrol. 104, 407-423.

Bateman, R., (1995). The interplay between crystallization, replenishment and hybridisation in large felsic magma chambers. Earth Sci. Rev. 39, 91–106.

Behrens H, Hahn M (2009) Trace element diffusion and viscous flow in potassium-rich trachytic and phonolitic melts. Chem Geol 259: 63-77

Bergantz, G.W., (2000). On the dynamics of magma mixing by reintrusion: implications for pluton assembly processes. J. Struct. Geol. 22, 1297-1309.

Bonnichsen, B., (1982). Rhyolite lava flows in the Bruneau-Jarbidge eruptive center, southwestern Idaho. Idaho Bur. Mines Geol. Bull. 26, 283-320.

Cathey, H.E., Nash, B.P., (2009). Pyroxene thermometry of rhyolite lavas of the Bruneau–Jarbidge eruptive center, Central Snake River Plain. J. Volcanol. Geotherm. Res. 188, 173-185.

Chakraborty, S., Dingwell, D.B., Rubie, D., (1995). Multicomponent diffusion in ternary silicate melts in the system K2O-Al2O3-SiO2: I. Experimental measurements. Geochim. Cosmochim. Acta 59, 255-264.

Costa, F., Chakraborty, S., (2004). Decadal time gaps between mafic intrusion and silicic eruption obtained by chemical zoning patterns in olivine. Earth Planet. Sci. Lett. 227, 517-530.

De Campos C P, Dingwell D B, Fehr K T (2004) Decoupled convection cells from mixing experiments with alkaline melts from Phlegrean Fields. Chem. Geol. 213:227-251

De Campos, C. P., Dingwell D.B., Perugini D., Civetta L., Fehr T. K., (2008). Heterogeneities in magma chambers: insight from the behaviour of major and minor elements during mixing experiments with natural alkaline melts. Chem. Geol., 256, 131-145

De Campos, C. P., Perugini, D., Ertel-Ingrisch, W., Dingwell, D. B., Poli, G., (2011). Enhancement of Magma Mixing Efficiency by Chaotic Dynamics: an Experimental Study. Contrib. Mineral. Petrol. 161, 863-881.

De Rosa R, Mazzuoli R, Ventura G (1996) Relationships between deformation and mixing processes in lava flows: a case study from Salina (Aeolian Islands, Tyrrhenian Sea) Bull Volcanol 58: 286-297

De Rosa, R., Donato, P., Ventura, G., (2002). Fractal analysis of min- gled/mixed magmas: an example from the Upper Pollara eruption (Salina Island, Southern Tyrrhenian Sea, Italy). Lithos 65, 299-311.

De Rosa, R., Mazzuoli, R., Ventura, G., (1996). Relationships between deformation and mixing processes in lava flows: a case study from Salina (Aeolian Islands, Tyrrhenian Sea). Bull. Volcanol. 58, 286-297.

Didier, J., Barbarin, B., (1991). Enclaves and Granite Petrology, Developments in Petrology, 13, Elsevier, Amsterdam, 625 pp.

Dingwell, D., (1986). Viscosity-temperature relationships in the system Na2Si2O5-Na4Al2O5. Geochim. Cosmochim. Acta, 50, 1261-1265.

Druitt, T. H., Costa, F., Deloule, E., Dungan, M., and Scaillet, B., (2012). Decadal to monthly timescales of magma transfer and reservoir growth at a caldera volcano. Nature 482, 77-80.

Eichelberger, J.C., (1975). Origin of andesite and dacite: evidence of mixing at Glass Mountain in California and other circum-Pacific volcanoes. Geol. Soc. Amer. Bull. 86, 1381-1391.

Flinders, J., Clemens, J.D., (1996). Non-linear dynamics, chaos, complexity and enclaves in granitoid magmas. Trans. R. Soc. Edinburgh Earth Sci. 87, 225-232.

Fourcade, S., Allegre, C. J., (1981). Trace element behaviour in granite genesis: a case study the calc-alkaline plutonic association from the Querigut Complex (Pyrenees France). Contrib. Mineral. Petrol. 76, 177-195.

Fung, J.C.H., Vassilicos, J.C., (1991). Fractal Dimensions of Lines in Chaotic Advection. Phys. Fluids A 11, 2725-2733.

Gouillart, E., Dauchot, O., Thiffeault, J.-L., (2011). Measures of mixing quality in open flows with chaotic advection. Phys. Fluids 23, 013604.

Grasset, O., Albarede, F., (1994). Hybridisation of mingling magmas with different densities. Earth Planet. Sci. Lett. 121, 327-332.

Hibbard M J (1981) The magma mixing origin of mantled feldspar. Contrib Mineral Petrol 76: 158-170

Hibbard, M.J., (1995). Petrography to petrogenesis. Prentice Hall 587 pp.

Janoušek V, Bowes DR, Rogers G, Farrow CM, Jelínek E (2000) Modelling diverse processes in the petrogenesis of a composite batholith: the Central Bohemian Pluton, Central European Hercynides. J Petrol 41: 511-543

Jochum, K.P., Dingwell, D.B., Rocholl, A. Stoll, B., Hofmann, A.W., et al., (2000). The preparation and preliminary characterisation of eight geological MPI-DING Reference glasses for in-situ microanalysis. Geostandards Newsletter 24, 87-133.

Kratzmann, D.J., Carey, S., Scasso, R., Naranjo, J.A., (2009). Compositional variations and magma mixing in the 1991 eruptions of Hudson volcano, Chile. Bull. Volcanol. 71, 419-439.

Leonard, G., Cole, J., Nairn, I., Self, S., (2002). Basalt triggering of the c. AD 1305 Kaharoa rhyolite eruption, Tarawera Volcanic Complex, New Zealand. J. Volcanol. Geotherm. Res. 115, 461-486.

Lesher, C.E., (1990). Decoupling of chemical and isotopic exchange during magma mixing. Nature 344, 235-237.

Liang, Y., Richter, F.M., Watson, E.B., (1996). Diffusion in silicate melts: II. Multicomponent chemical diffusion in CaO-Al2O3-SiO2 at 1500 °C and 1 GPa, Geochim. Cosmochim. Acta 60, 5021-5036.

Liu, W., Haller, G., (2004). Strange eigenmodes and decay of variance in the mixing of diffusive tracers. Physica D, 188, 1-39.

Lundstrom, C.C., (2000). Rapid diffusive infiltration of sodium into partially molten peridotite. Nature 403, 527-530.

Makridakis S, Wheelwright S, Hyndman R (1998) Forecasting: Methods and Applications (3rd Ed.). New York Wiley

Mandelbrot, B.B., (1982). The Fractal Geometry of Nature. W.H. Freeman, New York.

Martin, V.M., Morgan, D.J., Jerram, D.A., Caddick, M.J., Prior, D.J., Davidson, J.P., (2008). Bang! Month-Scale Eruption Triggering at Santorini Volcano. Science 321, 1178.

Mathew G, Mezic I, Grivopoulos S, Vaidya U, Petzold L (2007) Optimal control of mixing in Stokes fluid flows. J. Fluid Mech 580: 261-28

Morgavi D., Perugini D., De Campos C.P., Ertl-Ingrisch W., Lavallee Y., Morgan L., Dingwell D.B., (2012) Interactions Between Rhyolitic and Basaltic Melts Unraveled by Chaotic Magma Mixing Experiments. Chem. Geol. in press

Mungall J E, Dingwell D B, Chaussidon M (1999) Chemical diffusivities of 18 trace elements in granitoid melts. Geochim Cosmochim Acta 63: 2599-2610

Mungall, J.E., (2002). Empirical models relating viscosity and tracer diffusion in magmatic silicate melts. Geochim. Cosmochim Acta 66, 125-143.

Murphy, M.D., (1998). The Role of Magma Mixing in Triggering the Current Eruption at the Soufriere Hills Volcano, Montserrat, West Indies. Geophys. Res. Lett. 25, 3433-3436.

Muzzio, F.J., Swanson, P.D., Ottino, L.M., (1992). Mixing distributions produced by multiplicative stretching in chaotic flows. Int. Jour. Bif. Chaos 2, 37-50.

Nakamura E, Kushiro I, (1998) Trace element diffusion in jadeite and diopside melts at high pressures and its geochemical implication. Geochim Cosmochim Acta 62: 3151-3160

Ott, E., Antonsen, T.M., (1988). Chaotic Fluid Convection and the Fractal Nature of Passive Scalar Gradients. Phys. Rev. Lett. 61, 2839-2842.

Ottino J M (1989) The Kinematics of mixing: stretching, chaos and transport. Cambridge University Press

Perugini D, Petrelli M, Poli G (2006) Diffusive fractionation of trace elements by chaotic mixing of magmas. Earth Planet Sci Lett 243: 669-680

Perugini D, Poli G (2005) Viscous fingering during replenishment of felsic magma chambers by continuous inputs of mafic magmas: field evidence and fluid- mechanics experiments. Geology 33: 5-8.

Perugini D, Poli G, Gatta G (2002) Analysis and Simulation of Magma Mixing Processes in 3D. Lithos 65: 313-330

Perugini D, Poli G, Mazzuoli R (2003) Chaotic Advection, Fractals and Diffusion During Mixing of Magmas: Evidence from Lava Flows. J Volcanol Geotherm Res 124: 255-279

Perugini D, Ventura G, Petrelli M, Poli G (2004) Kinematic significance of morphological structures generated by mixing of magmas: a case study from Salina Island (Southern Italy). Earth Planet Sci Lett 222: 1051-1066

Perugini, D., (2002). MorphoUt 1.0: Utilities for Closed Shape Morphometry. Comput. Geosci. 28, 73-79.

Perugini, D., De Campos, C. P., Dingwell, D. B., Petrelli, M., Poli, G., (2008). Trace element mobility during magma mixing: preliminary experimental results. Chem. Geol. 256, 146-157.

Perugini, D., De Campos, C.P., Ertel-Ingrisch, W., Dingwell, D.B., (2012). The space and time complexity of chaotic mixing of silicate melts: implications for igneous petrology. Lithos, http://dx.doi.org/10.1016/j.lithos.2012.09.010.

Perugini, D., Petrelli, M., Poli, G., (2006). Diffusive fractionation of trace elements by chaotic mixing of magmas. Earth Planet. Sci. Lett. 243,669-80.

Perugini, D., Petrelli, M., Poli, G., De Campos, C., Dingwell, D.B., (2010). Time-Scales of Recent Phlegrean Fields Eruptions Inferred from the Application of a 'Diffusive Fractionation' Model of Trace Elements. Bull. Volcanol. 72, 431-447.

Perugini, D., Poli G., Mazzuoli, R. (2003). Chaotic Advection, Fractals and Diffusion During Mixing of Magmas: Evidence from Lava Flows. J. Volcanol. Geotherm. Res., 124, 255-279.

Perugini, D., Poli, G., 2005. Viscous fingering during replenishment of felsic magma chambers by continuous inputs of mafic magmas: field evidence and fluid- mechanics experiments. Geology 33, 5-8.

Perugini, D., Poli, G., (2012). The mixing of magmas in plutonic and volcanic environments: analogies and differences, Lithos, http://dx.doi.org/10.1016/j.lithos.2012.02.002.

Perugini, D., Poli, G., Valentini, L., (2005). Strange attractors in plagioclase oscillatory zoning: petrological implications. Contrib. Mineral. Petrol. 149, 482-497.

Perugini, D., Valentini, L., Poli, G., (2007). Insights into Magma Chamber Processes from the Analysis of Size Distribution of Enclaves in Lava Flows: a Case Study from Vulcano Island (Southern Italy). J. Volcanol. Geotherm. Res. 166, 193-203.

Perugini, D., Ventura, G., Petrelli, M., Poli, G., (2004). Kinematic significance of morphological structures generated by mixing of magmas: a case study from Salina Island (Southern Italy). Earth Planet. Sci. Lett. 222, 1051-1066.

Petrelli M, Perugini D, Poli G (2011) Transition to Chaos and Implications for Time-Scales of Magma Hybridization During Mixing Processes in Magma Chambers. Lithos 125: 211-220

Petrelli, M., Perugini, D., Alagna, K. E., Poli, G., Peccerillo, A., (2008). Spatially resolved and bulk trace element analysis by laser ablation-inductively coupled plasma-mass spectrometry (LA-ICP-MS). Periodico di Mineralogia 77, 3-21.

Petrelli, M., Perugini, D., Poli, G., (2011). Transition to Chaos and Implications for Time-Scales of Magma Hybridization During Mixing Processes in Magma Chambers. Lithos, 125, 211-220.

Petrelli, M., Perugini, D., Poli, G., Peccerillo, A., (2007). Graphite electrode lithium tetraborate fusion for trace element determination in bulk geological samples by laser ablation ICP-MS. Microchim. Acta 158, 275-282.

Poli, G., Perugini D., (2002). Strange Attractors in Magmas: Evidence from Lava Flows. Lithos 65, 287-297.

Poli, G., Tommasini, S., Halliday, A.N., (1996). Trace elements and isotopic exchange during acid-basic magma interaction processes. Trans. Royal Soc. Edinburgh: Earth Sci. 87, 225-232.

Pouchou, L., Pichoir, F., (1984). A new model for quantitative X-ray microanalysis: Part I: Applications to the analysis of homogeneous samples. Rech. Aerosp. 3, 13-38.

Rothstein, D., Henry, E., Gollub, J. P., (1999). Persistent patterns in transient chaotic fluid mixing. Nature, 401, 770-772.

Roth, J. (1861). Tabellarischen Uebersicht der Gesteins- analysen. Berlin, Besserische Buchhandlung, p. i–xxvi, 1–66.

Shannon, R. D. (1976). Revised effective ionic radii and systematic studies of interatomic distances in halides and chalcogenides. Acta Crystallographica A32, 751-767.

Slaby, E., Gotze, J., Worner, G., Simon, K., Wrzalik, R., Smigielski, M., (2010). K-feldspar phenocrysts in microgranular magmatic enclaves: a cathodoluminescence and geochemical study of crystal growth as a marker of magma mingling dynamics. Lithos 105, 85–97.

Slaby, E., Smigielski, M., Smigielski, T., Domonik, A., Simon, K., Kronz, A., (2011). Chaotic three-dimensional distribution of Ba, Rb, and Sr in feldspar megacrysts grown in an open magmatic system. Contrib. Mineral. Petrol. 162, 909-927.

Smith, J.V., (2000). Structures on interfaces of mingled magmas, Stew- art Island, New Zealand. J. Struct. Geol. 22, 123-133.

Snyder, D., (2000). Thermal effects of the intrusion of basaltic magma into a more silicic magma chamber and implications for eruption triggering, Earth Planet. Sci. Lett. 175, 257-273.

Solgadi F, Moyen JF, Vanderhaeghe O, Sawyer EW, Reisberg L (2007) The role of crustal anatexis and mantle-derived magmas in the genesis of synorogenic Hercynian granites of the Livradois area, French Massif Central. Can. Mineral 45: 581-606

Sparks, S.R.J., Marshall, L.A., (1986). Thermal and mechanical constraints on mixing between mafic and silicic magmas. J. Volcanol. Geotherm. Res. 29, 99-124.

Sparks, S.R.J., Sigurdsson, H., Wilson, L., (1977). Magma mixing: a mechanism for triggering acid explosive eruptions. Nature 267, 315–318.

Strogatz, S.H., (1994). Nonlinear Dynamics and Chaos. Addison-Wesley. 498 pp.

Swanson, P.D., Ottino, J.M., (1990). A comparative computational and experimental study of chaotic mixing of viscous fluids. J. Fluid. Mech. 213, 227-249.

Toussaint, V., Carriere, P., (1999). Diffusive cut-off of fractal surfaces in chaotic mixing, Int. J. Bifurcation Chaos 9, 443.

Ventura, G., (1998). Kinematic significance of mingling-rolling struc- tures in lava flows: a case study from Porri volcano (Salina Southern Tyrrhenian Sea), Bull. Volcanol. 59, 394-403.

Wada, K., (1995). Fractal structure of heterogeneous ejecta from the Meakan volcano, eastern Hokkaido, Japan: implications for mixing mechanism in a volcanic conduit. J. Volcanol. Geotherm. Res. 66, 69-79.

Walker, G.P.L., Skelhorn, R.R., (1966). Some associations of acid and basic igneous rocks. Earth Sci Rev 2, 9-109.

Wallace, G., Bergantz, G., (2002). Wavelet-based correlation (WBC) of crystal populations and magma mixing. Earth Planet. Sci. Lett. 202, 133-145.

Wiebe, R. A., (1994). Silicic magma chambers as traps for basaltic magmas: the Cadillac mountain intrusive complex, Mount Desert island, Maine. J. Geol. 102, 423-427.